Technische Universität München
TUM School of Life Sciences

Nutritional programming of white adipose tissue growth and metabolism in adulthood

Kristina Then

Vollständiger Abdruck der von der TUM School of Life Sciences der Technischen Universität München zur Erlangung einer

Doktorin der Naturwissenschaften (Dr. rer. nat.)

genehmigten Dissertation.

Vorsitz: Prof. Dr. Dietmar Zehn

Prüfer*innen der Dissertation:

1. Prof. Dr. Martin Klingenspor
2. Prof. Dr. Alexander Bartelt

Die Dissertation wurde am 27.03.2023 bei der Technischen Universität München eingereicht und durch die TUM School of Life Sciences am 28.06.2023 angenommen.

Table of Contents

Abbreviations

Acaca	Acetyl-CoA carboxylase alpha
Acc	Acetyl-CoA carboxylase
Adipoq	Adiponectin
ADP	Adenosine diphosphate
AF	Alexa fluor®
AGC	Automatic gain control
AMPS	2-acrylamido-2-methylpropane sulfonic acid
ANCOVA	Analysis of covariance
ANOVA	Analysis of variance
APC	Adipocyte progenitor cell
Ar	Androgen receptor
Areg	Adipogenesis-regulatory cell
Aoc3	Amine oxidase copper containing 3
AS3MT	Arsenite methyltransferase
Atgl	Adipose triglyceride lipase
ATP	Adenosine triphosphate
ATP5A	ATP synthase F1 subunit alpha
ATXN2	Ataxin 2
Bmp7	Bone morphogenetic protein 7
BSA	Bovine serum albumin
BV	Blue violet
CD	Control diet
CD55	Complement decay-accelerating factor
CD142	Platelet tissue factor, coagulation factor III
cDNA	Complementary DNA
CET	Central European time
Clec11a	C-type lectin domain family 11 member A
CLMP	CXADR like membrane protein
CS	Citrate synthase
Cy	Cyanine
DAPI	4′,6-diamidino-2-phenylindole
DDA	Data dependent acquisition
ddH_2O	Double distilled water
DGAT2	Diacylglycerol O-acyltransferase 2
DMEM	Dulbecco's modified eagle medium

DMSO	Dimethyl sulfoxide
DNA	Deoxyribonucleic acid
DPP4	Dipeptidyl peptidase-4
DTNB	5,5’dithiobis(2-nitrobenzoic) acid
EDTA	Ethylenediaminetetraacetic acid
EdU	5-ethynyl-2’-deoxyuridine
EFHD2	EF-hand domain-containing protein D2
EGTA	Ethylene glycol tetraacetic acid
EtOH	Ethanol
eWAT	Epididymal white adipose tissue
F3	Platelet tissue factor, coagulation factor III
Fabp	Fatty acid binding protein
FBS	Fetal bovine serum
FAM129B	Niban-like protein 1
Fasn	Fatty acid synthase
Fmo2	Flavin-containing monooxygenase 2
FSC-A	Forward scatter area
FSC-H	Forward scatter height
FSC-W	Forward scatter width
FTH1	Ferritin heavy chain 1
g	Gram
g	Gravitational acceleration
GC	Vitamin D-binding protein
GOCC	Gene ontology cellular component
h	Hour
HBSS	Hanks' balanced salt solution
HE	Hematoxylin and eosin
HEPES	4-(2-hydroxyethyl)-1-piperazineethanesulfonic acid
HFD	High-fat diet
HPLC	High performance liquid chromatography
HPX	Hemopexin
Hsl	Hormone-sensitive lipase
KEGG	Kyoto encyclopedia of genes and genomes
LFQ	Label-free quantification
Lin	Lineage
Lpl	Lipoprotein lipase
Ly6a	Lymphocyte antigen 6 complex

ICAM1	Intercellular adhesion molecule 1
iWAT	Inguinal white adipose tissue
k	One thousand
kg	Kilogram
kJ	Kilo joule
nl	Nanolitter
µg	Microgram
µl	Microliter
maxIT	Maximum injection time
min	Minute
MJ	Mega joule
ml	Milliliter
mm	Millimeter
MS	Mass spectrometric
msec	Millisecond
MTCO1	Mitochondrially encoded cytochrome C oxidase I
NUP210	Nuclear pore membrane glycoprotein 210
OPA1	Optic atrophy 1
PAGE	Polyacrylamide gel electrophoresis
PBS	Phosphate-buffered saline
PCA	Principal component analysis
Pdgfra	Platelet derived growth factor receptor alpha
PE	Phycoerythrin
pf	Pair-fed
PHLDA3	Pleckstrin homology-like domain family A member 3
Pi16	Peptidase inhibitor 16
Plin1	Perilipin 1
Pparg	Peroxisome proliferator-activated receptor
Pref1	Preadipocyte factor 1
RCC2	Regulator of chromosome condensation 2
RCR	Respiratory control ratio
RIPA	Radioimmunoprecipitation assay buffer
RNA	Ribonucleic acid
rpm	Revolutions per minute
SCA1	Stem cells antigen 1
SDHB	Succinate dehydrogenase complex iron sulfur subunit B
SDS	Sodium dodecyl-sulfate

SERPINB6B	Serpin family B member 6 B
SH3BGRL3	SH3 domain-binding glutamic acid-rich-like protein 3
SLC37A2	Sugar phosphate exchanger 2
SORBS1	Sorbin and SH3 domain-containing protein 1
Sox9	SRY-Box Transcription Factor 9
Srebp1c	Sterol regulatory element-binding transcription factor 1 c
SSC-A	Side scatter area
STE	Sucrose/Tris/EGTA
SVF	Stromal-vascular fraction
SZT2	Seizure threshold 2 homolog
T3	Triiodothyronine
TBS	Tris-buffered saline
TEMED	Tetramethylethylenediamine
TfIIb	Transcription factor II B
TRIM14	Tripartite motif-containing protein 14
RT-qPCR	Real-time quantitative polymerase chain reaction
U	Unit
UQCRC2	Ubiquinol-cytochrome-c reductase complex core protein 2
VAP1	Vascular adhesion protein 1
v/v	Volume per volume
WAT	White adipose tissue
Wnt2	Wingless-type MMTV integration site family member 2
w/v	Weight in volume

List of Figures

List of Tables

Abstract

Diet-induced obesity is a rapidly increasing health concern in modern society and has been associated with the development of numerous health issues, including cardiovascular disease and type 2 diabetes. Despite multiple interventions designed to promote body mass loss, affected patients often experience limited success in maintaining long-term outcomes. One underlying mechanism that contributes to this phenomenon is commonly known as the 'yo-yo effect' and remains poorly understood. To investigate the underlying role of adipogenic potential, we conducted a study on male C57BL/6N mice, examining cell fate decisions, terminal differentiation, and proliferation of adipocyte progenitor cells. Mice were initially fed a high-fat diet until they reached a body mass of at least 40 g, followed by a one-week control diet or caloric-restricted, pair-fed high-fat diet. In addition, we assessed mitochondrial function in white adipocytes during body mass loss and subsequent regain by feeding the male C57BL/6N mice a high-fat diet for 24 weeks, followed by an eight-week control diet-induced obesity remission and a high-fat diet refeeding for 12 weeks.

Short-term high-fat diet recovery had a significant impact on the fate of stromal-vascular fraction cells, as determined by cell culture and flow cytometry experiments. Specifically, we focused on three distinct white adipose tissue subpopulations, characterized by the expression of CD55, VAP1, or CD142, which contribute to diet- and fat depot-specific changes in adipogenic potential. Flow cytometry and immunofluorescence imaging revealed a proliferation stop in epididymal white adipose tissue in its plateau phase at 40 g body mass. Following full control diet-induced obesity remission, mitochondrial capacity and content remained reduced in epididymal adipocytes, as determined by high-resolution respirometry and citrate synthase activity. In contrast, inguinal adipocyte mitochondria retained their function. Protein expression analysis revealed only minor effects in the expression levels of proteins that belong mainly to adipocyte differentiation, lipid metabolism, and inflammation. High-fat diet refeeding doubled body mass and fat mass gain within the first weeks of the diet change in comparison to mice receiving a high-fat diet for the first time.

Our results emphasize the importance of fat depot specificity for metabolic obesity consequences and associated treatments. We identified $CD142^{+}$ adipogenesis-regulatory cells as a reversible silencer of differentiation capacity of adipocyte progenitor cells. Additionally, we found that epididymal adipocyte mitochondria exhibit a persisting restriction due to high-fat diet feeding, while inguinal adipocyte mitochondria are more resilient. These alterations are concomitant and likely implicated in the etiology of a 'yo-yo effect', characterized by enhanced body mass gain upon re-exposure to a high-fat diet.

Zusammenfassung

Diätbedingte Fettleibigkeit stellt in der modernen Gesellschaft ein rasch wachsendes Gesundheitsproblem dar und wird mit der Entwicklung zahlreicher Gesundheitsprobleme in Verbindung gebracht, darunter Herz-Kreislauf-Erkrankungen und Typ-2-Diabetes. Trotz zahlreicher Maßnahmen zur Förderung der Gewichtsabnahme sind die Erfolge der betroffenen Patienten bei der Aufrechterhaltung der langfristigen Ergebnisse oft begrenzt. Ein zugrundeliegender Mechanismus, der zu diesem Phänomen beiträgt, ist gemeinhin als Jo-Jo-Effekt" bekannt und wird nach wie vor nur unzureichend verstanden. Um die zugrundeliegende Rolle des adipogenen Potenzials zu untersuchen, führten wir eine Studie an männlichen C57BL/6N-Mäusen durch, in der wir die Entscheidungen über das Zellschicksal, die terminale Differenzierung und die Proliferation von Vorläuferzellen der Adipozyten untersuchten. Die Mäuse wurden zunächst mit einer fettreichen Diät gefüttert, bis sie eine Körpermasse von mindestens 40 g erreichten, gefolgt von einer einwöchigen Kontrolldiät oder einer kalorisch eingeschränkten, paarweise gefütterten fettreichen Diät. Außerdem untersuchten wir die mitochondriale Funktion in den weißen Adipozyten während des Verlusts an Körpermasse und der anschließenden Wiederzunahme, indem wir die männlichen C57BL/6N-Mäuse 24 Wochen lang mit einer fettreichen Diät fütterten, gefolgt von einer achtwöchigen Kontrolldiät, die zu einer Remission der Fettleibigkeit führte, und einer erneuten Fütterung mit einer fettreichen Diät für 12 Wochen.

Die kurzzeitige Erholung von der fettreichen Diät hatte einen signifikanten Einfluss auf das Schicksal der Zellen der stromal-vaskulären Fraktion, wie durch Zellkultur- und Durchflusszytometrie-Experimente festgestellt wurde. Insbesondere konzentrierten wir uns auf drei verschiedene Subpopulationen des weißen Fettgewebes, die durch die Expression von CD55, VAP1 oder CD142 charakterisiert sind und die zu den diät- und fettdepotspezifischen Veränderungen des adipogenen Potenzials beitragen. Durchflusszytometrie und Immunfluoreszenzbildgebung zeigten einen Proliferationsstopp im epididymalen weißen Fettgewebe in der Plateauphase bei 40 g Körpermasse. Nach der vollständigen Reduktion der Fettleibigkeit durch eine Kontrolldiät blieben die Kapazität und der Gehalt der Mitochondrien in den epididymalen Adipozyten reduziert, wie durch hochauflösende Respirometrie und die Aktivität der Zitrat-Synthase festgestellt wurde. Im Gegensatz dazu behielten die Mitochondrien der inguinalen Adipozyten ihre Funktion bei. Die Analyse der Proteinexpression ergab nur geringfügige Auswirkungen auf die Expressionsniveaus von Proteinen, die hauptsächlich zur Differenzierung der Adipozyten, zum Lipidstoffwechsel und zur Entzündung gehören. Die Wiederaufnahme einer fettreichen Diät verdoppelte die Körpermasse und die Zunahme der Fettmasse innerhalb der ersten Wochen nach der Ernährungsumstellung im Vergleich zu Mäusen, die zum ersten Mal eine fettreiche Diät erhielten.

Unsere Ergebnisse unterstreichen die Bedeutung der Spezifität der Fettdepots für die Folgen der metabolischen Adipositas und die damit verbundenen Behandlungen. Wir identifizierten $CD142^+$ adipogenese-regulierende Zellen als reversiblen Silencer der Differenzierungskapazität von Adipozyten-Vorläuferzellen. Darüber hinaus fanden wir heraus, dass die Mitochondrien epididymaler Adipozyten eine anhaltende Einschränkung aufgrund einer fettreichen Ernährung aufweisen, während die Mitochondrien inguinaler Adipozyten widerstandsfähiger sind. Diese Veränderungen treten gleichzeitig auf und sind wahrscheinlich an der Entstehung des "Jo-Jo-Effekts" beteiligt, der durch eine verstärkte Zunahme der Körpermasse bei erneuter fettreicher Ernährung gekennzeichnet ist.

1 Introduction

Obesity has become a worldwide health concern, presenting a challenge for medical research in the areas of prevention and targeted interventions to address the symptoms of the disease. According to the World Health Organization (WHO), in 2016, over 1.9 billion adults were classified as overweight (BMI 25 - 29.9) and over 650 million adults were classified as obese (BMI > 30) (OECD/WHO, 2020). The Western diet, which is characterized by high levels of processed foods, sugar, and saturated fats, has been implicated as a major contributor to the development of obesity (Christ et al., 2019). Obesity is associated with a plethora of comorbidities, including type 2 diabetes, cardiovascular and renal diseases, and certain types of cancer (Kitahara et al., 2014; Kovesdy et al., 2017; Renehan et al., 2008; Xu et al., 2018). These comorbidities are responsible for millions of deaths annually, including an estimated 2.8 million deaths worldwide each year caused by obesity (Ellulu et al., 2014).

The management of obesity is hampered by the lack of effective body mass reduction strategies. While up to 80 % of patients may achieve initial body mass loss through dieting, long-term maintenance of body mass loss is frequently unsuccessful. Instead, recurrent body mass gain and relapsing metabolic complications are commonly observed within 12 months of initial body mass loss, which may even surpass pre-dieting metabolic abnormalities (Anastasiou et al., 2015). This phenomenon, commonly referred to as body mass cycling or ‘yo-yo effect’, highlights the need for improved, evidence-based body mass loss interventions and further investigation into the underlying mechanisms that promote the development of obesity (Dulloo and Montani, 2015).

Obesity is a systemic disease that affects the entire body. However, white adipose tissue (WAT) is crucial for the development of obesity-related comorbidities. Generally, WAT is a highly dynamic and complex multi-depot organ. It is capable of storing and releasing energy from its lipid-laden adipocytes in the form of intracellular triglycerides, resulting in significant morphological changes (Cinti, 2005; Hepler and Gupta, 2017; Rosen and Spiegelman, 2014). However, prolonged periods of positive energy balance can lead to excessive fat mass accumulation, which has been associated with persistent pathologies even after re-establishment of a lean phenotype (Cottam et al., 2022; Droyvold et al., 2005; Nanri et al., 2010). WAT comprises two distinct subtypes, namely subcutaneous and visceral WAT. They are key determinants of the development of 'healthy' or 'unhealthy' obesity in response to excessive caloric intake (Longo et al., 2019). Specifically, in male mice, inguinal WAT (iWAT) is a representative of subcutaneous fat, while epididymal WAT (eWAT) is a representative of visceral fat. The two subtypes of WAT are distinguished by their different origins and intrinsic characteristics, which encompass differential secretion profiles of adipokines, insulin sensitivity, and propensity for inflammation. These distinct features contribute to the functional divergence between iWAT as

an energy reserve and eWAT as a higher risk depot for adverse health outcomes. (Chau et al., 2014; Foster et al., 2013; Macotela et al., 2012; Wajchenberg et al., 2002). Moreover, transplantation experiments have demonstrated that iWAT transplantation to the intra-abdominal space has an inverse association with metabolic risk. These findings highlight the significance of the origin of the WAT rather than its location (Hocking et al., 2008; Hocking et al., 2015; Tran et al., 2008). Furthermore, the behavior of both WAT depots during development and expansion exhibits distinct characteristics detailed in the following section (Spalding et al., 2008; Wang et al., 2013).

1.1 White adipose tissue development and expansion

Adipocytes originate from multipotent, fibroblast-like mesenchymal precursor cells and have the potential to differentiate into osteoblasts, chondroblasts, adipocytes, and myoblasts (Ghaben and Scherer, 2019). These adipocyte progenitor cells (APCs) are located in the perivasculature (Gupta et al., 2012; Schwalie et al., 2018; Tang et al., 2008). The process of forming mature adipocytes is referred to as adipogenesis. It comprises of two distinct stages: 1) determination and 2) differentiation. During the determination stage, mesenchymal stem cells differentiate into preadipocytes, thereby committing to the adipocyte lineage. The differentiation stage is characterized by the activation of peroxisome proliferator-activated receptor-γ (*Pparg*), a master regulator of adipogenesis, which leads to the formation of mature adipocytes that are capable of accumulating lipids (Ghaben and Scherer, 2019).

Childhood is a critical period for adipocyte formation as it mainly determines the number of adipocytes in an individual. Thus, the onset of obesity during childhood has lifelong consequences. Obese children have a higher adipocyte count than their lean counterparts, which increases their capacity for lipid storage and body mass. After adolescence, the total number of fat cells is tightly regulated and WAT primarily expand through an increase in the size of adipocytes (Spalding et al., 2008). In general, tissue expansion can occur through two distinct mechanisms: hyperplasia (increase in cell number) and hypertrophy (increase in cell size) (Jo et al., 2009). Hypertrophy is associated with various pathological conditions such as inflammation, hypoxia, fibrosis, and insulin resistance (Hepler and Gupta, 2017). In adult individuals, adipocytes exposed to a chronic state of positive energy balance will expand in size until they become lipid-overloaded and insulin-resistant. Subsequently, new precursor cells are recruited (Spalding et al., 2008). It has been proposed that hyperplasia is the primary contributor to the expansion of visceral WAT in humans (Arner et al., 2013). This phenomenon has also been observed in rodent models. Particularly, in adult mice, iWAT exhibits primarily hypertrophy and limited adipogenesis in response to high-fat diet (HFD) feeding, whereas eWAT experiences hypertrophy only during the initial phase of HFD feeding (Kim et al., 2014; Wang et al., 2013).

C57BL6/J mice fed HFD for 60 days displayed an average increase in adipocyte diameter of 17 % in iWAT compared to 65 % in eWAT. These results indicate that eWAT mostly expanded through the mechanism of hypertrophy during the initial phase of tissue expansion (Joe et al., 2009). However, after this initial hypertrophic expansion period of eWAT, hyperplasia occurs (Kim et al., 2014; Wang et al., 2013). Concerning body mass regain, it has been reported that the number of adipocytes increased by 30 % additionally during the relapse period (HFD refeeding) (MacLean et al., 2006). As a result of prolonged HFD feeding and during the relapse period, the number of adipocytes increases. This can ultimately shift the balance from available lipid storage to excess storage of lipids that are diverted from oxidation. This process can favor body mass regain. (Kim et al., 2014; MacLean et al., 2006; Wang et al., 2013). Additionally, a positive correlation between adipocyte turnover and insulin sensitivity has been observed in both humans and mice (Guillermier et al., 2017; Kim et al., 2014).

An essential aspect of the expansion of WAT and the distinction between iWAT and eWAT is the emergence of an expansion plateau in eWAT in adult C57BL6/J mice. Upon reaching a body mass of approximately 40 g, the eWAT depot does not further expand in mass and size, while the iWAT continues to increase proportionally to body mass (van Beek et al., 2015). These observations are consistent with increased adipogenesis in eWAT following prolonged HFD feeding. Obesity activates pro-apoptotic signals that result in enhanced adipocyte death in eWAT, and an expansion plateau is reached despite increased adipogenesis (Alkhouri et al., 2010; Kim et al., 2014). Additionally, the physiological process associated with eWAT expansion leads to significant immune cell infiltration into the fat depot, resulting in the formation of crown-like structures around dying adipocytes (Alkhouri et al., 2010; van Beek et al., 2015). Body mass loss cannot reverse the pro-inflammatory signals that persist within eWAT, promoting the development of metabolic syndrome upon regained body mass (Fischer et al., 2018). The phenomenon of eWAT reaching a plateau may cause nutritional programming of adipogenic potential within progenitor cells from eWAT, resulting in a decline of the adipogenic potential of APCs (consistently observed in our laboratory; unpublished data). This may be attributed to the depletion of the APCs pool or silencing of them during HFD feeding. Accordingly, nutritional programming of adipogenic potential within APCs during the body mass loss phase may promote hyperplasia in eWAT and contribute to the propensity for regained body mass. In conclusion, APCs appear to play a vital role in the development and expansion of WAT.

1.2 The importance of primary adipocytes subpopulations

The majority of cells within WAT belongs to the stromal-vascular fraction (SVF), which is largely composed of blood cells, endothelial cells, fibroblasts, pericytes, preadipocytes, macrophages,

and other immune cells (Sarjeant and Stephens, 2012). The highly heterogeneous cellular composition of SVF cells without apparent macrostructure is characteristic for WAT (Cristancho and Lazar, 2011). Mature adipocytes constitute over 80 % of WAT mass; on the cellular level, however, WAT is composed of only one-third mature adipocytes (Tsiloulis and Watt, 2015). The numerous different cell types of the SVF cells need to be a highly coordinated to result in a proper WAT expansion (Sun et al., 2011). According to several studies, increase of infiltration with immune cells (Fischer et al., 2018; van Beek et al., 2015) and changes in the abundance and expression patterns of distinct cell subpopulations is observed during the development of obesity (Burl et al., 2018; Cho et al., 2019; Emont et al., 2022; Hepler et al., 2018; Merrick et al., 2019; Sarvari et al., 2021; Schwalie et al., 2018). APCs and their development and fate decision appear to play an important role that is not yet fully understood. The study of distinct subpopulations of adipose stem and precursor cells within the SVF has only been possible in recent years through the application of single-cell ribonucleic acid (RNA) sequencing (Kolodziejczyk et al., 2015). Recent research has focused on the characterization of $CD142^+$ adipogenesis-regulatory cells (Aregs) as committed preadipocytes and inhibitors of adipogenesis (Merrick et al., 2019; Schwalie et al., 2018).

Depending on the approach used, biological and technical variances can be observed. These discrepancies lead to the identification of distinct subpopulations of APCs, immune cells, fibro-inflammatory cells, mesothelial-like cells, and Aregs in both mice and humans in various studies (Burl et al., 2018; Cho et al., 2019; Emont et al., 2022; Hepler et al., 2018; Merrick et al., 2019; Sarvari et al., 2021; Schwalie et al., 2018). Despite these variances, an overall match between subpopulations has been detected by overlapping the results of different studies (Cho et al., 2019; Emont et al., 2022; Merrick et al., 2019; Sarvari et al., 2021). Specific markers for adipogenic stem and precursor cells are used to characterize subpopulations of SVF cells, and their unique expression patterns are verified using fluorescence-activated cell sorting (FACS). Based on the work of Schwalie *et al*. and Merrick *et al*., three main clusters are defined, which show high expression of the adipogenic stem and precursor cell markers *Cd34* and *Ly6a* (encoding stem cells antigen 1 (SCA1)) (Merrick et al., 2019; Schwalie et al., 2018). Cluster 1 is identified as the population of adipogenic stem cells, characterized by the expression of $CD55^+$ (Schwalie et al., 2018). This cluster corresponds to the $DPP4^+$ (dipeptidyl peptidase-4 (DPP4)) interstitial progenitor cell subpopulation, which expresses *Dpp4*, *Wnt2*, *Bmp7*, and *Pi16*, but not adipocyte markers (Merrick et al., 2019). Cluster 2 represents the $VAP1^+$ (vascular adhesion protein 1 (VAP1)) pre-adipogenic specific cell subpopulation, characterized by the expression of *Aoc3* (encoding VAP1) (Schwalie et al., 2018). This cluster is similar to the $ICAM1^+$ (intercellular adhesion molecule–1 (ICAM1)) cell population, expressing the preadipocyte marker *Pref1* and several adipocyte markers such as *Pparg*, *Fabp4*, and *Cd36* (Merrick et al.,

2019). Cluster 3 is defined as the CD142$^+$ subpopulation, expressing genes such as *F3* (encoding CD142), *Clec11a*, and *Fmo2* (Merrick et al., 2019; Schwalie et al., 2018). The role of the CD142$^+$ subpopulation in adipogenesis is controversial. While some studies suggest that CD142$^+$ cells inhibit adipogenesis both *in vivo* and *in vitro*, others propose that they can differentiate into mature adipocytes. These discrepancies may be attributed to different FACS strategies employed for cell purification and the age of mice used in the studies (Merrick et al., 2019; Schwalie et al., 2018). In particular, Schwalie *et al*. find that CD142$^+$ cells inhibit adipogenesis in adult mice, as demonstrated by reduced differentiation of preadipocytes to lipid-laden adipocytes in *ex vivo* cell culture experiments. Furthermore, they transplant Matrigel plugs containing or lacking Aregs into mice and show that Aregs reduced the development of mature adipocytes within the transplanted Matrigel plugs in comparison to the Areg-depleted Matrigel plugs. (Schwalie et al., 2018). Transcriptomic data confirm that Aregs have a non-adipogenic nature since the genes related to adipogenesis, such as *Pparg*, *Fasn*, *Fabp4*, *Lpl*, and *Fabp12*, are significantly reduced in these cells (Rosen and Spiegelman, 2014; Schwalie et al., 2018). However, transplantation experiments performed by Merrick *et al.* on 10-day-old mice demonstrate an interconversion of CD142$^+$ cells into ICAM1$^+$ cells. Furthermore, no inhibition of adipogenesis is observed in postnatal mice both *in vivo* and *in vitro* (Merrick et al., 2019). In summary, Aregs can be identified as CD142$^+$ cells within the lineage-negative/SCA1$^+$ (Lin$^-$/SCA1$^+$) SVF cells, and they seem to exert an inhibitory effect on the adipogenesis of APCs in adult mice. Furthermore, the developmental trajectory of CD55$^+$ adipocyte stem cells and VAP1$^+$ preadipocytes is gaining attention as a promising tool to gain new insights into adipocyte development.

Recent studies on the adipose tissue of iWAT and eWAT have demonstrated distinct subpopulation compositions and alterations associated with obesity. The frequency of the CD142$^+$ subpopulation is significantly elevated in eWAT of obese mice (Merrick et al., 2019; Schwalie et al., 2018). However, iWAT of diet-induced obese mice does not show an increase in the CD142$^+$ frequency (Merrick et al., 2019). In a recent study, gene expression patterns of eWAT in lean and obese adult mice reveals significant changes in subpopulation expression associated with obesity. Specifically, the VAP1$^+$ comparable subpopulations exhibit a decrease in the expression of genes involved in *de novo* lipogenesis, such as *Fasn* and *Acaca*, while general adipocyte markers, such as *Pparg*, *Lpl*, and *Fabp4*, remain unchanged. Intriguingly, the CD142$^+$ population demonstrates a reduction in the expression of adipogenesis inhibitors, including *Ar*, *Sox9*, and *Pdgfra*. Furthermore, this study supports a transition from CD142$^+$ cells (early preadipocytes expressing adipocyte marker genes at low levels) to VAP1$^+$ cells (late preadipocytes) (Sarvari et al., 2021). Additionally, recent studies have failed to prove an increase of the CD142$^+$ subpopulation in eWAT upon HFD feeding (Emont et al., 2022; Sarvari et al., 2021). These findings raise questions about the role of CD142$^+$ cells in adipogenesis

and nutritional programming. Further research is required to gain a better understanding of the role of $CD142^+$ cells in obesity. This research should include a comparison with previous findings that indicated reduced adipogenic potential in APCs after prolonged HFD feeding (unpublished data). Furthermore, it is essential to investigate the effect of APCs on mitochondria in less differentiated mature adipocytes (Schottl et al., 2015a; Schottl et al., 2015b). Overall, during obesity, the eWAT is more prone to alterations in distinct SVF cell subpopulations and mitochondrial function than to the obesity-resilient iWAT.

1.3 Effects of obesity on mitochondria

Mitochondrial integrity is a crucial aspect of adipocyte physiology. The main function of mitochondria is to produce adenosine triphosphate (ATP), the primary energy source for the cell, through the oxidative phosphorylation (OXPHOS). In addition, mitochondria play a vital role in generating and neutralizing reactive oxygen species (ROS). They are essential in regulating apoptotic cell death, controlling intracellular calcium levels, synthesizing iron-sulfur clusters, and metabolite turnover (Brand and Nicholls, 2011; Stehling et al., 2014). Mitochondria in WAT are also involved in several processes such as lipogenesis, lipolysis, secretion of adipokines, and differentiation of adipocytes (De Pauw et al., 2009; Koh et al., 2007).

Recent studies in rodent models have consistently demonstrated a reduction of mitochondrial integrity, content, and protein levels during obesity and type 2 diabetes (Fischer et al., 2015; Heinonen et al., 2017; Kusminski and Scherer, 2012; Mustelin et al., 2008; Schottl et al., 2015b; Schottl et al., 2020; Wessels et al., 2019). Collectively, these changes have been described as mitochondrial dysfunction and are implicated in the development of inflammation and insulin resistance in WAT (Woo et al., 2019). Notably, eWAT appears to be more susceptible to these negative effects of obesity on mitochondrial bioenergetics and inflammation compared to iWAT (Giordano et al., 2013; Gonzalez-Franquesa et al., 2022; Schmitz et al., 2016; Schottl et al., 2015b). Furthermore, the immunometabolic crosstalk between adipocytes and macrophages is compromised in the eWAT of obese mice. HFD feeding reduces the expression of heparin sulfates on WAT macrophages, resulting in reduced mitochondrial transfer from adipocytes to macrophages. This, in turn, affects metabolic homeostasis and leads to a persistent immune response (Brestoff et al., 2021; Schmitz et al., 2016). Indeed, experimental disruptions in mitochondrial gene homeostasis compromise WAT size, metabolism, and mitochondrial structure (Gonzalez-Franquesa et al., 2022; Kusminski et al., 2012; Vernochet et al., 2012). In line, perturbing mitochondrial fission and fusion results in decreased mitochondrial bioenergetics in obese WAT (Tol et al., 2016). Long-term consumption of HFD has been shown to have particularly negative effects on epididymal mitochondria, which cannot be reverted by

short-term low-fat control diet (CD) interventions (Schottl et al., 2015b). Furthermore, the abundance of mitochondrial membrane proteins is strongly downregulated upon HFD consumption, which particularly affects OXPHOS processes (Schottl et al., 2020). Thereby, a functional complex I and a proper ROS production at complex III are also required for the adipocyte differentiation (Lu et al., 2010; Tormos et al., 2011).

Depending on their persistence, the phenomena described above are assumed to play a role in body mass cycling. The underlying mechanisms remain largely unknown, but persistent alterations may contribute to poor long-term outcomes (Anderson et al., 2001; Freedhoff and Hall, 2016; Wing and Hill, 2001). Defining standard thresholds for body mass cycling is still lacking, and the level of susceptibility to additional body mass gain as a result of body mass cycling remains controversial (Cutter et al., 1996; National, 1994). Studies investigating body mass cycling in athletes and identical twins with at least one episode of body mass loss have demonstrated a negative impact on body mass compared to non-athletes or non-dieting co-twins (Pietilainen et al., 2012; Saarni et al., 2006). Additionally, twin studies have revealed a downregulation of mitochondrial transcripts and expression of mitochondrial OXPHOS proteins in obese compared to non-obese co-twins (Heinonen et al., 2017; Mustelin et al., 2008). The potential underlying mechanisms are multifaceted, but evidence in both mice and humans supports the role of mitochondria in the context of body mass cycling (Heinonen et al., 2017; Kusminski and Scherer, 2012; Mustelin et al., 2008; Schottl et al., 2015b; Schottl et al., 2020; Wessels et al., 2019), rather than just the re-partitioning of lean mass and fat mass (Dulloo, 2021; Keys et al., 1950; Pasquet and Apfelbaum, 1994; Pasquet et al., 1992). These findings underscore the importance of further investigating the role of mitochondria in body mass cycling.

1.4 Research objectives

This thesis investigated the underlying mechanisms of obesity-related WAT adaptations and their associated health risks by exploring the concept of nutritional programming. Despite considerable research on the central regulation and metabolism of obesity, the impact of nutritional programming on the growth and metabolism of WAT during body mass cycling remains incomplete (MacLean et al., 2015; MacLean et al., 2006). The primary focus of this thesis was to examine the effects of various diet-induced changes on adipose tissue function in the homeostatic control of body mass. As body mass is gained, lost, and regained during body mass cycling, the entire WAT depot must adapt to the fluctuations in stored energy (Lee et al., 2010). The recurrent body mass fluctuations may render adipose tissue more susceptible to increased uptake and storage of ingested energy, leading to metabolic complications. We hypothesized

that nutritional programming of the adipogenic potential of progenitor cells and the mitochondrial functionality in mature adipocytes exacerbated body mass regain and intensified metabolic aberrations after re-exposure to an obesogenic diet. Furthermore, we proposed that nutritional programming played a critical role in these metabolic adaptations of adipose tissue via caloric density and macronutrient composition of diets. We tested two mechanism-based hypotheses of how nutritional programming affected adipose tissue metabolism in response to HFD feeding and body mass loss:

1) HFD feeding altered the adipogenic potential of APCs, thereby limiting the expandability of the intra-abdominal eWAT depot.
2) HFD feeding induced long-term deficiencies in mitochondrial function of mature adipocytes, independent of body mass and adiposity.

To investigate the adipogenic potential, we evaluated the effects of HFD and short-term diet-induced obesity reduction on SVF cell proliferation in mice. We determined if HFD-induced changes in progenitor cell proliferation were reversible by low-fat diet or calorie-restricted pair-fed (pf) HFD feeding. In addition, we investigated whether HFD resulted in a depletion or silencing of the progenitor cell pool. To examine the effects of HFD on mitochondrial function, we studied the long-term effects of HFD feeding on adipocyte mitochondrial function after a full recovery from obesity. We assessed whether HFD-induced changes in mitochondrial function were persistent and could increase propensity to obesity and represent a novel mechanism of nutritional programming.

This thesis investigated the cellular composition of SVF cells in obese mice, and for the first time, we demonstrated that a reversible reduction in adipogenic potential occurred at the level of adipogenic stem and precursor cells. However, we did not observe an improvement in HFD-induced mitochondrial function and abundance, even after full remission from obesity. Taken together, the rapid recovery of adipogenic potential combined with the persistent reduction in mitochondrial function may promote body mass regain in mice.

2 Material and Methods

A detailed list of chemicals, consumables, and equipment used can be found in the appendix. Relevant materials are mentioned in the methods section.

2.1 Animals

All male wild-type C57BL/6N mice were bred in a specific-pathogen-free animal facility at the Technical University of Munich registered at the local authorities according to §11 of the German Animal Welfare Act (AZ32-568, 01/22/2015). The mice were housed in groups of 2 – 3 in individual ventilated cages at an ambient temperature of 23 °C ± 1 °C on a 12/12 hour (h) light/dark cycle (5:00 am/pm CET) with *ad libitum* access to water and food.

All animal experiments were conducted in accordance with German animal welfare law and with the permission of the Government of Upper Bavaria (Regierung von Oberbayern, reference number Az. ROB-55.2.1.54-2532.Vet_02-19-84). At 8 weeks of age, male mice were switched from chow diet (Ssniff, V1124-3M-Z) to a purified research control diet (CD, 12 kJ% fat, Ssniff, SS745-E702, **Table 1**) and assigned to experimental groups. At 12 weeks of age, non-control mice were switched to a high-fat diet (HFD, 48 kJ% fat, Ssniff, SS745-E712, **Table 1**).

Table 1: Nutrient composition of diets.

	CD	**HFD**
Metabolized energy [MJ/kg]	**15.3**	**19.7**
Protein [MJ%]	23	18
Fat [MJ%]	13	48
Carbohydrate [MJ%]	64	34
Total protein [g/kg]	**240**	**240**
Casein	240	240
Total fat [g/kg]	**50**	**250**
Soybean oil	50	50
Palm oil	-	200
Total carbohydrate [g/kg]	**634**	**434**
Corn starch	478	278
Maltodextrin	56	56
Sucrose	50	50
Cellulose	50	50

Other [g/kg]	**76**	**76**
L-cystine	2	2
Choline chloride	2	2
Vitamins	12	12
Minerals	60	60

2.1.1 Animal experimentation protocol for studying the adipogenic potential of primary adipocytes

It was previously demonstrated that the epididymal white adipose tissue (eWAT) of male C57BL mice reaches a plateau in mass expansion at a body mass of 40 g (van Beek et al., 2015). To investigate the effect of reduced mass expansion on primary adipocytes, mice were fed HFD until they reached a body mass greater than 40 g. Based on their assigned experimental group (**Figure 1**), the diet was switched to CD one week before the end of the experiment for the HFD-CD group. The mice in the HFD-pfHFD group were pair-fed (pf) with HFD one week before the end of the experiment. They received the same caloric intake as the average caloric intake of the experimental mice in the HFD-CD group receiving CD for one week.

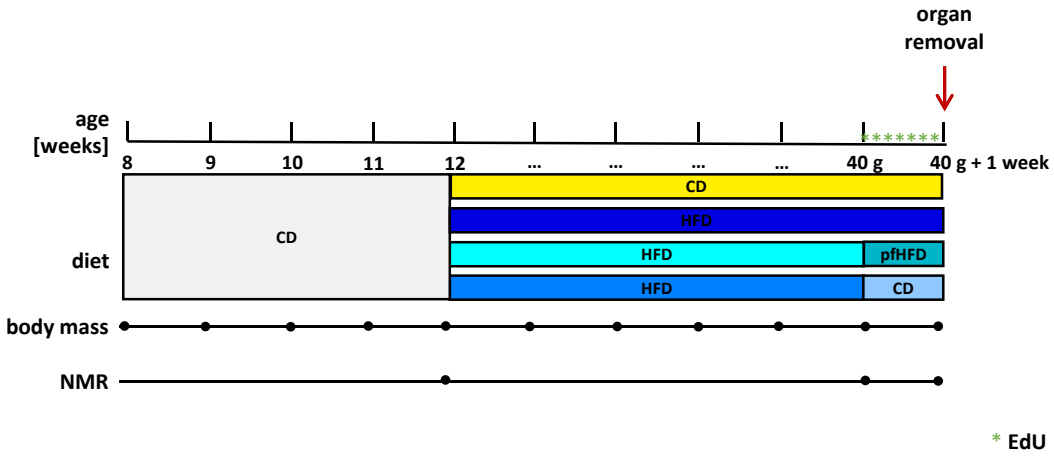

Figure 1: Overview of animal experimentation protocol for studying the adipogenic potential of primary adipocytes. Mice were fed a chow diet until the age of 8 weeks, followed by a control diet (CD) for 4 weeks. Mice in the high-fat diet (HFD) group were fed a HFD until they reached a minimum body mass of 40 g before their diet was switched to either CD or pair-fed (pf) HFD for one week in the HFD-CD and HFD-pfHFD groups. A subset of mice were injected with 5-ethynyl-2'-deoxyuridine (EdU) during the last seven days of the experiment.

Unless stated otherwise, body mass was determined weekly until the end of the experiment. Body composition was analyzed using nuclear magnetic resonance spectroscopy (The Minispec mq7.5, Bruker BioSpin GmbH) at 12 weeks of age, seven days before death, and at day of death.

To investigate the proliferation of stromal-vascular fraction (SVF) cells, mice were injected intraperitoneally with 20 mg/kg 5-ethynyl-2'-deoxyuridine (EdU) for seven days until death (* = injection, **Figure 1**). Body mass was determined daily.

2.1.2 Animal experimentation protocol for investigating the mitochondrial capacity of mature adipocytes

To examine the persistent effects of obesity after complete remission from obesity, mice were fed either CD or HFD for 24 weeks (**Figure 2**). After this period, the HFD-CD group (CD remission group) and the HFD-CD-HFD group (HFD refeeding group) received CD for eight weeks, while the CD groups and the HFD group stayed on their previous diet. The remaining CD mice and the HFD-CD-HFD group were fed HFD for 12 weeks. Subsequently, all mice were killed and dissected.

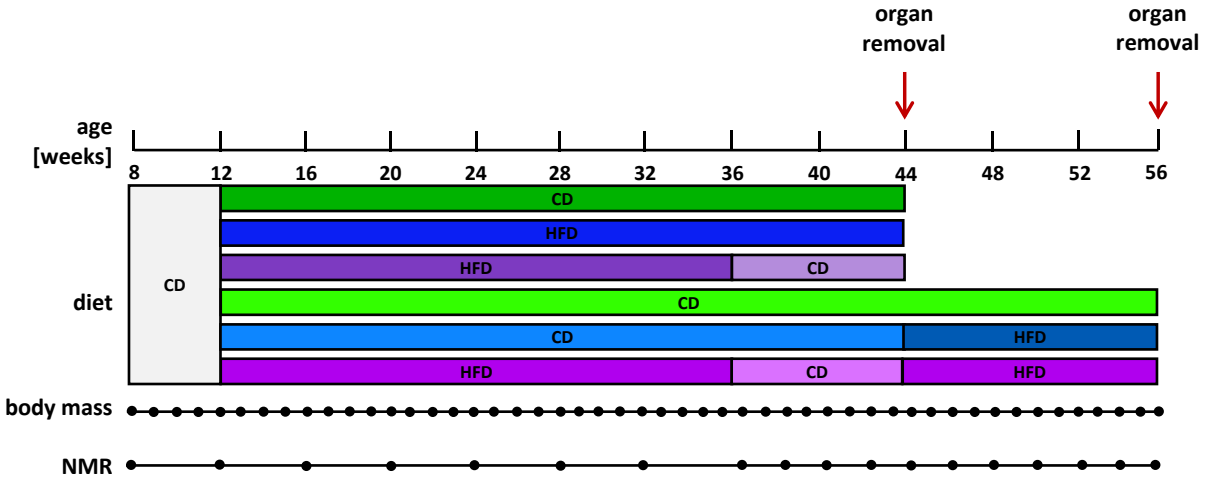

Figure 2: Overview of animal experimentation protocol for examining the mitochondrial capacity of mature adipocytes. The mice were initially fed a chow diet until they reached 8 weeks of age, after which they were fed a control diet (CD) for 4 weeks. Subsequently, the high-fat diet (HFD) groups were fed a HFD for either 24 weeks (HFD-CD and HFD-CD-HFD groups) or 32 weeks (HFD group), followed by CD feeding in the HFD-CD and HFD-CD-HFD groups for 8 weeks. The HFD-CD-HFD and CD-HFD groups were subsequently (re)fed with HFD for 12 weeks.

Body mass was determined weekly until the end of the experiment. Body composition was analyzed using nuclear magnetic resonance spectroscopy every four weeks from 12 to 36 weeks of age, followed by biweekly measurements until the end of the experiment.

2.2 Histology of murine white adipose tissue

Mice were killed by cervical dislocation and sampled eWAT and iWAT were weighed and incubated for 72 h in 4 % (v/v) formaldehyde at room temperature. Afterward, tissues were transferred to 70 % (v/v) ethanol (EtOH) until they were dehydrated. Tissues were automatically

dehydrated for 12 h using sequential 60 minutes (min) units per solvent (70 % (v/v) EtOH, 70 % (v/v) EtOH, 80 % (v/v) EtOH, 96 % (v/v) EtOH, 96 % (v/v) EtOH, 96 % (v/v) EtOH, 100 % (v/v) EtOH, 100 % (v/v) EtOH, 100 % (v/v) EtOH, 100 % (v/v) Xylene, 100 % (v/v) Xylene, 100 % (v/v) Paraffin, 100 % (v/v) Paraffin) in a tissue processing machine (Leica TP1020). Tissues were then embedded in paraffin using a Leica EG1150C embedding machine and stored at room temperature until further processing.

The embedded WAT was sliced into 5 µm thick slices using a Leica RM2255 microtome for Hematoxylin & Eosin (HE) staining. The slices were placed in a 37 °C water bath until the wrinkles smoothened out, then transferred to Superfrost® microscope slides and dried for a minimum of 12 h. Before the staining procedure, the slides were deparaffinized by pretreatment in a heating chamber for 20 min at 60 °C. Next, the slides were placed in a Leica ST5020 Multistainer and stained using the HE staining program (**Table 2**) before being mounted using mounting medium and coverslips.

Table 2: HE staining program.

Step	Solution	Duration [min]
1	Xylene	3
2	Xylene	3
3	100 % (v/v) EtOH	2
4	96 % (v/v) EtOH	2
5	70 % (v/v) EtOH	1
6	ddH_2O	1
7	Hematoxylin	4
8	Tap water	2
9	Eosin	2
10	70 % (v/v) EtOH	1
11	96 % (v/v) EtOH	1
12	100 % (v/v) EtOH	1
13	100 % (v/v) EtOH	1.5
14	Xylene/Alcohol	1.5
15	Xylene	1
16	Xylene	2

After drying and cleaning of the mounted slides, pictures were taken at 20x magnification using a microscope equipped with a scanner (M8, PreciPoint) and ViewPoint software (Version 1.0.0.8712, PreciPoint). The analysis of adipocyte diameter and number was performed using the ImageJ plugin Adiposoft. To do this, the pictures were divided into randomly chosen sec-

tions with the same zoom (60x) covering approximately 1/3 of each slide in total. The parameters "Auto mode" and "Exclude on edges" were selected. The Adiposoft output was converted from pixel to unit µm. The "Minimum diameter" was set to 3 µm and the "Maximum diameter" to 150 µm. The mean adipocyte diameter and mean adipocyte number was each calculated per tissue and mouse.

2.3 Isolation of murine stromal-vascular fraction cells

Mice were killed by cervical dislocation for cell culture and flow cytometry experiments with unfixed cells. For experiments with EdU-injected mice, the mice were killed by CO_2 asphyxiation in a closed tank, followed by a cut through the diaphragm. The EdU-injected mice were then perfused with 50 ml of phosphate-buffered saline (PBS). iWAT and eWAT were collected, weighed, and stored in PBS (with antibiotics for cell culture experiments) separately until the isolation of SVF cells started. For cell culture experiments, SVF cells from three individual mice per feeding regime were pooled in one experiment, with SVF cells from 1.5 mice isolated together in the same tube.

Prior to experimentation, PBS with antibiotics, wash medium, isolation medium, and culture medium were prepared for cell culture experiments. For flow cytometry experiments, isolation medium, red blood cell lysis buffer, culture medium, and fluorescence-activated cell sorting (FACS) buffer were also prepared (**Table 3**). Wash medium, isolation medium, red blood cell lysis buffer, and culture medium were pre-warmed to 37 °C.

Table 3: Media and buffer composition for SVF cell isolation.

Solution	Reagent	Stock Concentration	Final Concentration
PBS with antibiotics	PBS	n/a	n/a
	Gentamycin	10 mg/ml	40 µg/ml
	Penicillin/Streptomycin	10000 units/ml, 10 mg/ml	40 units/ml, 40 µg/ml
*Isolation medium**	1x HBSS w/o Mg^{2+} and Ca^{2+}	n/a	n/a
	Albumin Fraction V	n/a	3.5 % (w/v)
	Glucose	n/a	0.55 mM
	Collagenase Type I	n/a	1 mg/ml
	Gentamycin	10 mg/ml	40 µg/ml
	Penicillin/Streptomycin	10000 units/ml, 10 mg/ml	40 units/ml, 40 µg/ml

	Amphotericin B	250 µg/ml	500 ng/ml
*Wash medium**	1x HBSS w/o Mg^{2+} and Ca^{2+}	n/a	n/a
	Albumin Fraction V	n/a	3.5 % (w/v)
Culture medium	DMEM high glucose	n/a	n/a
	FBS	n/a	20 % (v/v) (cell culture) 10 % (v/v) (flow cytometry)
	Gentamycin	10 mg/ml	40 µg/ml
	Penicillin/Streptomycin	10000 units/ml, 10 mg/ml	40 units/ml, 40 µg/ml
Red blood cell lysis buffer,***	ddH_2O	n/a	n/a
	K_2HPO_4	n/a	10 mM
	EDTA	500 mM	0.1 mM
	NH_4Cl	n/a	154 mM
*FACS buffer**	PBS	n/a	n/a
	FBS	n/a	3 % (v/v)
	Penicillin/Streptomycin	10000 units/ml, 10 mg/ml	1 % (v/v)
	EDTA	500 mM	1 mM

*Solutions were sterilize using a 0.22 µm filter.

**Solution adjust to pH 7.3.

The dissected tissue was minced with approximately 6 ml collagenase-containing isolation medium in a 15 ml tube using surgical scissors. Afterward, iWAT was digested for 80 min and eWAT for 40 min at 37 °C with continuous vortex mixing (120 rpm) and intermittent shaking (300 rpm for one minute every 10 minutes). After complete digestion, the cell suspension was filtered through a 250 µm pore-size nylon mesh into a new tube. The nylon mesh was washed with 6 ml of wash medium (cell culture experiment) or 6 ml of culture medium (flow cytometer experiment) to stop collagenase activity. SVF cells were centrifuged at 250 g for 5 min, followed by vigorously shaking and a second centrifugation step to fully separate SVF cells from primary adipocytes. The floating fraction, composted of mature adipocytes, was discarded. The pellet containing the SVF cells was resuspended in 2 ml of red blood cell lysis buffer and incubated for 5 min at room temperature for flow cytometry experiments. Following the incubation period, the cells were passed through a 40 µM pore-size cell strainer in a 50 ml tube before adjusting

the volume with ice-cold FACS buffer to a final volume of 10 ml. The cells were centrifuged at 500 g for 5 min, and the supernatant was aspirated. The pellet was resuspended with 1 ml of culture medium for cell culture experiments or 2 ml of FACS buffer for flow cytometry experiments.

2.4 Cell culture of murine white stromal-vascular fraction cells

For *in vitro* cell culture experiments, SVF cells isolated from iWAT and eWAT were used. The appropriate medium (**Table 4**) was freshly prepared and pre-warmed to 37 °C. To ensure equivalent cell seeding for the four dietary groups per experiment, the adenosine triphosphate (ATP) concentration was utilized as a surrogate marker for cell number. For this purpose, the CellTiter-Glo® Luminescent Cell Viability Assay (Promega) was applied. Reagents were prepared as stated in the protocol of the manufacture. 50 µl of CellTiter-Glo® Reagent was added to 50 µl of 1:4 diluted cells (total dilution 1:8). The mixture was mixed with an orbital shaker at 120 rpm for 2 min in the dark at room temperature. Afterward, the tube contents were vortexed, and the luminescent signal was immediately quantified (delay time: 10 seconds (sec), integration time: 1 sec, per tube) using a luminometer FB12 (Berthold Detection Systems).

Following the determination of cell numbers via ATP measurement, the remaining cells were centrifuged at 500 g for 5 min and the supernatant was aspirated. Then, the cell pellet was resuspended in the appropriate volume of culture medium. Equal cell numbers were seeded into two 12-well cell culture plates (with equivalent ATP concentrations for all four dietary groups of one experiment/replicate). Cell attachment to the plates occurred within 3 – 4 h. The media was removed from the wells, and the cells were rinsed with pre-warmed PBS. PBS was aspirated, and fresh culture medium was added to the wells. The culture medium was replaced approximately 14 – 16 h later, and subsequently every 24 h until confluence was reached. Upon reaching confluence within one to three days, the differentiation was induced with induction medium for 48 h and continued for the following six days with differentiation medium that was changed every 48 h. Images were taken at the end of the experiment.

Table 4: Media composition for cell culture experiments.

Media	Reagent	Stock Concentration	Final Concentration
Culture medium	DMEM high glucose	n/a	n/a
	FBS	n/a	20 % (v/v)
	Gentamycin	10 mg/ml	40 µg/ml
	Penicillin/Streptomycin	10000 units/ml, 10 mg/ml	40 units/ml, 40 µg/ml

Induction medium	DMEM high glucose	n/a	n/a
	FBS	n/a	10 % (v/v)
	Gentamycin	10 mg/ml	40 µg/ml
	Penicillin/Streptomycin	10000 units/ml, 10 mg/ml	40 units/ml, 40 µg/ml
	Insulin	10 mg/ml	850 nM
	T3	n/a	1 nM
	Isobutylmethylxanthine	n/a	500 µM
	Indometacin	n/a	125 µM
	Dexamethason	n/a	1 µM
	Rosiglitazone	n/a	1 µM
Differentiation medium	DMEM high glucose	n/a	n/a
	FBS	n/a	10 % (v/v)
	Gentamycin	10 mg/ml	40 µg/ml
	Penicillin/Streptomycin	10000 units/ml, 10 mg/ml	40 units/ml, 40 µg/ml
	Insulin	10 mg/ml	850 nM
	T3	n/a	1 nM
	Rosiglitazone	n/a	1 µM

2.5 Lipid droplet staining and quantification

The degree of differentiation of intracellular neutral lipids (lipid droplets) was visualized at the end of the *in vitro* culture experiment through staining with Oil Red O (Sigma-Aldrich). To prepare the staining solution, a 0.5 % (w/v) concentrated Oil Red O stock solution was prepared in 100 % (v/v) isopropanol. After proper mixing, the solution was allowed to rest for 20 min before being filtered through a 0.45 µm filter. For staining, the cells were washed twice in their cell culture plate with PBS and then fixed with 3.7 % (v/v) formaldehyde for 1 h. A working solution was generated by mixing 3 parts of the Oil Red O stock solution with 2 parts deionized water (dH_2O) and filtering the mixture through a 0.22 µm filter. Afterward, the fixed cells were rinsed twice with dH_2O and incubated for 5 min in 60 % (v/v) isopropanol. Isopropanol was removed, and the cells were incubated for 1 h with 1 ml of the Oil Red O working solution per cell culture well. After two rinsing steps with dH_2O, the stained lipid droplets were recorded using a light microscope (Olympus FluoView FV10i) with bright-field (20X magnification).

To determine the number and distribution of lipid droplets (mean area [μm^2]) in fully differentiated adipocyte cultures, bright-field images (20X magnification) of unstained lipid droplets were acquired using a light microscope (Olympus FluoView FV10i).These images were automatically analyzed through the use of a validated pattern recognition algorithm for lipid droplets (WimLipid) on the image analysis platform Wimasis (Onimagin Technologies).

2.6 Total RNA isolation of murine white adipose tissue and cultured adipocytes

Total ribonucleic acid (RNA) was isolated from tissue or cell homogenates using the SV Total RNA Isolation System (Promega) modified for use with fat rich samples. Solutions and reagents were prepared according to the instructions of the manufacturer. To do so, tissue samples were snap-frozen with liquid nitrogen and ground into tissue powder using a mortar and pestle. Approximately 100 mg of the resulting powder was transferred to a 5 ml tube with 1 ml of TRIsure (BioLine) and homogenized using an Ultra-Turrax D-1 disperser (Miccra GmbH) for ~20 sec. For the preparation of a homogenate from adherent cells in culture, media was removed and the cells were washed once with PBS. After aspirating PBS, the cells were scraped by pipetting and scratching from the plate and lysed in TRIsure (400 µl/well for a 12-well cell culture plate). The tissue or cell homogenate was further incubated for 5 min at room temperature with TRIsure. Afterward, the cells were centrifuged at 2500 g for 5 min and 4 °C. The fraction without the formed pellet or floating fat layer was transferred to a fresh tube containing chloroform in a TRIsure:chloroform ratio of 5:1. The mixture was thoroughly shaken by hand for 15 sec, incubated for 2 min at room temperature, and centrifuged at 12,000 g for 15 min and 4 °C. The sample separated into a pale greenish phenol-chloroform phase, a whitish interphase with proteins and deoxyribonucleic acid (DNA), and a colorless watery phase on top that contained the RNA. The RNA fraction was mixed with 500 µl of 75 % (v/v) EtOH in diethylpyrocarbonate (DEPC) water (tissue homogenate) or 200 µl of 75 % (v/v) EtOH in DEPC water (cell culture homogenate). 700 µl of the prepared sample was added to a spin column provided in the kit system, centrifuged at 8000 g for 15 sec at room temperature. The flow-through was discarded and the remaining sample was added onto the same column. After centrifugation (centrifugation 12000 g, 1 min), the columns with attached RNA were transferred to fresh tubes and washed with 600 µl of EtOH-containing RNA-Wash-Solution (centrifugation 12000 g, 1min). On-column DNA-digestion was performed for 15 min at room temperature with a DNase-mix prepared according to the kit protocol (40 µl Yellow Core Buffer, 5 µl $MnCl_2$, and 5 µl DNase I per sample). Afterward, the column was washed with 200 µl of DNase Stop Solution (centrifugation 12000 g, 1 min), 600 µl of EtOH-containing RNA-Wash-Solution (centrif-

ugation 12000 g, 1 min), and a second time with 250 µl of ethanol-containing RNA-Wash-Solution (centrifugation 12000 g, 2 min). All flow-throughs were discarded. RNA was eluted with nuclease free water into a fresh tube. For tissue samples, 50 µl of nuclease-free water was directly added to the column and those tubes were centrifuged at 12000 g for 1 min. For cell culture samples, 30 µl of nuclease-free water was directly added to the column and incubated for 10 min at room temperature before centrifugation at 12000 g for 1 min. For higher RNA yields, the eluate was added to the column again and centrifuged at 12000 g for 1 min. The final concentration of purified RNA samples was determined spectrophotometrically using a TECAN InfiniteM2000 NanoQuant (Tecan Group Ltd.). RNA samples were stored at – 80 °C for future analyses.

2.7 Gene expression

Reverse transcription of RNA into complementary DNA (cDNA) was carried out using the SensiFAST™ cDNA Synthesis kit (BioLine). 1 µg of total RNA was prepared with 4 µl of 5x TransAmp buffer, 1 µl of reserve transcriptase, and DNase/RNase free-water up to a final volume of 20 µl. Reverse transcription was conducted in a thermal cycler using the following program (**Table 5**):

Table 5: Program for cDNA synthesis.

Step	Temperature	Duration
Primer annealing	25 °C	10 min
Reverse transcription	42 °C	15 min
Inactivation	85 °C	5 min
Cooling	4 °C	∞

Samples were diluted 1:10 with DNase/RNase free-water and stored at – 20 °C.

Real-time quantitative polymerase chain reaction (RT-qPCR) was performed using the SensiMix SYBR® No-ROX Kit system (BioLine). A small fraction of all cDNA samples was pooled and serially diluted (1:2) until a final dilution of 1:256 (cell culture) or 1:512 (tissue) was achieved to create a standard curve. 1 µl of 1:10 diluted cDNA from all investigated samples (Primers listed in **Table 6**) was added to a 384-well plate (4titude) in a volume of 11.5 µl of reaction mix per well (6.25 µl 2x SensiMix SYBR® No-ROX master mix, 0.03125 µl forward primer [100 µM], 0.03125 µl reverse primer [100 µM], 5.1875 µl nuclease-free water). Standard samples were run in duplicates, and target samples in triplicates.

Table 6: Primers of target genes.

Target gene	5' - 3' forward primer [100 µM] (Eurofines Genomics)	5' - 3' reverse primer [100 µM] (Eurofines Genomics)
Acc	TTTTCGATGTCCTCCCAAAC	ACATTCTGTTTAGCGTGGGG
Adipoq	CTTGTGCAGGTTGGATGGC	CAGCTCCTGTCATTCCAACA
Atgl	GGAAATTGGGTGACCATCTG	AAGGCCACATTGGTGCAG
Fabp4	GAAAGAAGTGGGAGTGGGCTT	CCCCGCCATCTAGGGTTATG
Fasn	TTGCTGGCACTACAGAATGC	GCATTCAGAATCGTGGCATA
Hsl	GCTTGGTTCAACTGGAGAGC	GCCTAGTGCCTTCTGGTCTG
Plin1	GAGACTGAGGTGGCGGTCTG	ATCCTTACTCTCCACGCTGTAACAC
Pparg	TCAGCTCTGTGGACCTCTCC	ACCCTTGCATCCTTCACAAG
Pref-1	TGTCAATGGAGTCTGCAAGG	CTTTCCAGAGAACCCAGGTG
Srebp1c	GGAGCCATGGATTGCACATT	GGCCCGGGAAGTCACTGT
TfIIb	TGGAGATTTGTCCACCATGA	GAATTGCCAAACTCATCAAAACT

RT-qPCR reactions (**Table 7**) were performed on a LightCycler 480 II (Roche). Transcript abundances were calculated using the absolute values of the standard curve, with general transcription factor II B (*TfIIb*) as housekeeper gene and all expression values normalized accordingly.

Table 7: Program for RT-qPCR for cDNA.

Step		Temperature	Duration
Initial denaturation		95 °C	7 min
Denaturation	45 cycles	97 °C	10 sec
Annealing		53 °C	15 sec
Extension		72 °C	20 sec
Melting curve		60 °C – 95 °C	
Cooling		4 °C	∞

2.8 Flow Cytometry

Cells were isolated following the protocol described in Section 2.3 (Isolation of murine stromal-vascular fraction cells) and resuspended in 2 ml of FACS buffer. A 20 µl aliquot of cell suspension was mixed with an equal volume of 0.4 % (v/v) trypan blue for the purpose of identifying dead cells. The viability of the cells was then determined using an automated cell counter (BioRad) to ensure equal numbers of intact cells per well for subsequent staining procedures. The cells were diluted to a final concentration of $5*10^6$ cells/ml in ice-cold FACS buffer (**Table 3**) and transferred to a 96-well V-bottom plate for staining.

2.8.1 Surface staining

After centrifugation at 300 g for 3 min, the supernatant was aspirated and the cells were incubated in 50 µl of FACS buffer containing a 1:10 dilution of Fc Block (Miltenyi Biotec, 130-092-575) for 10 min at 4 °C. After centrifugation at 300 g for 3 min at 4 °C, the Fc Block solution was discarded and the cells were incubated with a primary antibody Master-Mix (**Table 8**) in FACS buffer (30 µl/well) for 20 min.

Table 8: Composition of primary antibody Master-Mix for live cell staining.

Primary antibody	Cat#	Source	Dilution factor
CD31-AF488	102513	BioLegend	1:600
CD45-AF488	103121	BioLegend	1:600
Ter119-AF488	116215	BioLegend	1:600
SCA1-PE-Cy7	122513	BioLegend	1:600
VAP1 conjugated to Lightning-Link Cy5.5 (Innova Biosciences)	ab81673	abcam	1:50
CD55 conjugated to Lightning-Link PE (Innova Biosciences)	131802	BioLegend	1:1000
CD142 conjugated to Lightning-Link APC (Innova Biosciences)	50413-R001	SinoBiological	1:350

The cells were washed twice with 100 µl of FACS buffer (centrifugation 300 g, 3 min, 4 °C) and resuspended in fresh FACS buffer. Prior to analysis, the samples were incubated with DAPI (final dilution: 1:2500, Sigma-Aldrich, D9542) at room temperature for 5 min to stain the nuclei of deceased cells. Unless otherwise stated, the cells were maintained on ice and in darkness. Fluorescence minus one (FMO) staining was performed to ensure the specificity of the acquired data. The immunofluorescence signals of the samples were subsequently quantified using a multicolor flow cytometer (BD LSRFortessaTM) (gating strategy: **Figure S1**).

2.8.2 Co-staining with intracellular staining

The SVF cells were centrifuged at 300 g for 3 min and supernatant was aspirated. Then, the cells were incubated with 50 µl of live/dead staining (1:1000 Zombie Aqua™, Biolegend, 423101) for 10 min at room temperature. After this treatment, the cells were washed with 100 µl of FACS buffer (centrifugation 300 g, 3 min) and stained with the conjugated primary antibody

VAP1 (1:50 dilution; abcam, ab81673, conjugated to Lightning-Link Cy5.5, Innova Biosciences)) in FACS buffer for 20 min to prevent non-specific intracellular staining. The cells were subsequently washed twice in 100 µl of FACS buffer (centrifugation 300 g, 3 min) and resuspended in 100 µl of IC fixation buffer (ThermoFisher Scientific) for 10 min. To permeabilize the cells, they were washed (centrifugation 400 g, 2 min, 4 °C) with 100 µl of 1x permeabilization buffer (ThermoFisher Scientific). For detecting EdU, the Click-iT® EdU Alexa Fluor™ 488 Imaging Kit (ThermoFisher Scientific) was used and components were prepared according to the protocol of the manufacturer. The cells were resuspended in 50 µl of the adapted Click-iT® reaction cocktail (**Table 9**) and incubated for 30 min at ambient temperature.

Table 9: Adapted Click-iT® reaction cocktail for flow cytometry.

Component	Volume
1x Click it reaction buffer (component D)	43.75 µl
Copper protectant (component E)	1 µl
Alexa Fluor picolyl azide (component B)	0.25 µl
Reaction Buffer Additive (component F)	5 µl

The cells were washed with 100 µl of 1x permeabilization buffer (centrifugation 400 g, 2 min, 4 °C). Afterward, the cell pellets were dissolved in 50 µl of FACS buffer containing 1:10 Fc Block and incubated at 4 °C for 10 min. The Fc Block solution was removed (centrifugation 400 g, 2 min, 4 °C) and the cells were incubated with a primary antibody Master-Mix (**Table 10**) in 1x permeabilization buffer (30 µl/well) for 30 min.

Table 10: Composition of primary antibody Master-Mix for co-staining.

Primary antibody	Cat#	Source	Dilution factor
CD31-BV421	562939	BD	1:400
CD45-BV421	103133	BioLegend	1:400
Ter119-BV421	116233	BioLegend	1:400
SCA1-PE-Cy7	122513	BioLegend	1:600
CD55 conjugated to Lightning-Link PE (Innova Biosciences)	ab81673	abcam	1:1000
CD142	AF3178	R&D	1:350

The cells were washed twice with 100 µl of 1x permeabilization buffer (centrifugation 400 g, 2 min, 4 °C). Subsequently, the cells were treated with 30 µl of secondary donkey-anti goat antibody (1:600; Jackson Immunoresearch, 705-605-147) diluted in 1x permeabilization buffer for 20 min to detect $CD142^+$ cells. The cells were again washed twice with 100 µl of 1x permeabilization buffer (centrifugation 400 g, 2 min, 4 °C) and resuspended in 100 µl of FACS buffer.

Unless stated otherwise, the cells were maintained on ice and in darkness. The samples and FMO controls were quantified using a multicolor flow cytometer (BD LSRFortessa™) (gating strategy: **Figure S2**).

2.9 3D imaging of proliferating preadipocytes in murine white adipose tissue

A distal tissue part of eWAT was obtained from mice perfused with PBS and fixed in 200 µl of IC fixation buffer (ThermoFisher Scientific) for 2 h at ambient temperature. Subsequently, the tissue sample was stored in a solution containing 25 % (v/v) fixation buffer in PBS at 4 °C for further processing.

Tissue samples underwent clearing, staining and imaging processes by our collaborative partner, Marie Goëss from the laboratory of Dr. Selina Keppler from the Institute for Clinical Chemistry and Pathobiochemistry at Technical University of Munich. The methodology for preparing and clearing the samples was previously described in detail (Hofmann et al., 2020).

The tissue sample was treated with blocking buffer (PBS containing 1 % (v/v) FBS, 1 % (v/v) mouse serum (Jackson Immunoresearch, AB_2337194), 0.3 % (v/v) Triton X-100) for a minimum of 12 h at 37 °C. Afterward, it was stained with Click-iT® EdU Alexa Fluor™ 488 Imaging Kit (ThermoFisher Scientific) as mentioned in the protocol of the manufacturer. The tissue was subsequently washed twice with 1 ml of 3 % bovine serum albumin (BSA) in PBS, and then fully immersed and incubated with an appropriate volume of Click-iT® reaction cocktail (**Table 11**) for 30 min at room temperature.

Table 11: Click-iT® reaction cocktail for 50 µl staining volume.

Component	Volume
1x Click it reaction buffer (component D)	43 µl
Copper protectant (component E)	2 µl
Alexa Fluor picolyl azide (component B)	0.12 µl
Reaction Buffer Additive (component F)	5 µl

The tissue sample was further washed with 1 ml of 3 % BSA in PBS and stained with the following antibodies in blocking buffer for 72 h at 37 °C: CD45.2 (1:200 dilution, BioLegend, 109850), SytoxTM Orange (1:50000 dilution, ThermoFisher Scientific, S34861), and CD31 (1:200 dilution, BioLegend, 102415). Then, the tissue sample was washed in PBS with 0.2 % (v/v) Triton X-100 and 0.5 % (v/v) 1-thioglycerol for 24 h at 37 °C. The tissue sample was dehydrated by sequential treatment with ascending dilution series of isopropanol (30 %, 50 %, and 70 %; pH~9) for 1 h each and for 2 h with 100 % isopropanol. The tissue was cleared

under visual inspection (< 1 h) using undiluted ethyl cinnamate. All staining steps were carried out in the dark.

Imaging was conducted unsing an inverted Leica TCS SP8 confocal microscope with white light laser and HyD photodetectors, and an HC PL APO CS2 20 × /0.75 IMM objective (zoom factor of 1; Leica Microsystems). Images were deconvolved using the LIGHTNING module in Leica Application Suite X (Leica Microsystems). Contrast adjustment for display purposes and image analysis was performed using Imaris (Bitplane, version 9.5.1). Binary masking of the investigated cells was achieved with the Surface Creation Wizard function in Imaris. Cells of interest were assigned into two groups (1: vessel associated proliferating primary adipocytes; 2: non-vessel associated proliferating primary adipocytes outside of crown-like structures) and were quantified manually.

2.10 Isolation of murine mature adipocytes

Mice were killed by cervical dislocation. iWAT and eWAT depots were dissected, weighed, and maintained in PBS until further processing. For respiratory measurements, total iWAT or eWAT were utilized. For immunoblotting and proteomics, exclusively one iWAT and eWAT depot were used. Tissue samples were mechanically minced using scissors and were subsequently subjected to collagenase digestion with 10 ml of isolation medium (**Table 3**) per tissue depot and mouse. Tissues were digested during shaking at 150 rpm for 30 min (iWAT, respiratory measurements), 25 min (iWAT, immunoblotting and proteomics), 20 min (eWAT, respiratory measurements), and 15 min (eWAT, immunoblotting and proteomics) at 37 °C. Any remaining tissue fragments were manually disrupted using a Pasteur pipette. The solution was filtered through a 250 µM nylon gauze to remove lymph nodes and undigested tissue. The gauze was rinsed with Sucrose/Tris/EGTA (STE)-buffer (250 mM sucrose, 5 mM Tris, 2 mM EGTA, pH = 7.4 at 4 °C, adjusted with HCl) containing 4 % (w/v) bovine serum albumin (BSA) (for respiratory measurements) or only STE-buffer (for immunoblotting and proteomics). After low-speed centrifugation (300 g, 2 min), mature adipocytes accumulated on top of the liquid phase, while the SVF cells formed a pellet at the bottom. The SVF cells for immunoblotting experiments were collected and washed twice with PBS (centrifugation 500 g, 5 min). Mature adipocytes for respirometry measurements were washed twice with STE-buffer containing 4 % (w/v) BSA (centrifugation 300 g, 2 min), followed by two washing steps with STE-buffer containing 4 % (w/v) essentially fatty-acid free BSA (centrifugation 300 g, 2 min). Mature adipocytes for non-respiratory measurements (immunoblotting and proteomics) were washed four times with STE-buffer (centrifugation 300 g, 2 min). The infranatants were thoroughly removed. The isolated mature adipocytes for respirometry measurements were stored on ice until respiratory

measurements were performed (≤ 4 h). Adipocytes and SVF cells were snap-frozen and stored at - 80 °C for subsequent analysis.

2.11 High resolution respirometry of murine mature adipocytes

We employed high-resolution respirometry (Oxygraph-2k, OROBOROS INSTRUMENTS) to measure the oxygen consumption of isolated mature adipocytes. The adipocyte suspension, composed of 60 µl inguinal adipocytes or 80 µl epididymal adipocytes, was added with a cut pipette tip to 2 ml mitochondrial respiration buffer (MIR05) (110 mM Sucrose, 60 mM potassium lactobionate, 0.5 mM EGTA, 3 mM $MgCl_2$ * $6H_2O$, 20 mM taurine, 10 mM KH_2PO_4, 20 mM HEPES, 1g/l BSA-essentially fatty acid free, pH 7.1 with 5 N KOH at 30 °C, (Gnaiger et al., 2000)), supplemented with 5 mM succinate, pyruvate, and malate each. Stirrer speed was set to 750 rpm.

Leak respiration (state 4) was induced by the addition of 20 µM α-chaconine, which effectively permeabilized the isolated mature adipocytes without causing cellular damage (data not shown). Maximal phosphorylating respiration (state 3) was elicited by the addition of 5 mM adenosine diphosphate (ADP), in the presence of aforementioned substrates. Background respiration was determined by the addition of 2.5 µM antimycin A (a complex III inhibitor) and subtracted from all respiratory state results obtained. After measurement, the permeabilized cells were frozen at – 20 °C for subsequent DNA quantification. The respiratory control ratio (RCR) was calculated by dividing state 3 by state 4 respiration to evaluate the integrity of the mitochondrial respiratory chain. All samples were analyzed in quadruplicate and the resulted mean values were utilized for analysis.

DNA quantification of the adipocyte suspension obtained from respiratory measurements was performed using RT-qPCR targeting a unique region of genomic DNA (promotor resistin; 5' - 3' forward primer [100 µM]: ACCTCTCTTGGGGTCAGATGT (Eurofines Genomics), 5' - 3' reverse primer [100 µM]: CTGGGTATTAGCTCCTGTCCC (Eurofines Genomics)) in order to normalize the oxygen consumption rate to the DNA content [pmol O2/(s*µg DNA)]. The frozen permeabilized cells were thawed on ice. After thorough vortexing (> 10 sec), 100 µl of the adipocyte suspension were diluted 1:5 in lysis buffer (10 mM Tris, pH 8.3 adjusted with 6 N HCl, 50 mM KCl, 0.45 % (v/v) Nonidet P-40, 0.45 % (v/v) Tween 20, 0.2 mg/ml Proteinase K). The samples were digested during shaking at 1000 rpm for 1 h at 65 °C. Proteinase K was inactivated by heating (95 °C, 10 min), the samples were cooled on ice, and 2.25 volumes of phenol/chloroform/isoamyl alcohol (25:24:1) were added. The samples were inverted and shaken for 2 min and centrifuged (16000 g, 5 min) for phase separation. 1 µl of the extracted DNA from the upper hydrophilic phase was directly added to a 384-well plate containing 11.5 µl

of reaction mix per well (6.25 µl 2x SensiMix SYBR No-ROX® master mix, 0.03125 µl forward primer [100 µM], 0.03125 µl reverse primer [100 µM], 5.1875 µl nuclease-free water). The RT-qPCR reaction (**Table 12**) was conducted on a LightCycler 480 II. A mouse genomic DNA standard series of known concentrations was used for calculating DNA concentrations of the adipocyte suspension. The standard samples were measured in duplicates and the adipocyte suspension samples in triplicates.

Table 12: Program for RT-qPCR for genomic DNA.

Step		Temperature	Duration
Initial denaturation		97 °C	7 min
Denaturation	45 cycles	97 °C	10 sec
Annealing		59 °C	15 sec
Extension		72 °C	20 sec
Cooling		4 °C	∞

2.12 Citrate synthase activity

The citrate synthase (CS) activity was determined as a surrogate measure for mitochondrial content. Isolated mature adipocytes were thawed on ice and diluted 1:25 in a CS lysis buffer (MIR05 supplemented with 1 % (v/v) Tween 20) to a final volume of 400 µl. Adipocytes were homogenized using an Ultra-Turrax homogenizer (30 sec. level 2, IKA). 10 µl of the adipocyte homogenate or CS-lysis buffer (negative control) was added to 240 µl of CS assay medium buffer (100 mM Tris, 1 mM EDTA, 1 mM MgCl2, adjusted pH 8.2 with HCl) containing freshly added 0.1 mM 5,5'dithiobis(2-nitrobenzoic) acid (DTNB) and 0.36 mM Acetyl-CoA. Measurements were performed on a 96-well plate at an excitation wavelength of 412 nm (TECAN InfiniteM2000 NanoQuant microplate reader) in triplicates at 30 °C. After shaking for 3 sec and measuring five kinetic cycles of 1 min, 50 µl of 3 mM oxaloacetate was injected per well. After shaking for 3 sec again, ten kinetic cycles of 1 min were measured. The enzyme activity was calculated by measuring the difference of absorption before and after the injection of oxaloacetate (by consideration of the dilution factor) and dividing it by the extinction coefficient of DTNB and the path length of the plate:

$$\text{CS activtiy } [\frac{\text{U}}{\mu\text{g DNA}}] = \frac{(\text{slope after oxaloacetate} - \text{slope before oxaloacetate}) * \text{dilution factor}}{\text{extinction coefficent of DNTB} * \text{path lenght of plate} * \mu\text{g DNA}}$$

Dilution factor = 30.
Extinction coefficient of DTNB = 13.6 ml * µmol^{-1} * cm^{-1} (Alexson and Nedergaard, 1988).
Path length of plate filled with 300 µl suspension = 0.75 cm.
DNA concentrations were determined as described in 2.11.

2.13 Protein expression

Total protein lysates of iWAT, eWAT, inguinal adipocytes, epididymal adipocytes, inguinal SVF cells, and epididymal SVF cells were generated in an appropriate volume of radio immunoprecipitation assay (RIPA) lysis buffer (50 mM Tris-HCl, 1 % (v/v) Nonidet P-40, 0.25 % (w/v) sodium deoxycholate, 150 mM NaCl, 1 mM EDTA, 0.1 % (w/v) protease inhibitor (Sigma-Aldrich)). Samples were incubated on ice for 30 min and vortexed every 10 min. Phase separation occurred during centrifugation for 15 min at 22000 g at 4 °C. The supernatant was harvested and protein concentration was determined by Pierce™ bicinchoninic acid (BCA) protein assay (ThermoFisher Scientific) as stated in the protocol of the manufacturer. BSA standard solutions and protein lysates (diluted 1:5 in dH_2O) were prepared. 10 µl of samples or standard solutions were incubated in a 96-well plate with 200 µl of BCA working reagent (50 parts Reagent A, 1 part Reagent B) per well for 30 min at 37 °C. The absorbance was measured at an excitation wavelength of 562 nm using a TECAN InfiniteM2000 NanoQuant microplate reader and the protein concentration was calculated accordingly.

2.13.1 Immunoblotting

Immunoblotting was performed utilizing protein lysates of 30 µg iWAT or eWAT and 50 µg inguinal adipocytes, epididymal adipocytes, inguinal SVF cells, or epididymal SVF cells. Samples were prepared in 4x ROTI®Load sample buffer (Carl Roth) and denatured for 5 min at 60 °C. Proteins were separated with 10 % sodium dodecyl sulfate-polyacrylamide gel electrophoresis (SDS-PAGE) (**Table 13**) (150 min, 80 V) using 1x ROTIPHORESE® SDS-PAGE running buffer (Carl Roth).

Table 13: Composition of 10 % SDS-PAGE.

Gel	Reagent	Volume [ml]
Resolving gel [10 %]	ROTIPHORESE® Gel 30	10 ml
	Resolving gel buffer (0.5 M Tris, pH 6.8 with HCl)	3.76 ml
	H_2O	15.8 ml
	10 % (w/v) SDS	300 µl
	10 % (w/v) AMPS	150 µl
	TEMED	15 µl
Stacking gel [5 %]	ROTIPHORESE® Gel 30	2.4 ml
	Stacking gel buffer (3 M Tris, pH 8.8 with HCl)	3.75 ml
	H_2O	8.58 ml

10 % (w/v) SDS	150 µl
10 % (w/v) AMPS	90 µl
TEMED	30 µl

Proteins were subsequently transferred onto a nitrocellulose membrane (LI-COR Bioscience; 1.5 mA/1 cm^2, 1 h) using a semi-dry blotter Biometra Fastblot™ (AnalyticJena) and blotting buffer (48 mM Tris, 39 mM glycine, 1.3 mM SDS, pH 9.2) with 20 % (v/v) methanol. The membranes were blocked in blocking buffer (3 % (w/v) BSA in Tris-buffered saline (TBS)) for a minimum of 2 h at ambient temperature. Subsequently, the membranes were incubated with a primary antibody combination specifically targeting representative subunits of the oxidative phosphorylation (1:500; Abcam, ab110413) in the aforementioned blocking buffer at 4 °C overnight. On the next day, the primary antibody solution was replaced by a primary antibody directed against the housekeeping protein, Vinculin (1:2000; Proteintech, 26520-1-AP), in the same blocking buffer and incubated overnight at 4 °C. The membranes were washed with TBS-0.1 % (v/v) Tween 20 for 10 min three times to remove any unbound antibodies. To detect the primary antibodies, the membranes were incubated with infrared dye-conjugated secondary antibodies (1:20000; IRDye® 680RD, 926-68072, LI-COR Biosciences; IRDye® 800CW, 925-32211, LI-COR Biosciences) for 2 h at room temperature during shaking. To ensure complete removal of unbound secondary antibodies, the membranes were again washed three times with TBS-0.1 % Tween-20 for 10 min between the incubation steps for the different secondary antibodies and at the end of the second secondary antibody staining. Finally, the fluorescence intensity of the separated bands was quantitatively analyzed using the Azure Sapphire™ Biomolecular Imager (Azur Biosystems) and Image StudioTM Lite Version 5.2 (LI-COR Bioscience).

2.13.2 Mass spectrometry proteomics

The sample preparation, measurement, and pre-analysis for mass spectrometric (MS) analysis were executed by our collaborative partner, Dr. Christina Ludwig, at the Bavarian Center for Biomolecular Mass Spectrometry, Technical University of Munich.

Mass spectrometric sample preparation

For each adipocyte sample, 25 µg of protein lysate was mixed 3:1 with 4x LDS sample buffer (NuPAGE™, ThermoFisher Scientific) and heated to 70 °C for 10 min. In-gel trypsin digestion was performed according to standard procedures (Shevchenko et al., 2006). Briefly, the samples were run on a Nu-PAGE™ 4 % – 12 % Bis-Tris protein gel (ThermoFisher Scientific) for

about 1 cm. Subsequently, the still not size-separated single protein band per sample was cut out, reduced (50 mM dithiothreitol), alkylated (55 mm chloroacetamide) and digested overnight with trypsin (Trypsin Gold, mass spectrometry grade, Promega). The peptides obtained were dried to completeness and resuspended in 25 µl of 2 % acetonitrile, 0.1 % formic acid in HPLC grade water. Finally, 2 µl of sample were injected per MS measurement.

LC-MS/MS data acquisition

LC-MS/MS data acquisition of all adipocyte samples was carried out on a Dionex Ultimate 3000 RSLCnano system coupled to a Q-Exactive HF-X mass spectrometer (ThermoFisher Scientific). Injected peptides were delivered to a trap column (ReproSil-pur C18-AQ, 5 µm, Dr. Maisch, 20 mm × 75 µm, self-packed) at a flow rate of 5 µl/min in 0.1 % formic acid in HPLC grade water. After 10 min of loading, peptides were transferred to an analytical column (ReproSil Gold C18-AQ, 3 µm, Dr. Maisch, 450 mm × 75 µm, self-packed) and separated using a 110 min gradient from 4 % to 32 % of solvent B (0.1 % formic acid, 5 % DMSO in acetonitrile) in solvent A (0.1 % formic acid, 5 % DMSO in HPLC grade water) at 300 nl/min flow rate. The Q-Exactive HF-X mass spectrometer was operated in data dependent acquisition (DDA) and positive ionization mode. MS1 spectra (360–1300 m/z) were recorded at a resolution of 60k using an automatic gain control (AGC) target value of 3e6 and maximum injection time (maxIT) of 45 milliseconds (msec). Up to 18 peptide precursors were selected for fragmentation. Only precursors with charge state 2 to 6 were selected and dynamic exclusion of 30 sec was enabled. Peptide fragmentation was performed using higher energy collision induced dissociation and a normalized collision energy of 26 %. The precursor isolation window width was set to 1.3 m/z. MS2 Resolution was 15.000 with an AGC target value of 1e5 and maxIT of 25 msec (full proteome).

LC-MS/MS data analysis and visualization

Peptide identification and quantification was performed using the software MaxQuant (version 1.6.3.4) (Tyanova et al., 2016) with its built-in search engine Andromeda (Cox et al., 2011). MS2 spectra were searched against the Uniprot mouse protein database (UP000000589, 55462 protein entries, downloaded July 2020), supplemented with common contaminants (built-in option in MaxQuant). Samples of inguinal and epididymal adipocytes were analyzed separately. Trypsin/P was specified as proteolytic enzyme. Carbamidomethylated cysteine was set as fixed modification. Oxidation of methionine and acetylation at the protein N-terminus was specified as variable modifications. Results were adjusted to 1 % false discovery rate on

peptide spectrum match level and protein level employing a target-decoy approach using reversed protein sequences. Label-Free Quantification (LFQ) intensities (Cox et al., 2014) were used for protein quantification with at least 2 peptides per protein identified. The minimal peptide length was defined as 7 amino acids and the “match-between-runs” functionality was enabled (matching time window 0.7 min, alignment time window 20 min). Missing values were imputed by a protein-specific constant value, which was defined as the lowest detected protein-specific LFQ-value over all samples divided by two. Additionally, a maximal imputed LFQ value was defined as 15 % quantile of the protein distribution from the complete dataset.

The Protein Groups result file from MaxQuant was loaded into Perseus (Version 2.0.6.0) for quantitative analysis. The raw LFQ intensity values were set as the main columns and transformed into their log2 values. The biological replicate groups were assigned according to the feeding regimens of the mice, and only values protein groups identified in at least three biological replicates in at least one feeding group were processed further. A principal component analysis (PCA) was performed to assess grouping patterns of the feeding groups and that of the biological replicates. Missing values in each column were imputated using a normal distribution method and normalized by the median protein group area. The normalized values were used to generate the column Pearson correlation coefficients. Multiple sample test using ANOVA was performed and the data were filtered for significant values and Z-score transformed by row to generate the hierarchical clustering and heat map visualization of feeding groups and for that of the biological replicates. In parallel, the Gene Ontology annotations, Pfam and Gene Set Enrichment Analysis terms were overlaid onto the protein groups. The overlaid terminologies were used to assess the representation of mitochondrial proteins in the total dataset. From the three feeding groups (CD, HFD, and HFD-CD), three categories of comparisons were made for the quantitative analysis: (i) HFD versus CD; (ii) HFD-CD versus CD, and (iii) HFD versus HFD-CD. For each comparison, two-sample t-test was performed and filtered for significant protein groups with fold change values of greater or lesser than 1.5. The lists of significantly expressed proteins from each comparison were extracted and saved in excel format for further *in silico* analysis. The PCA was performed in RStudio environment, showing individual values. Functional annotation of differentially regulated proteins was carried out using the Kyoto Encyclopedia of Genes and Genomes (KEGG) mapper tool (https://www.genome.jp/kegg/mapper/) and the Enrichr tool (https://maayanlab.cloud/Enrichr/). For conversion of protein IDs, the Retrieve/ID mapping tool in Uniprot (https://www.uniprot.org/id-mapping/) and g:Convert tool in g:Profiler (https://biit.cs.ut.ee/gprofiler/convert) were used. Vent diagrams were generated with Venny 2.1 (https://bioinfogp.cnb.csic.es/tools/venny/).

2.14 Statistical analysis and data presentation

Data were presented in bar charts as individual and mean values ± standard deviation, or in line charts of mean values ± standard deviation. Unless otherwise stated, one-way or two-way repeated-measures ANOVA followed by post-hoc Dunn-Šidák correction were conducted for statistical comparison (Matlab R2022b). *P* values with a threshold less than 0.05 were considered statistically significant.

3 Results

White adipose tissue (WAT) is a highly adaptable organ that can respond to various environmental and lifestyle conditions. Body and fat mass increase or decrease plastically depending on energy intake and expenditure. However, this system has limits. Excessive energy intake combined with reduced energy expenditure can drive WAT to its maximal sustainable limit. At this point, adaptation to energy overload turns into pathology with persistent metabolic consequences, even after reduction of body and fat mass (Fothergill et al., 2016). In this work, we focused on two aspects that exhibit residual effects following a return to normal body mass: 1) the adipogenic potential of adipocyte progenitor cells (APCs), and 2) the mitochondrial function of adipocytes.

3.1 Diet-induced obesity causes diet-dependent, persisting alterations in the adipogenic potential and fate of progenitor cells

Adipocytes have a low cell turnover rate, with an annual renewal rate of only 10 % (Spalding et al., 2008). WAT can expand through hypertrophy and hyperplasia. Hypertrophy refers to the expansion of adipocytes in size and is linked to inflammation, hypoxia, insulin resistance, and impaired adipocyte differentiation (Hammarstedt et al., 2018; Isakson et al., 2009). Hyperplasia is the increase of adipocyte number. In humans, hyperplastic expansion is limited and mainly occurs in childhood (Spalding et al., 2008). Therefore, excess caloric intake in adulthood tends to promote hypertrophic adipocyte expansion.

Initial cell culture experiments showed a reduction in proliferation and differentiation of primary adipocytes from epididymal white adipose tissue (eWAT) of obese mice (data not published). Therefore, we suppose that a significant positive energy balance not only has persistent effects on adipocytes (Schottl et al., 2015b), but it also impacts APCs, resulting in lasting reduced preadipocyte proliferation and differentiation. As eWAT reaches its expansion limit at approximately 40 g body mass in mice (van Beek et al., 2015), we conducted a detailed analysis of the effect of limited tissue expansion on the adipogenic potential of APCs.

3.1.1 Short-term CD feeding reduces body and fat mass

To evaluate the adipogenic potential of APCs, we conducted a study with four different feeding regimes. All mice, except for the control group, received a high-fat diet (HFD) starting at 12 weeks of age until they reached a minimum body mass of 40 g. Afterward, two short-term obesity intervention groups were fed a control diet (CD) for one week (HFD-CD group) or a caloric-restricted HFD that matched the caloric intake of the HFD-CD group (pair-fed HFD

group (HFD-pfHFD)). As previously shown eWAT reaches its storage capacity at 40 g body mass in mice (van Beek et al., 2015), so it was crucial to ensure that all HFD-fed mice reached at least 40 g body mass. Therefore, the feeding duration was determined by body mass (**Figure 3 G**) rather than time and varied among mice and feeding groups. For control mice, we adjusted their age to match the three HFD-fed groups. We initially assessed the body mass and body composition of C57BL/6N mice (**Figure 3**) at the start of the experiment (12 weeks of age) and when they reached a minimum body mass of 40 g (> 40 g).

We observed a significant increase in body, fat, and lean mass, as well as organ masses of inguinal white adipose tissue (iWAT) and eWAT in the HFD group compared to the control group (CD group) (**Figure 3 A**, **C**, **D**, **H**, and **I**). To account for potential factors that may influence body mass and composition, we considered the effects of litter size, as this could possibly affect feeding duration. However, contrary to earlier reports (Anderson et al., 1968; Parra-Vargas et al., 2020; Toth et al., 2015), we did not observe litter size or housing density effects on body mass gain in adult mice (data not shown).

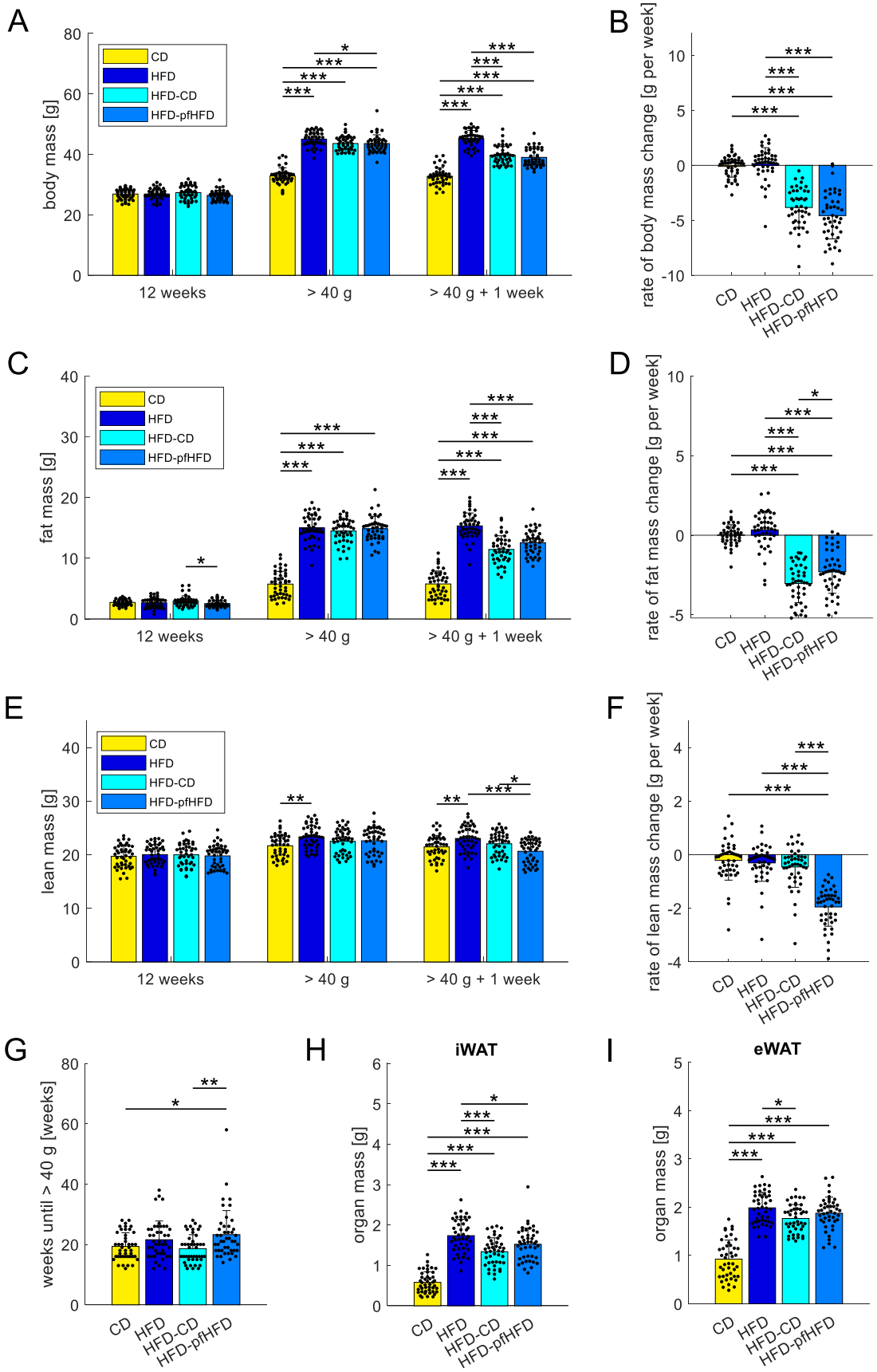

Figure 3: Alterations in body composition in mice following dietary interventions. All male C57BL/6N mice were given a control diet (CD) at 8 weeks of age. A high-fat diet (HFD) was introduced at 12 weeks of age. Mice in the HFD-CD and HFD-pfHFD groups were fed CD or pair-fed (pf) HFD for one week once they had reached a body mass of at least 40 g. (**A**) Comparison of body mass in four

feeding regimes at the following time points: start of the experiment (12 weeks of age), minimum body mass of 40 g (> 40 g), and end of the experiment (> 40 g + 1 week). Body mass was measured weekly. (**B**) Rate of body mass change in four feeding regimes during the final week of the experiment. (**C**) Comparison of fat mass in four feeding regimes at the following time points: start of the experiment (12 weeks of age), minimum body mass of 40 g (> 40 g), and end of the experiment (> 40 g + 1 week). (**D**) Rate of fat mass change in four feeding regimes during the final week of the experiment. (**E**) Comparison of lean mass in four feeding regimes at the following time points: start of the experiment (12 weeks of age), minimum body mass of 40 g (> 40 g), and end of the experiment (> 40 g + 1 week). (**F**) Rate of lean mass change in four feeding regimes during the final week of the experiment. (**G**) Duration of feeding in the four investigated feeding regimes until one week before the end of the experiment (> 40 g). (**H**) Organ mass of inguinal white adipose tissue (iWAT) in the depicted feeding regimes. (**I**) Organ mass of epididymal white adipose tissue (eWAT) in the depicted feeding regimes. All data were analyzed by one-way ANOVA (Dunn-Šidák correction). Data are presented as individual values and means ± standard deviation, n = 44 (biological replicates). * = $p < 0.05$, ** = $p < 0.01$, *** = $p < 0.001$.

To determine whether short-term obesity intervention is sufficient to overcome the storage limit of eWAT, we fed mice CD or pfHFD for one week. The pfHFD group was calorie-restricted to match the intake of the HFD-CD group. When switching from HFD to low-fat CD, mice reduce caloric intake. In fact, switching to low-fat CD has been shown to have more beneficial effects on insulin resistance than energy restriction alone (Muurling et al., 2002). By performing a one-week obesity intervention with CD or pfHFD, we also sought to determine whether diet quality, rather than diet quantity, could affect the adipogenic potential. After one week of CD or pfHFD feeding, we observed a clear reduction in body, fat, and lean mass compared to the HFD group (**Figure 3 A** – **F**). Interestingly, the changes in body composition differed between the one-week CD and one-week pfHFD feeding groups, despite similar caloric intake. Specifically, fat mass decreased more in the HFD-CD group, while only lean mass decreased in the HFD-pfHFD group. Furthermore, pfHFD feeding had a greater effect on lean mass compared to CD, HFD, and HFD-CD feeding groups (**Figure 3 E** and **F**). One week of CD feeding lowered already organ masses, with a more pronounced reduction in iWAT than in eWAT (**Figure 3 H** and **I**). One week of pfHFD feeding showed only a slight reduction in iWAT organ mass, with no decrease in eWAT organ mass compared to the HFD group.

These findings suggest that diet quality is more important for body and fat mass loss than diet quantity and support previous findings that low-fat CD is a stronger inducer of negative energy balance than energy restriction alone (Muurling et al., 2002).

3.1.2 Epididymal adipocytes exhibit a lower degree of expansion compared to inguinal adipocytes

Adipogenic differentiation can be divided into two stages: determination and terminal differentiation (Ghaben and Scherer, 2019). To determine the differences of terminal differentiation within different feeding regimes and fat depots, we studied the morphology of adipocytes in WAT.

HFD feeding led to a significant increase in the diameter of iWAT adipocytes, accompanied by a reduction in the mean number of iWAT adipocytes per mm^2 (**Figure 4 A**, **B**, and **E**) compared to the control group. As adipocytes in eWAT reach their expansion capacity quickly in adult obese mice (van Beek et al., 2015), they could not expand much (**Figure 4 C** and **F**). However, eWAT generally had larger, and therefore fewer, adipocytes than iWAT. The diameter of eWAT adipocytes also increased with HFD feeding, leading to a decrease in the mean number of eWAT adipocytes per mm^2 (**Figure 4 C** and **D**). These findings on WAT morphology are consistent with previous reports (Dong et al., 2017; Parlee et al., 2014; van Beek et al., 2015) and demonstrate the differences in expansion capacity between inguinal and epididymal fat depots.

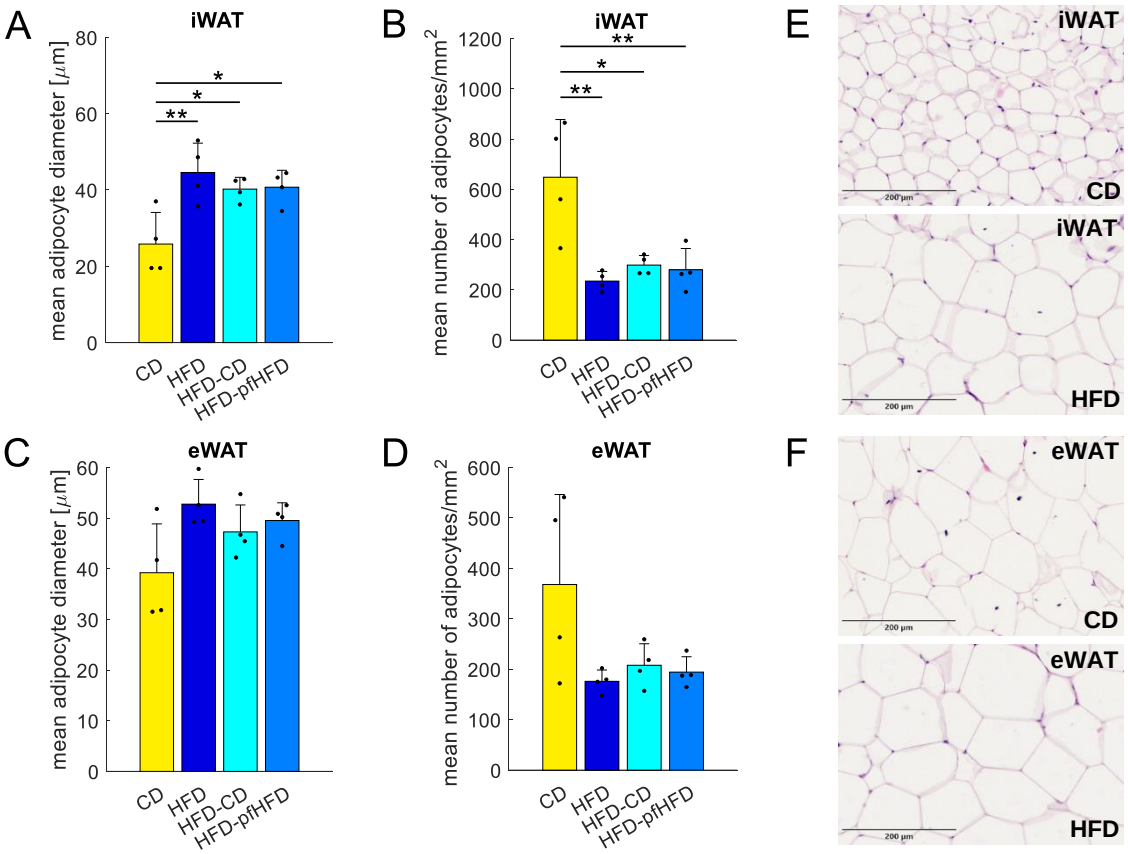

Figure 4: Diet-induced morphological changes in white adipose tissue. Hematoxylin & eosin (HE) staining of white adipose tissue (WAT). (**A**) Mean adipocyte diameter [µm] in four feeding regimes in inguinal white adipose tissue (iWAT). (**B**) Mean number of adipocytes per mm^2 in four feeding regimes in iWAT. (**C**) Mean adipocyte diameter [µm] in four feeding regimes in epididymal white adipose tissue (eWAT). (**D**) Mean number of adipocytes per mm^2 in four feeding regimes in eWAT. (**E**) Example for HE staining with 5 µm sliced paraffin-embedded iWAT from control diet (CD) (top) and high-fat diet (HFD) (bottom) group. Scale bar 200 µm. (**F**) Example for HE staining with 5 µm sliced paraffin-embedded eWAT from CD (top) and HFD (bottom) group. Scale bar 200 µm. **A** – **D** were analyzed by one-way ANOVA (Dunn-Šidák correction). Data are presented as individual values and means ± standard deviation, n = 4 (biological replicates). * = $p < 0.05$, ** = $p < 0.01$. pf = pair-fed.

To investigate the effects of diet quality and quantity on the structure of WAT, we fed obese mice CD or pfHFD for one week. We observed slight divergent effects on the adipocyte diameter and mean number of adipocytes per mm^2 in the inguinal fat depot (**Figure 4 A** - **C**). On

the morphological level, both short-term obesity interventions appeared generally to be equivalent with a very small tendency of a stronger reverse effect of one week CD. In the epididymal fat depot, we observed a reduced level of WAT restructuring within the short-term obesity interventions (**Figure 4 C** and **D**). However, the epididymal adipocytes in the control group showed only slight expansion in size, implying that they were already close to their expansion limit. Therefore, a short-term obesity intervention did not reduce the mean adipocyte diameter or increase the mean number of adipocytes per mm^2 in this tissue.

On the level of terminal differentiation, obesity had huge effects on the mean adipocyte diameter and number in both tissue depots. Feeding obese mice CD or pfHFD for one week showed only initial reverse effects in both WAT depots. To restore the WAT morphology fully, longer periods of body mass reduction through CD or pfHFD feeding are necessary.

3.1.3 Epididymal primary adipocytes from obese mice display persisting, reduced differentiation capacity on morphological level

For studying the proliferation and differentiation capacity of APCs, we isolated stromal vascular fraction (SVF) cells from iWAT and eWAT of mice that received CD or mice that had reached a minimum body mass of 40 g. The primary adipocytes were cultured until they reached confluence and were then induced and differentiated. We analyzed the morphology of the resulting lipid droplets to assess the adipogenic potential of these cells.

The overall distribution of adipocyte sizes was consistent across different fat depots and dietary interventions (data not shown). Analysis of inguinal primary adipocytes revealed a slight reduced trend in the number of lipid droplets, while the area covered by lipid droplets remained unchanged upon comparison of HFD to CD feeding (**Figure 5 A**, **B**, and **E**). This suggests that inguinal primary adipocytes responded to the HFD challenge by producing fewer, but larger and better developed lipid droplets. In contrast, epididymal primary adipocytes exhibited a tendency of an increase in lipid droplet number and a slight decrease in lipid droplet area (**Figure 5 C**, **D**, and **F**), indicating a reduction in differentiation capacity with more small and less matured lipid droplets. These results highlighted the differences between primary adipocytes derived from iWAT and eWAT and suggested that HFD feeding decreased the differentiation potential in epididymal, but not inguinal preadipocytes. Nevertheless, both types of preadipocytes were able to grow to confluence, indicating that the proliferation potential of cultured preadipocytes from obese mice was unaffected.

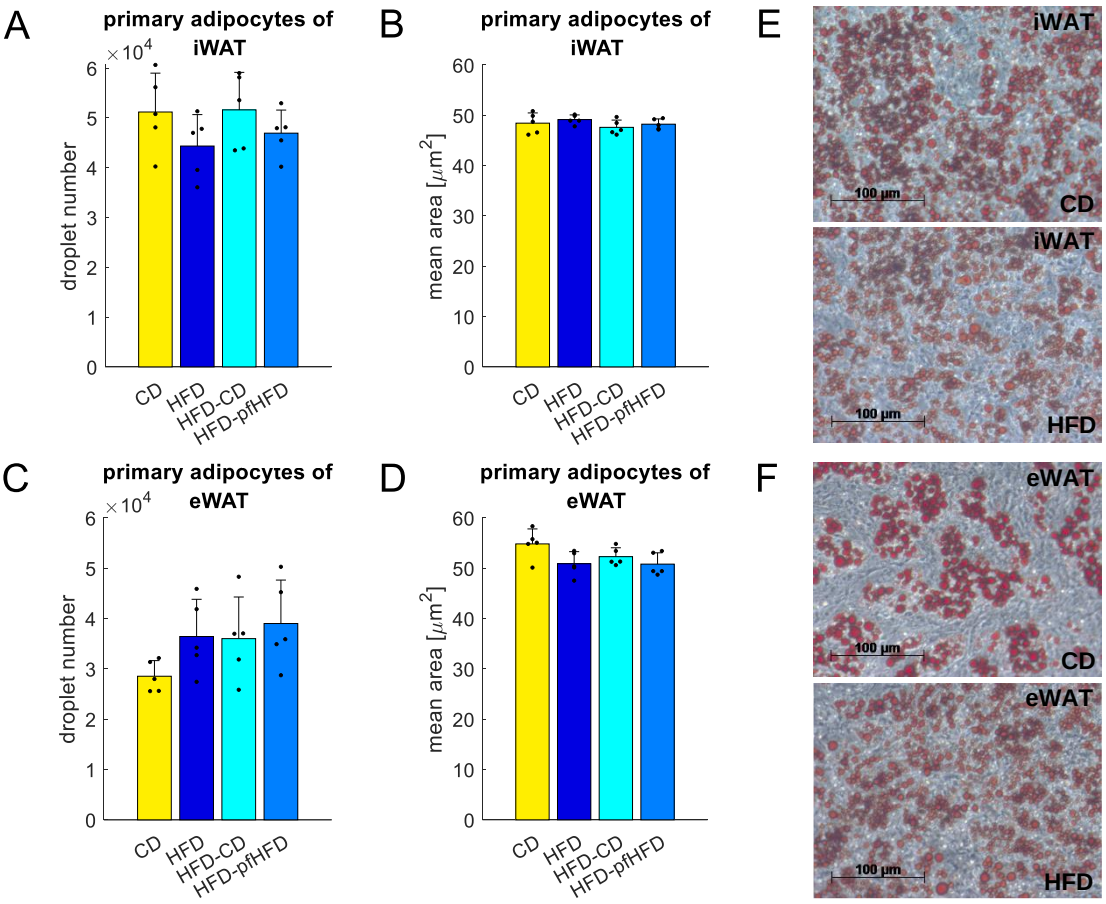

Figure 5: Diet-induced morphological changes of terminal differentiation in cultured primary adipocytes. Isolated stromal-vascular fraction (SVF) cells were cultured until confluence, induced for 48 h, and differentiated for six days. The morphology of lipid droplets was analyzed using WimLipid by Wimasis. (**A**) Droplet number in four feeding regimes of differentiated primary adipocytes of inguinal white adipose tissue (iWAT). (**B**) Lipid droplet size (mean area [µm²]) in four feeding regimes of differentiated primary adipocytes of iWAT. (**C**) Droplet number in four feeding regimes of differentiated primary adipocytes of epididymal white adipose tissue (eWAT). (**D**) Lipid droplet size (mean area [µm²]) in four feeding regimes of differentiated primary adipocytes of eWAT. (**E**) Example for Oil Red O stained differentiated primary adipocytes of iWAT from control diet (CD) (top) and high-fat diet (HFD) (bottom) group. Scale bar 100 µm. (**F**) Example for Oil Red O stained differentiated primary adipocytes of eWAT from CD (top) and HFD (bottom) group. Scale bar 100 µm. **A** – **D** were analyzed by one-way ANOVA (Dunn-Šidák correction). Data are presented as individual values and means ± standard deviation, n = 5 (biological replicates). pf = pair-fed.

After switching from HFD to CD or pfHFD for one week, inguinal primary adipocytes did not show any alteration in lipid droplet area (**Figure 5 A** and **B**). However, a trend of normalization in the number of lipid droplets were observed in the HFD-CD group, but not in HFD-pfHFD group, comparable to control group (**Figure 5 A**). Interestingly, the differentiation potential of epididymal primary adipocytes did not appear to be recovered after switching from HFD to CD or pfHFD (**Figure 5 B** and **D**), as we observed a remaining tendency for many small lipid droplets rather than fewer, larger, and more developed lipid droplets.

Overall, the adipogenic potential of epididymal primary adipocytes in culture indicated a reduced terminal differentiation on the morphological level that could not be reversed by a one-week CD or pfHFD obesity intervention.

3.1.4 Short-term control diet feeding restores impaired epididymal primary adipocyte differentiation capacity on gene expression level

To analyze the adipogenic potential of cultured primary adipocytes further, we performed gene expression analysis. In inguinal differentiated primary adipocytes, we detected no alterations in differentiation potential when comparing CD- and HFD-fed mice, as indicated by the lack of changes in terminal differentiation markers (**Figure 6 A** and **Figure S3 A**) and in the expression of the preadipocyte marker *Pref1* (**Figure 6 C**). Similarly, no diet-induced differences were observed in the expression of various markers of lipogenesis (*Acc*, *Fasn*), lipid storage (*Plin1*, *Srebp1c*), lipolysis (*Atgl*, *Hsl*), adipokines (*Adipoq*, *Fabp4*), adipogenesis (*Pparg*), and the preadipocyte marker *Pref1* in epididymal primary adipocytes (**Figure 6 B** and **D**). However, individual mice from the HFD group exhibited a slightly reduced differentiation potential compared to those from the CD group (**Figure S3 B**). Analysis of *Pref1* expression showed a slightly reduced expression in iWAT and eWAT upon HFD feeding (**Figure 6 D** and **F**). A slightly more pronounced reduction in differentiation potential was observed in eWAT compared to iWAT of HFD-fed mice compared to CD-fed mice.

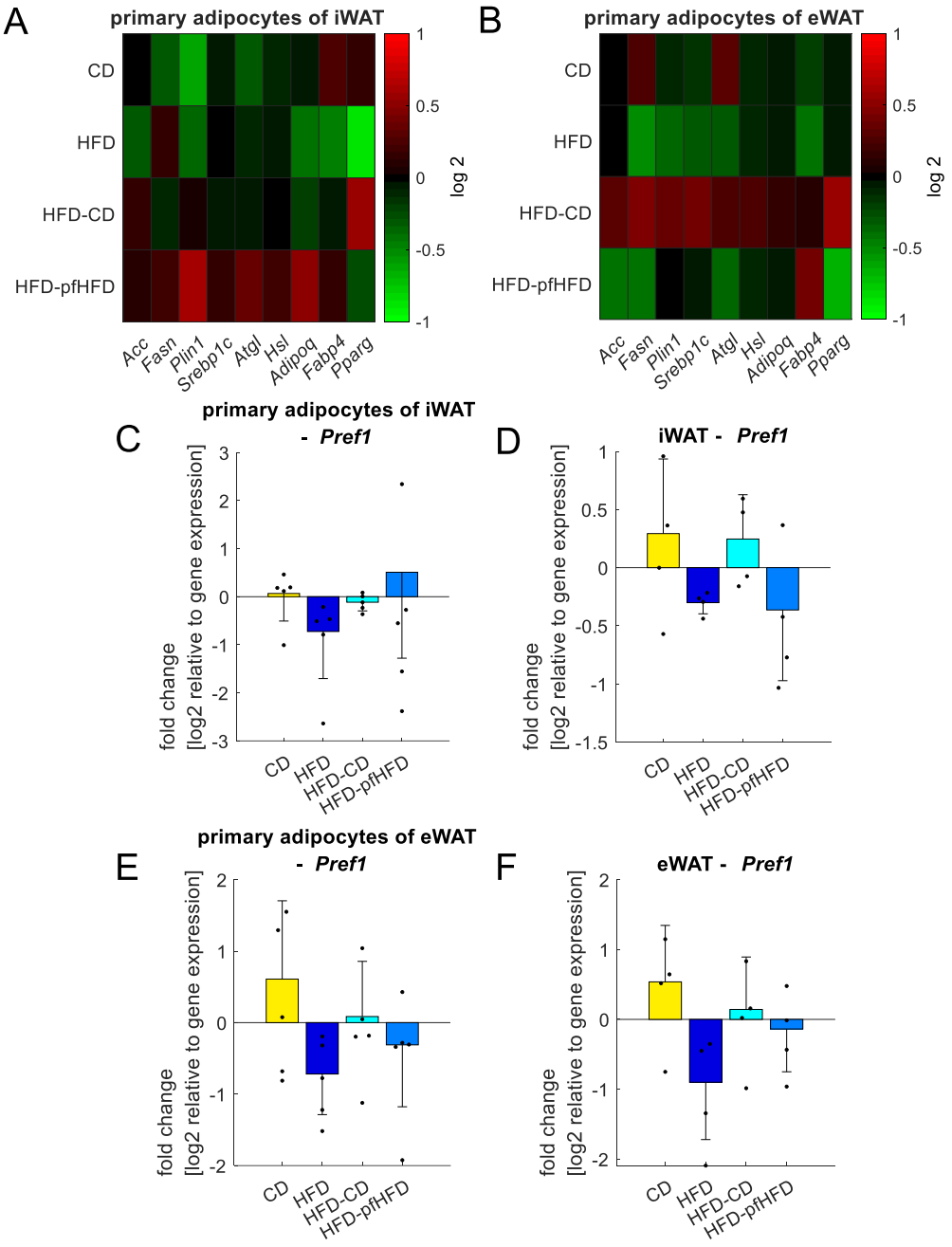

Figure 6: The effects of obesity and short-term control diet or pair-fed high-fat diet on markers of terminal differentiation associated with adipogenic potential. Isolated stromal-vascular fraction (SVF) cells were cultured until confluence, induced for 48 h, and differentiated for six days. Terminal differentiation capacity was determined by real-time quantitative polymerase chain reaction (RT-qPCR) (**A**) Heat map of selected terminal differentiation markers in differentiated inguinal primary adipocytes in four feeding regimes. Every value represents the mean of all biological replicates with three technical replicates. Values are standardized in a way that each column (mean of single protein) has the same mean (0) and standard deviation (1). (**B**) Heat map of selected terminal differentiation markers in differentiated epididymal primary adipocytes in four feeding regimes. Every value represents the mean of all biological replicates with three technical replicates. Values are standardized in a way that each column (mean of single protein) has the same mean (0) and standard deviation (1). (**C**) Fold change gene expression of preadipocyte marker preadipocyte factor 1 (*Pref1*) in differentiated inguinal primary adipocytes in four feeding regimes. (**D**) Fold change gene expression of preadipocyte marker *Pref1* in differentiated epididymal primary adipocytes in four feeding regimes. (**E**) Fold change gene expression of preadipocyte marker *Pref1* in inguinal white adipose tissue (iWAT) in four feeding regimes. (**F**) Fold change gene expression of preadipocyte marker *Pref1* in epididymal white adipose tissue (eWAT) in

four feeding regimes. **C** – **F** were analyzed by one-way ANOVA (Dunn-Šidák correction). Data are presented as individual values and means ± standard deviation, n = 5 (biological replicates). CD = control diet, HFD = high-fat diet, pf = pair-fed.

We then investigated whether one week of CD or one week of pfHFD feeding could reverse the trend of reduced gene expression of terminal differentiation markers in differentiated primary adipocytes from obese mice. Previously, we observed only minimal restoration of the adipogenic potential on a morphological level. However, changes at the gene level may be more easily detected sooner. We fed mice with a body mass of at least 40 g a one-week CD or pfHFD, which contained the same caloric quantity as the CD. In inguinal primary adipocytes, we observed no significant restoration of the differentiation potential after feeding obese mice a one-week CD (**Figure 6 A** and **Figure S3 A**). Despite a huge variation between individual mice after one-week pfHFD feeding (**Figure S3 A**), the mean values of terminal differentiation markers of nearly all selected genes indicated an enhanced differentiation capacity (**Figure 6 A**). Interestingly, we also found an acceleration in the differentiation potential of epididymal primary adipocytes when examining the mean values of the terminal differentiation markers during a one-week CD feeding, but not pfHFD, in contrast to HFD feeding (**Figure 6 B** and **Figure S3 B**). Examination of the preadipocyte marker *Pref1* in cultured primary adipocytes demonstrated a consistent gene expression pattern with the set of terminal differentiation markers (**Figure 6 A** – **C**, and **E**). Analysis of *Pref1* expression in the entire tissue of iWAT and eWAT revealed distinct patterns in response to short-term obesity interventions in iWAT (**Figure 6 D and F**). In iWAT, one-week CD feeding restored *Pref1* expression to levels comparable to the control group, whereas one-week pfHFD reduced its expression.

Our results highlighted the diverse behaviors of inguinal and epididymal SVF cells and WAT in response to diet quality. The fat depots responded differently to variations in diet quality, rather than solely quantity. The differentiation capacity of inguinal primary adipocytes increased in average when obese mice were fed a one-week pfHFD, but not CD. In contrast, epididymal primary adipocytes showed an increase in their adipogenic potential when obese mice were fed a low-fat CD for one week, whereas feeding a one-week pfHFD did not restore the adipogenic potential of these cells.

3.1.5 High-fat diet increases the frequency of adipogenesis-regulatory cell in epididymal primary adipocytes

The preadipocyte pool consists of several subpopulations. $CD142^+$ APCs have gained recent attention due to their inhibitory properties on adipocyte differentiation, leading to their designation as adipogenesis-regulatory cells (Aregs) (Schwalie et al., 2018). $CD142^+$ Aregs and vascular adhesion protein 1-positve ($VAP1^+$) preadipocytes are committed preadipocytes and give

rise to differentiated mature adipocytes. As CD142$^+$ and VAP1$^+$ subpopulations can transit into one another in mice (Ferrero et al., 2020; Merrick et al., 2019), we concentrated our examinations on both preadipocytes. Additionally, we were interested in changes in the CD55$^+$ adipose stem cell pool, as they give rise to both CD142$^+$ Aregs and VAP1$^+$ preadipocytes (Ferrero et al., 2020).

We detected alterations in terminal differentiation at the histological level of eWAT and at the gene expression level of epididymal primary adipocytes following HFD feeding (see 3.1.2 and 3.1.4). To clarify differences in subpopulations and obesity-induced cell fate determination in inguinal and epididymal SVF cells of control mice and mice with a body mass of at least 40 g, we performed flow cytometry analysis (Schwalie et al., 2018). We analyzed the three distinct subpopulations of unfixed isolated SVF cells (**Figure 7 A** and **C**). In inguinal SVF cells, we observed no changes in the frequency of CD142$^+$ Areg subpopulation in Lineage-negative/stem cells antigen 1-positive (Lin$^-$/SCA1$^+$) cells between CD and HFD feeding (**Figure 7 A**). In line with the notion of CD142$^+$ Aregs being able to convert to VAP1$^+$ preadipocytes and *vice versa*, we observed that two-third of all CD142$^+$ cells were also VAP1$^+$ cells (data not shown), highlighting their shared origins as committed preadipocytes. Additionally, we detected a decrease of CD55$^+$ adipose stem cells and an increase of VAP1$^+$ preadipocytes in HFD-fed mice compared to CD-fed mice (**Figure 7 A**), demonstrating an ongoing transition and differentiation form CD55$^+$ adipose stem cells into VAP1$^+$ preadipocytes following HFD feeding. In contrast, we detected more CD55$^+$ adipose stem cells and fewer VAP1$^+$ preadipocytes undergoing differentiation to mature adipocytes in control mice (**Figure 7 A**). This demonstrated that CD feeding resulted in fewer adipose stem cells and preadipocytes that needed to progress in their trajectory to expand the tissue and provide more energy storage. To demonstrate the robustness of these findings, we performed the same analysis on fixed isolated SVF cells using a different antibody-staining panel. Flow cytometry analyses on fixed samples (**Figure 7 B**) were consistent with the unfixed experimental setup, verifying previous findings. Generally, inguinal SVF cells displayed proper differentiation potential in response to HFD at all investigated subpopulation levels. At the CD55$^+$ adipogenic stem cell level, we observed a reduced frequency following HFD feeding. At the VAP1$^+$ preadipocyte level, we demonstrated an increase, and on the CD142$^+$ Areg level, we showed no alterations in the frequency of the subpopulation following HFD feeding. The proper differentiation occurred as CD55$^+$ adipogenic stem cells differentiated into VAP1$^+$ preadipocytes, resulting in a depletion of the CD55$^+$ pool and an increase in the VAP1$^+$ pool. As the CD142$^+$ pool remained unchanged, Aregs were not able to inhibit angiogenesis significantly. Therefore, HFD feeding activated the differentiation process in inguinal SVF cells to produce primary adipocytes from CD55$^+$ adipogenic stem cells to VAP1$^+$ preadipocytes. The adipogenic potential was not diminished in inguinal SVF cells following HFD feeding.

Contrary, we observed a 2-fold increase of differentiation inhibitory CD142$^+$ Aregs in epididymal Lin$^-$/SCA1$^+$ cells following HFD (**Figure 7 C** and **D**). The CD55$^+$ adipogenic stem cell and VAP1$^+$ preadipocyte subpopulations of Lin$^-$/SCA1$^+$ cells remained unchanged when comparing CD to HFD. For epididymal SVF cells, approximately 80 % of CD142$^+$ cells were also VAP1$^+$ (data not shown). This showed the close association between these two types of committed preadipocyte. The findings were consistent across both unfixed and fixed sample preparations using a modified antibody-staining panel, demonstrating the robustness of these results. The elevated CD142$^+$ Areg frequency combined with no decrease in CD55$^+$ adipose stem cells and no increase in VAP1$^+$ preadipocytes confirmed the lack of further processing towards mature adipocytes in epididymal SVF cells. The unchanged frequency of CD55$^+$ adipogenic stem cells and their failure to differentiate into VAP1$^+$ preadipocytes, along with the inhibitory effect of increased CD142$^+$ Aregs on adipogenesis, indicated a reduced adipogenic potential in SVF cells of eWAT. Our data aligned with previous observations in ob/ob mice and diet-induced obese mice, showing an increase in Aregs in obese mice in compared to lean mice (Merrick et al., 2019; Schwalie et al., 2018). In conclusion, Aregs are the main factor contributing to a reduced adipogenic potential. The increased CD142$^+$ Areg subpopulation was accompanied by the previously observed lowered differentiation capacity. Our data showed that HFD feeding determines the cell fate decision and thus affects the adipogenesis.

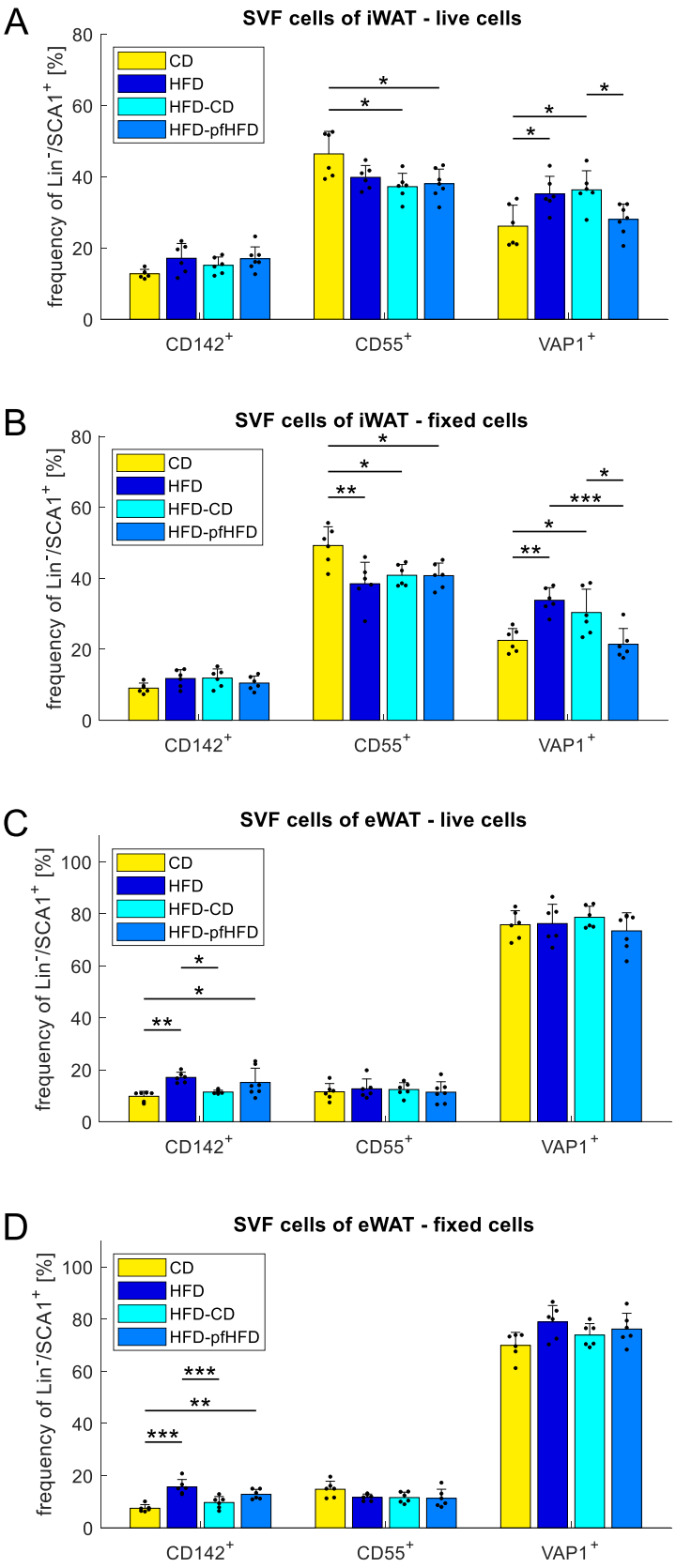

Figure 7: Influence of obesity and short-term control diet or pair-fed high-fat diet on the determination of cell fate in stromal-vascular fraction cells. Flow cytometry analysis of live and fixed stromal-vascular fraction (SVF) cells from inguinal (iWAT) and epididymal white adipose tissue (eWAT) in four feeding regimes. (**A**) Fraction of CD142$^+$, CD55$^+$ and VAP1$^+$ cells in the Lin$^-$/SCA1$^+$ population of unfixed SVF cells of iWAT. (**B**) Fraction of CD142$^+$, CD55$^+$ and VAP1$^+$ cells in the Lin$^-$/SCA1$^+$ population of fixed SVF cells of iWAT. (**C**) Fraction of CD142$^+$, CD55$^+$ and VAP1$^+$ cells in the Lin$^-$/SCA1$^+$ population of

unfixed SVF cells of eWAT. (**D**) Fraction of CD142$^+$, CD55$^+$ and VAP1$^+$ cells in the Lin$^-$/SCA1$^+$ population of fixed SVF cells of eWAT. All data were analyzed by one-way ANOVA (Dunn-Šidák correction). Data are presented as individual values and means ± standard deviation, n = 6 (biological replicates). * = $p < 0.05$, ** = $p < 0.01$, *** = $p < 0.001$. CD = control diet, HFD = high-fat diet, Lin = Lineage, pf = pair-fed, SCA1 = stem cells antigen 1, VAP1 = vascular adhesion protein 1.

To clarify whether feeding obese mice for one week CD or pfHFD is sufficient to restore subcellular composition of resident preadipocytes in WAT, we implemented a caloric restriction in mice with a minimum body mass of 40 g. Additionally, we distinguished between dietary quality by using CD or pfHFD for caloric restriction following HFD feeding. Analysis of inguinal SVF cells revealed no changes in the abundance of CD142$^+$ Aregs with either diet, or in unfixed and fixed sample preparations (**Figure 7 A** and **B**). The frequency of CD55$^+$ adipogenic stem cells remained comparable to HFD feeding after one week of CD or pfHFD, and was therefore reduced in comparison to the control group (**Figure 7 A** and **B**). For one week of CD, the frequency of VAP1$^+$ preadipocyte subpopulation was similar to the HFD group. Therefore, feeding mice with a body mass greater than 40 g for one week of CD resulted in well-differentiating cells with CD55$^+$ adipogenic stem cells giving rise to VAP1$^+$ preadipocytes and no inhibition of the adipogenic potential by increased CD142$^+$ Areg frequencies. After one week of pfHFD, we observed a reduction in VAP1$^+$ preadipocyte frequencies compared to HFD feeding (**Figure 7 A** and **B**). As the committed preadipocyte pool normalized to the control group, it indicated a reduced demand for new VAP1$^+$ preadipocytes that can differentiate into mature adipocytes. However, the CD55$^+$ adipogenic stem cell subpopulation was still decreased compared to the control group, indicating their ongoing development into committed preadipocytes and differentiation into mature adipocytes caused by caloric reduction with a fat-rich diet. In epididymal SVF cells, we demonstrated a reduction of CD142$^+$ Aregs in both sample preparations upon feeding obese mice for one week of CD (**Figure 7 C** and **D**). Using pfHFD for obesity intervention had no reverse effect on the adipogenic potential, as CD142$^+$ Areg frequency remained as high as in the HFD group. The frequency of CD55$^+$ adipogenic stem cells and VAP1$^+$ preadipocytes in the Lin$^-$/SCA1$^+$ population remained unchanged when comparing all four different feeding regimes (**Figure 7 C** and **D**), indicating the importance of CD142$^+$ Aregs in regulating the differentiation capacity.

With our findings, we proved an increase in the adipogenic potential of epididymal SVF cells of obese mice after just one week of feeding with CD. Furthermore, we demonstrated again the importance of diet-dependent caloric restriction. Only obesity intervention with a low-fat CD had a positive effect on the adipogenic potential of epididymal SVF cells. HFD feeding caused signals that reached the SVF cells and influenced their further progression. In iWAT, these signals resulted in an appropriate expansion of the fat depot through the development and differentiation of preadipocytes from adipogenic stem cells to mature adipocytes. However, in eWAT, HFD feeding also leads to inflammation, hypoxia, and insulin resistance (Hammarstedt

et al., 2018; Isakson et al., 2009), releasing further signals that inhibit the expansion of eWAT. These signals influence the composition of the subpopulations of eWAT and favor the inhibition of adipogenesis by increasing the frequency of Aregs. The elevated $CD142^+$ Areg frequency then interferes with the transition of $CD55^+$ adipogenic stem cells into $VAP1^+$ preadipocytes and mature adipocytes. Feeding obese mice a low-fat CD for one week stopped the inhibitory signal cascade and the Areg frequency decreased. As a result, the differentiation capacity increased again and the SVF cell composition started to normalize to control group levels, as demonstrated by our findings above.

3.1.6 High-fat diet feeding does not induce an *in vivo* proliferation arrest in stromal-vascular fraction cells

In our final step to investigate the adipogenic potential of SVF cells, we performed *in vivo* studies. Feeding mice HFD until they reach a minimum body mass of 40 g may exhaust the adipocyte progenitor pool, limiting further expansion of eWAT. We sought to resolve whether reaching the limit of eWAT expansion causes an *in vivo* proliferation stop of SVF cells. To investigate this, we injected control mice and obese mice with a body mass greater than 40 g with EdU for the last seven days to detect deoxyribonucleic acid (DNA) synthesis. Afterward, we examined previously studied SVF cell subpopulations and the frequency of their cells that were proliferating.

Comparing CD to HFD feeding, inguinal SVF cells showed no significant differences in the frequency of EdU^+ cells in the Lin-/$SCA1^+$ population (**Figure 8 A**). Both feeding regimes revealed a low proliferation rate, with approximately 1.7 % EdU^+ cells in the $Lin^-/SCA1^+$ population. Examining the three previously examined subpopulations of $Lin^-/SCA1^+$ cells demonstrated a similar, low abundance of EdU^+ cells upon CD and HFD feeding (**Figure 8 B** – **D**). However, there was a slight increase in EdU^+ cells in HFD-fed mice. Therefore, the proliferation potential was not impaired in inguinal SVF cells in response to HFD feeding. The low frequency of EdU^+ cells was expected, as the turnover of adipocytes is low (Spalding et al., 2008). A low percentage of EdU^+ cells of the $Lin^-/SCA1^+$ population was also detected in epididymal SVF cells of CD- and HFD-fed mice (**Figure 8 E**). The frequency of EdU^+ cells in the three studied subpopulations showed no substantial differences between epididymal SVF cells of CD- and HFD-fed mice (**Figure 8 F** – **H**). Only a minor reduction of EdU^+ cells was visible, representing a slight reduced proliferation potential mainly in $CD55^+$ adipocyte stem cells and $VAP1^+$ preadipocytes. Overall, in both tissue depots we did not observe an *in vivo* proliferation arrest, highlighting the importance of Aregs and its frequency in WAT in terms of a reduced adipogenic potential.

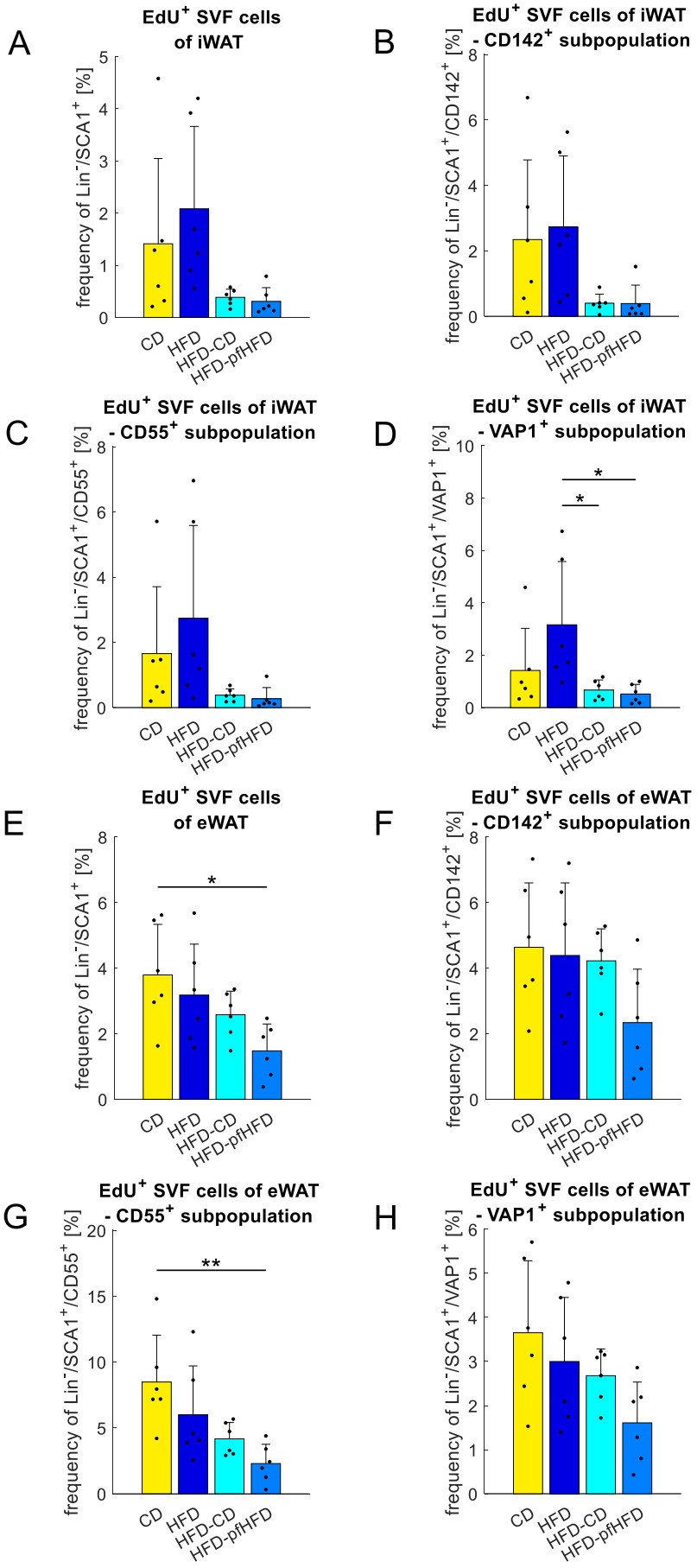
A
EdU+ SVF cells of iWAT
frequency of Lin-/SCA1+ [%]
B
EdU+ SVF cells of iWAT - CD142+ subpopulation
frequency of Lin-/SCA1+/CD142+ [%]
C
EdU+ SVF cells of iWAT - CD55+ subpopulation
frequency of Lin-/SCA1+/CD55+ [%]
D
EdU+ SVF cells of iWAT - VAP1+ subpopulation
frequency of Lin-/SCA1+/VAP1+ [%]
E
EdU+ SVF cells of eWAT
frequency of Lin-/SCA1+ [%]
F
EdU+ SVF cells of eWAT - CD142+ subpopulation
frequency of Lin-/SCA1+/CD142+ [%]
G
EdU+ SVF cells of eWAT - CD55+ subpopulation
frequency of Lin-/SCA1+/CD55+ [%]
H
EdU+ SVF cells of eWAT - VAP1+ subpopulation
frequency of Lin-/SCA1+/VAP1+ [%]
CD
HFD
HFD-CD
HFD-pfHFD
*
**

Figure 8: High-fat diet feeding does not affect the *in vivo* proliferation of stromal-vascular fraction cells. Flow cytometry analysis of fixed stromal-vascular fraction (SVF) cells from inguinal (iWAT) and epididymal white adipose tissue (eWAT) in four feeding regimes. (**A**) Fraction of proliferating (EdU^+) cells in the $Lin^-/SCA1^+$ population of SVF cells in iWAT. (**B**) Fraction of proliferating (EdU^+) cells in the $Lin^-/SCA1^+/CD142^+$ population of SVF cells in iWAT. (**C**) Fraction of proliferating (EdU^+) cells in the $Lin^-/SCA1^+/CD55^+$ population of SVF cells in iWAT. (**D**) Fraction of proliferating (EdU^+) cells in the $Lin^-/SCA1^+/VAP1^+$ population of SVF cells in iWAT. (**E**) Fraction of proliferating (EdU^+) cells in the $Lin^-/SCA1^+$ population of SVF cells in eWAT. (**F**) Fraction of proliferating (EdU^+) cells in the $Lin^-/SCA1^+/CD142^+$ population of SVF cells in eWAT. (**G**) Fraction of proliferating (EdU^+) cells in the $Lin^-/SCA1^+/CD55^+$ population of SVF cells in eWAT. (**H**) Fraction of proliferating (EdU^+) cells in the $Lin^-/SCA1^+/VAP1^+$ population of SVF cells in eWAT. All data were analyzed by one-way ANOVA (Dunn-Šidák correction). Data are presented as individual values and means ± standard deviation, n = 6 (biological replicates). * = $p < 0.05$, ** = $p < 0.01$. CD = control diet, HFD = high-fat diet, Lin = Lineage, pf = pair-fed, SCA1 = stem cells antigen 1, VAP1 = vascular adhesion protein 1.

We next examined the effect of one week of CD or pfHFD on cell proliferation. We sought to determine whether the adipogenic potential of SVF cells could be quickly restored by increased cell proliferation after just one week of reduced caloric intake, or whether adipogenic stem and precursor cells were only silenced by long-term HFD feeding and reprogrammed in response to low-fat CD refeeding, as previously shown. We also aimed to determine whether the proliferation rate in the short-term obesity intervention phase could be influenced by the quality of the diet, in terms of low- or high-fat content. We fed mice that weighed at least 40 g for one week of CD or pfHFD. In inguinal SVF cells, we found that both obesity interventions resulted in almost complete proliferation arrest, particularly in the $VAP1^+$ preadipocyte subpopulation (**Figure 8 A** – **D**). Thus, caloric restriction affected the inguinal APCs after just one week. The proliferation arrest was independent of diet quality, with only diet quantity being important. In epididymal SVF cells, we observed a slight reduction in the proliferation rate in the studied subpopulations when feeding obese mice for one week of CD (**Figure 8 E** – **H**). In contrast, feeding mice that weighed at least 40 g for one week of pfHFD resulted in decreased proliferation of the $Lin^-/SCA1^+$ population of epididymal SVF cells (**Figure 8 E**). The reduced proliferation rate was particularly evident in the $CD55^+$ adipose stem cell pool subpopulations (**Figure 8 G**) when compared to the control group. The caloric restriction of the HFD (pfHFD) was largely responsible for the reduction in proliferation potential in epididymal APCs. Feeding obese mice for one week with either control diet or pfHFD did not improve the proliferation rate.

The adipogenic potential of SVF cells in iWAT showed only minor diet-induced effects, while in epididymal SVF cells, the adipogenic potential was diminished by certain diets. The adipogenic potential of epididymal SVF cells in obese mice was decreased due to decreased differentiation capacity compared to the control group. The adipogenic potential in the HFD-CD group was restored through increased differentiation capacity and unchanged proliferation rate compared to the HFD group. In contrast, pfHFD feeding resulted in reduced adipogenic potential in epididymal SVF cells through decreased differentiation and proliferation capacity in comparison to the HFD group. Our findings highlighted fat depot-specific differences and the importance of diet composition, particularly on the adipogenic potential of epididymal SVF cells.

Additionally, we have demonstrated the significant role of high Areg frequency in reducing the adipogenic potential compared to low Areg frequency.

3.1.7 HFD feeding and short-term obesity intervention have pronounced impact on the proliferation and structure of eWAT

To visualize the effects of low-fat CD and HFD on the adipogenic potential in eWAT, we conducted 3D imaging. We stained for vessels ($CD31^+$) to assess the overall tissue structure, $CD45.2^+$ cells to identify immune cells, and EdU^+ cells to identify cells that had proliferated within the previous seven days.

Upon comparison of CD with HFD, we observed clear differences between lean and obese mice (**Figure 9 A**, **C**, and **D**). As previously seen in the flow cytometry data for epididymal SVF cells, we observed the highest proliferation rate in the CD group. We distinguished between vessel-associated and freely distributed EdU^+ preadipocytes by excluding immune cells and crown-like structures. Our findings supported the notion that most preadipocytes are located in close proximity to vessels (Cawthorn et al., 2012; Schwalie et al., 2018). In lean mice, we observed only a few infiltrating immune cells in the tissue (**Figure 9 A**). HFD feeding caused the formation of crown-like structures, which were characterized by an infiltration of numerous immune cells into the tissue to clear up cell debris and dying adipocytes (**Figure 9 A right**). In addition, it slightly reduced the *in vivo* proliferation rate, particularly for tissue-distributed preadipocytes (**Figure 9 D**). However, we did not observe an *in vivo* proliferation stop in obese mice. As the Areg population increased with HFD feeding, we were able to demonstrate their global effect on preadipocytes in the whole tissue, with a mild influence on proliferation and a strong impact on differentiation capacity.

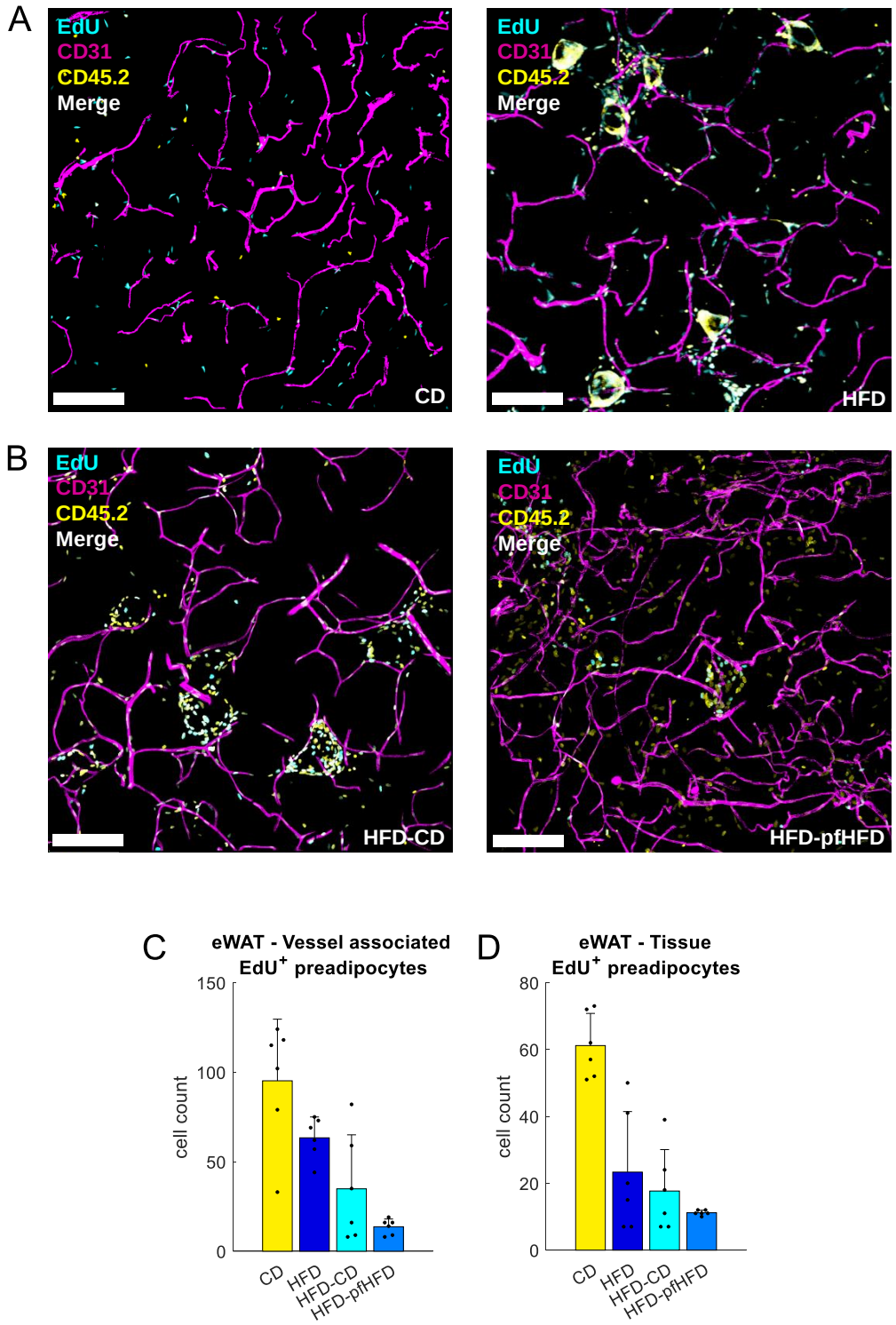

Figure 9: The effects of obesity and short-term control diet or pair-fed high-fat diet on the morphology of epididymal white adipose tissue. Randomly chosen Z-stacks of epididymal white adipose tissue (eWAT) after *in vivo* treatment with 5-ethynyl-2'-deoxyuridine (EdU) for seven days. (**A**) Example of eWAT from control diet (CD) (left) and high-fat diet (HFD) (right). Scale bar 100 µm (**B**) Example of eWAT from HFD-CD (left) and HFD-pair-fed (pf) HFD (right). Scale bar 100 µm (**C**) Vessel-associated EdU⁺ preadipocytes. (**D**) Non-vessel and non-crown-like structure associated separated EdU⁺ preadipocytes. **C** and **D** are presented as individual values and means ± standard deviation, N = 6 (technical replicates) of n = 2 (biological replicates). blue = EdU, pink = CD31, yellow = CD45.2, white = merge.

While investigating mice with body mass greater than 40 g that received either CD or pfHFD for one week, we observed diet-dependent differences (**Figure 9 B**, **C**, and **D**). In both short-

term obesity intervention groups, a huge number of crown-like structures were present (**Figure 9 B**). In the HFD-pfHFD group, there was also a notable infiltration of immune cells in the tissue in addition to the crown-like structures (**Figure 9 B right**). Furthermore, the vasculature structures in the HFD-pfHFD group were deteriorated, with numerous small branches present. In line with our previous data, we confirmed slight reductions in *in vivo* proliferation rates in both obesity intervention groups (**Figure 9 C** and **D**).Thereby, the proliferation reduction was more dominant in the HFD-pfHFD group compared to the HFD-CD group.

The findings from 3D imaging of eWAT indicated that obesity had a global impact on eWAT structure, including immune cell infiltration and slightly reduced *in vivo* proliferation in response to HFD feeding. These results corroborated and extended our previous findings in the SVF. Furthermore, the influence of diet quality on obesity intervention was demonstrated. While caloric restriction with a HFD resulted in massive immune cell infiltration, vascular deterioration, and a near complete proliferation stop of preadipocytes, these negative effects were not observed with CD. These findings suggest that body mass reduction may be more sustainable and beneficial when achieved through low-fat CD rather than energy-restricted HFD.

3.2 Diminished mitochondrial function of epididymal adipocytes in diet-induced obese mice persists after complete remission from obesity

The pathological expansion of WAT and positive energy balance not only affects the adipogenic potential of preadipocytes, but also reduces the mitochondrial function of adipocytes. Thus, HFD feeding in mice has been shown to impair mitochondrial fission activity, bioenergetics, and alterations in mitochondrial protein expression (Schottl et al., 2015b; Schottl et al., 2020; Tol et al., 2016). Certain alterations in mitochondrial architecture are not reversible even after initial body mass loss (Schottl et al., 2015b). We aimed to investigate persistent mitochondrial alterations after complete remission from obesity with a low-fat CD. Additionally, we were interested in their potential contribution to handle again an obesogenic environment and thereby contributing to body mass cycling, coined as ‘yo-yo effect’.

3.2.1 Body mass and fat mass normalize during control diet-induced obesity remission

Diet-induced obesity causes a fat depot-specific reduction in mitochondrial function. A decrease in respiratory capacity and mitochondrial integrity in eWAT remains even after one week of CD feeding (Schottl et al., 2015b). For investigating whether this effect is reversible

after the mice have reestablished a lean body and fat mass, body mass and composition were continuously determined during an eight-week long return to CD after established, diet-induced obesity.

Body mass, fat mass and fat depot masses increased drastically during HFD feeding (**Figure 10 A** – **D**, **I**, and **J**). However, body mass adjusted fat mass showed no differences between CD and HFD feeding (**Figure 10 E** and **F**). The adjusted fat mass demonstrated an appropriate fat mass for the body mass at any time. Furthermore, body composition analysis detected no differences in lean mass after 24 weeks of HFD feeding compared to CD feeding (**Figure 10 G** and **H**). The eWAT depot accumulated a similar mass in both diet groups, consistent with a eWAT plateau in mice at around 40 g body mass (van Beek et al., 2015).

After eight weeks of CD-induced obesity remission, the body mass and fat mass of the HFD-CD group had normalized to levels comparable to the CD group (**Figure 10 A** – **D**). Additionally, the iWAT mass of the HFD-CD group was again comparable to that of the CD group (**Figure 10 I**), while the eWAT mass had decreased below that of the CD group (**Figure 10 J**). The adjusted fat mass showed differences already four weeks after the diet switch from age 40 weeks (data not shown) until the end of the experiment when comparing the HFD and HFD-CD groups (**Figure 10 F**). The lean mass remained unchanged throughout the experiment (**Figure 10 G** – **H**).

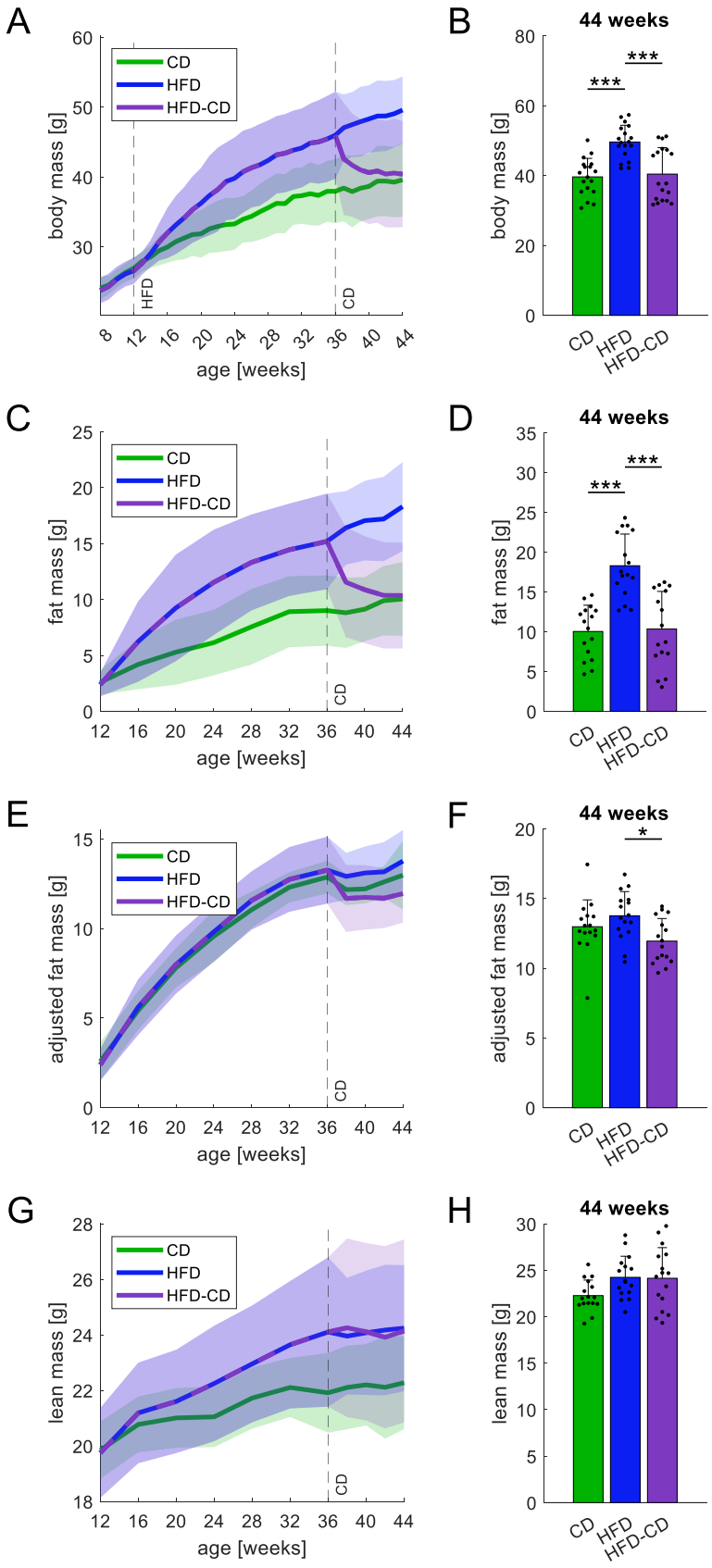

Continue page 53

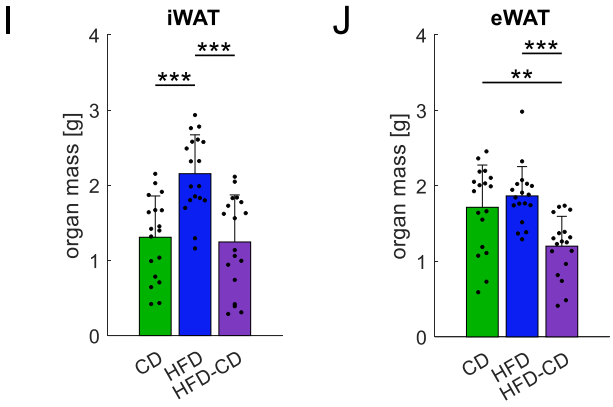

Figure 10: Normalization of body mass and fat mass during control diet-induced obesity remission on a low-fat control diet. All male C57BL/6N mice received a control diet (CD) at 8 weeks of age. High-fat diet (HFD) feeding started at 12 weeks of age for mice in the HFD and HFD-CD groups. CD-induced obesity remission began at 36 weeks of age for HFD-CD mice. (**A**) Body mass development between 8 and 44 weeks of age. Body mass was determined weekly. (**B**) Comparison of body mass at 44 weeks of age between the three feeding regimes. (**C**) Fat mass development between 12 and 44 weeks of age. Fat mass was measured monthly until 36 weeks of age and biweekly thereafter. (**D**) Comparison of fat mass at 44 weeks of age between the three feeding regimes. (**E**) ANCOVA-adjusted fat mass development between 12 and 44 weeks of age. Fat mass was measured monthly until 36 weeks of age and biweekly thereafter. (**F**) Comparison of ANCOVA-adjusted fat mass at 44 weeks of age between the three feeding regimes. (**G**) Lean mass development between 12 and 44 weeks of age. Lean mass was measured monthly until 36 weeks of age and biweekly thereafter. (**H**) Comparison of lean mass at 44 weeks of age between the three feeding regimes. (**I**) Organ mass of inguinal white adipose tissue (iWAT). (**J**) Organ mass of epididymal white adipose tissue (eWAT). **B**, **D**, **F**, **H**, **I**, and **J** were analyzed by one-way ANOVA (Dunn-Šidák correction). Data are presented as individual values and means ± standard deviation, n = 16 (**C** – **H**) – 18 (**A**, **B**, **I**, **J**) (biological replicates). * = $p < 0.05$, ** = $p < 0.01$, *** = $p < 0.001$.

Overall, HFD feeding resulted in an increase in body mass, fat mass, and iWAT mass without a corresponding increase in lean mass and with an appropriate adjusted fat mass. CD-induced obesity remission reduced body mass, fat mass, and organ mass to levels comparable to the control group.

3.2.2 Diminished mitochondrial capacity and content persist in epididymal adipocytes after body mass and fat mass normalization

Body mass, fat mass, and organ mass were comparable or even reduced to the levels observed in the CD group after eight weeks of CD-induced obesity remission. In this setting, we analyzed the capacity, content, and integrity of mitochondrial to investigate whether a long-term CD-induced obesity remission restores mitochondrial function of epididymal adipocyte mitochondria. Therefore, we measured the mitochondrial respiration (state 3 and 4) of permeabilized inguinal and epididymal adipocytes. Mitochondrial integrity was calculated using the respiratory control ratio (RCR), and mitochondrial content was determined using a citrate synthase (CS) activity assay.

There were no differences in respiration rates (state 3 and 4) in inguinal adipocytes among the three feeding groups (**Figure 11 A**). Additionally, mitochondrial abundance (**Figure 11 B**) and RCR (**Figure 11 C**) remained unchanged among the three different feeding groups. However, respiratory rates were reduced in epididymal adipocytes upon HFD feeding and remained diminished after an eight-week CD-induced obesity remission phase (**Figure 11 D**). Analysis of mitochondrial content via CS activity revealed a reduction in the HFD group. This reduced mitochondrial abundance per cell did not recover after CD-induced obesity remission and remained unchanged compared to the HFD group (**Figure 11 E**). The RCR, which is independent of mitochondrial mass, was also reduced in the HFD group and did not recover upon CD-induced obesity remission (**Figure 11 F**). Therefore, respiratory rates were not only diminished by a reduced mitochondrial abundance, but also by respiratory capacity itself.

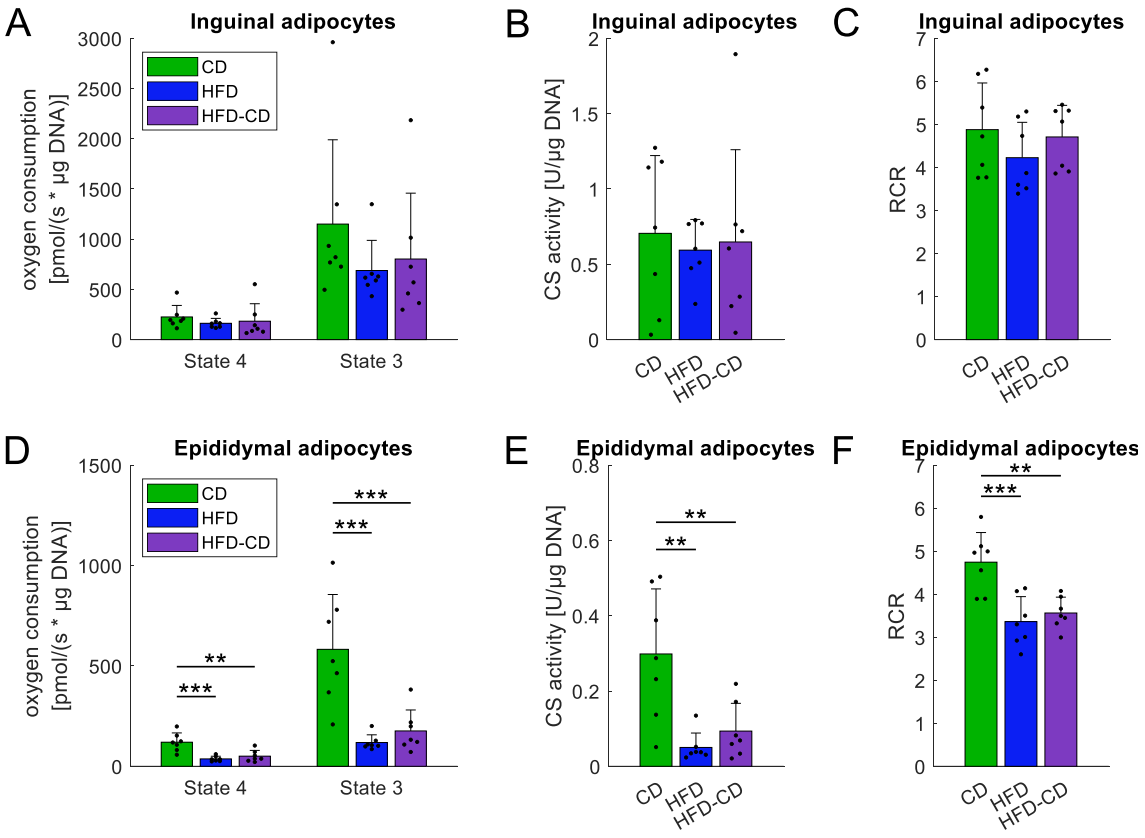

Figure 11: Diminished mitochondrial capacity, content, and integrity persist in epididymal adipocytes. (**A**) Bioenergetics of α-chaconine permeabilized inguinal adipocytes in the presence of substrates (pyruvate, malate, succinate). State 4 represents substrate-only respiration. Phosphorylating state 3 respiration was assessed in the presence of substrates and adenosine diphosphate (ADP). Non-biological background respiration was subtracted from respiration rates after electron flow at complex III was blocked with antimycin A. Respiration rates were normalized to deoxyribonucleic acid (DNA) content of inserted cells. (**B**) Citrate synthase (CS) activity measurements of inguinal adipocytes. CS activity was normalized to DNA content. (**C**) Respiratory control ratio (RCR) of inguinal adipocytes, defined as the ratio of state 3 to state 4 respiration. (**D**) Bioenergetics of α-chaconine permeabilized epididymal adipocytes in the presence of substrates (pyruvate, malate, succinate). State 4 represents substrate-only respiration. State 3 is respiration in the presence of substrates and ADP. Non-biological background respiration was subtracted from respiration rates after electron flow at complex III was blocked with antimycin A. Respiration rates were normalized to DNA content of inserted cells. (**E**) CS activity measurements of epididymal adipocytes. CS activity was normalized to DNA content. (**F**) RCR of epididymal

adipocytes, defined as the ratio of state 3 to state 4 respiration. Data were analyzed by one-way ANOVA (Dunn-Šidák correction). Data are presented as individual values and means ± standard deviation, n = 7 (biological replicates). ** = $p < 0.01$, *** = $p < 0.001$. CD = control diet, HFD = high-fat diet.

These findings clearly demonstrated that HFD feeding had far-reaching consequences on epididymal adipocyte mitochondria that were not reversed in the short-term by reducing body and fat mass. In contrast, inguinal adipocyte mitochondria were resilient to the HFD challenge with no effect on respiratory capacity and abundance.

3.2.3 Obesity has no effects on the oxidative phosphorylation protein expression

As reduced mitochondrial function persisted in epididymal adipocytes after restoration of control mass, we examined the effects on oxidative phosphorylation complexes. To detect whether there is compensation of protein expression levels, we investigated whole tissue and SVF cells.

Western blot analysis of subunits from complexes II to V revealed only minor changes in adipocytes, whole tissue, and SVF cells of both fat depots due to HFD feeding and CD-induced obesity remission (**Figure 12 A** – **F**). Only complex II of inguinal mature adipocytes showed reduced expression upon HFD feeding and recovery upon CD-induced obesity remission (**Figure 12 A**). Protein expression of the oxidative phosphorylation complexes was stable between all three feeding groups in the whole tissue samples **(Figure 12 B** and **E**). Interestingly, SVF cells nearly had no complex II expression (**Figure 12 C** and **F**). This is in line with a diminished role of oxidative phosphorylation in highly proliferative cells (DeBerardinis et al., 2008). Additionally, inguinal SVF cells slightly reduced expression of all four detected complexes upon HFD, while epididymal SVF cells slightly increased expression of oxidative phosphorylation complexes (**Figure 12 C** and **F**). CD-induced obesity remission mostly affected complex expression in a direction similar to the CD group. Investigation of the ratio of total protein per organ mass (**Figure 12 H** and **I**) also revealed no differences caused by obesity or CD-induced obesity remission.

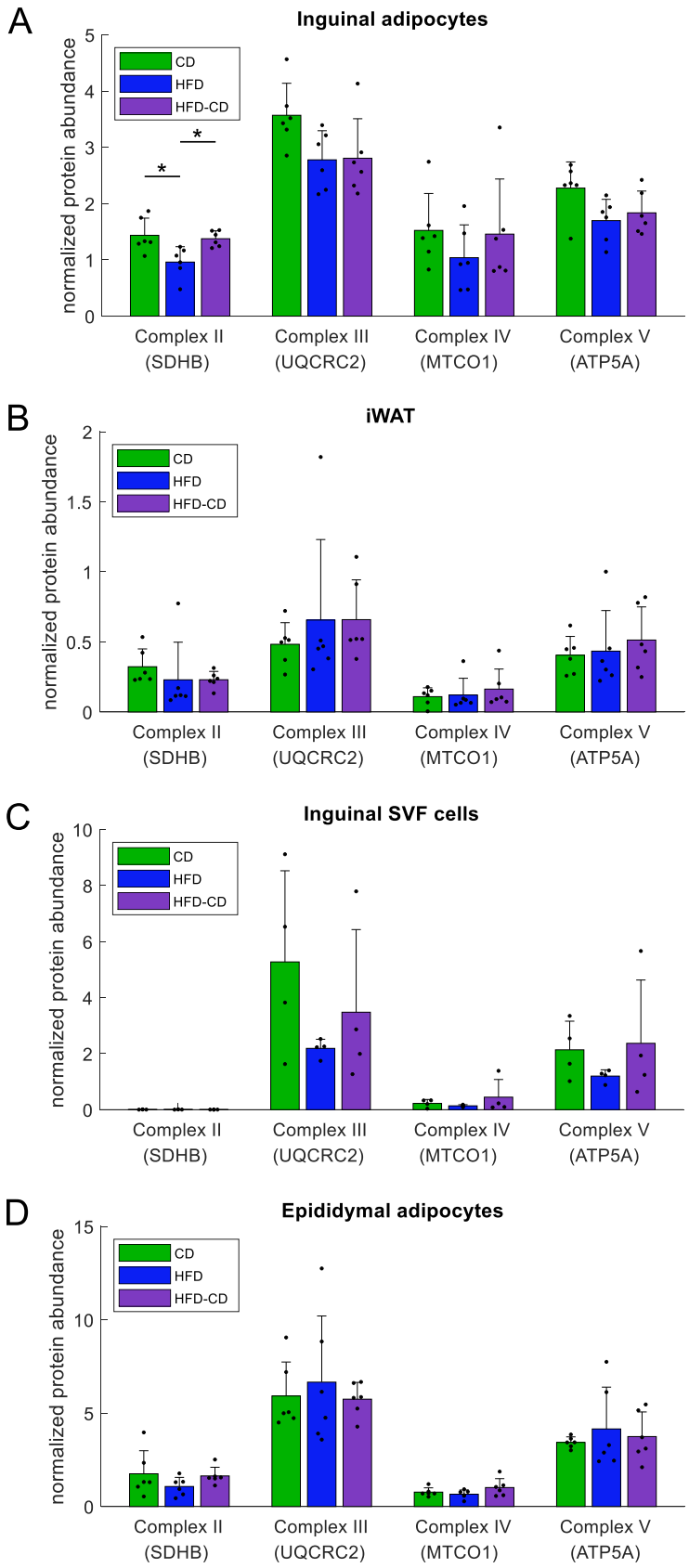

Continue page 57

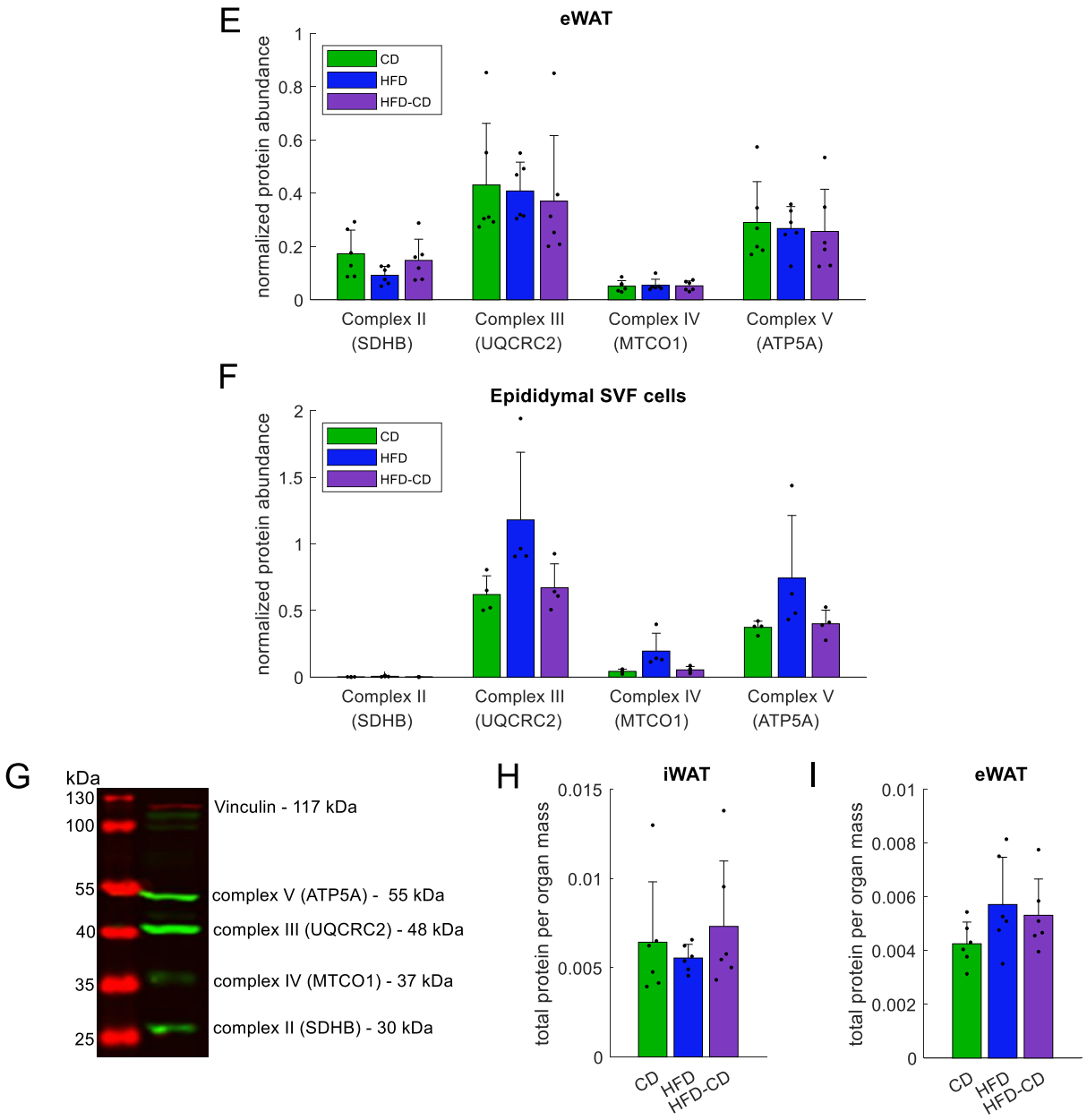

Figure 12: Minor changes in protein expression of oxidative phosphorylation complexes. Western blot analysis of oxidative phosphorylation complexes. Complex signals were normalized to vinculin signal. (**A**) Inguinal adipocytes. (**B**) Inguinal white adipose tissue (iWAT). (**C**) Inguinal stromal-vascular fraction (SVF) cells. (**D**) Epididymal SVF cells. (**E**) Epididymal white adipose tissue (eWAT). (**F**) Epididymal SVF cells. (**G**) Example of eWAT western blot with oxidative phosphorylation and vinculin antibodies. (**H**) Total protein per organ mass ratio of iWAT. (**I**) Total protein per organ mass ratio of eWAT. Data were analyzed by one-way ANOVA (Dunn-Šidák correction). Data are presented as individual values and means ± standard deviation, n = 4 (**C**, **F**) – 6 (**A**, **B**, **D** – **F**, **H**, and **I**) (biological replicates). * = $p < 0.05$. CD = control diet, HFD = high-fat diet.

In summary, the expression of subunits of mitochondrial oxidative phosphorylation complexes, as well as the total protein abundance per organ mass, were largely unaffected by diet. These findings showed that other factors, such as additional proteins or signals from primary adipocytes, play an important role in the regulation of mitochondrial capacity and abundance in mature adipocytes.

3.2.4 Obesity causes no mitochondrial protein expression changes

Extending our analysis beyond oxidative phosphorylation complexes, we sought to identify mitochondrial pathways and proteins that could lead to differences in mitochondrial integrity and abundance. We performed mass spectrometry on inguinal and epididymal adipocytes to identify additional mitochondrial proteins and gain a deeper understanding of the differences between inguinal and epididymal adipocytes.

When examining the principal component analysis (PCA) of inguinal adipocytes, we did not observe any clear clustering between lean mice, obese mice, and mice in CD-induced obesity remission (**Figure 13 A**). In contrast, the PCA of epididymal adipocytes showed a clear separation in protein expression between the CD and HFD groups (**Figure 13 B**). The CD-induced obesity remission mice displayed intermediate protein expression between the CD and HFD groups in the PCA. The hierarchical clustering analysis showed no separation between the three feeding groups in inguinal adipocytes, but a clear distinction was observed between the groups in epididymal adipocytes (**Figure 13 C** and **13 D**). No significant expressed proteins were identified when comparing CD-induced obesity remission mice with control mice in inguinal adipocytes (data not shown). The epididymal adipocytes exhibited two major patterns, one comprising non-mitochondrial proteins and the other comprising mitochondrial proteins (**Figure 13 D**). However, to our surprise, when evaluating biologically relevant proteins using a 1.5-fold cutoff, a coefficient of variation less than 0.5, and differently regulated proteins ($p < 0.05$) for HFD versus CD and HFD-CD versus CD mice, we did only observe one single mitochondrial protein (upregulation: FTH1) that differed between obesity-recovered and control mice (**Figure 13 E**). The analysis of proteins exhibiting significant differences with a 1.5-fold change in epididymal adipocytes at the cellular level revealed the differential regulation of 18 non-mitochondrial proteins (downregulation: SORBS1, DGAT2, CLMP, SZT2, TRIM14, ATXN2, PHLDA3; upregulation: SH3BGRL3, SERPINB6B, SLC37A2, RCC2, GC, HPX, CD9, NUP210, FAM129B, AS3MT, EFHD2) that differed between obese mice or those undergoing CD-induced obesity remission and control mice. The downregulated proteins were predominantly involved in processes such as adipocyte differentiation (SORBS1, CLMP, ATXN2, PHLDA3) (Eguchi et al., 2005; Song et al., 2021; Yang et al., 2003; Yousof et al., 2022) and lipid metabolism (DGAT2, TRIM14) (Cases et al., 1998; Xu et al., 2019). The upregulated proteins were primarily related to processes such as increased adipose tissue mass (GC, FAM129B) (Mutt et al., 2014; Vazquez-Sandoval et al., 2023), adipose tissue fibrosis (CD9) (Marcelin et al., 2017), macrophage infiltration (SLC37A2) (Kim et al., 2007), mitosis (RCC2) (Yenjerla et al., 2013), elevated triglyceride levels (HPX) (Lawson et al., 2017), and oxidative stress in WAT (FTH1) (Moreno-Navarrete et al., 2014). Furthermore, the observed increase in ferritin heavy chain 1 (FTH1) expression is consistent with a prior study that linked dysregulated iron homeostasis to reduced adipogenic differentiation capacity (Moreno-Navarrete et al., 2014). The

limited number of proteins, out of the 104 significantly differentially regulated proteins, that exhibited a 1.5-fold difference suggests that alterations in protein expression alone may not entirely explain the sustained decline in mitochondrial function observed in obesity. Nevertheless, these identified protein candidates offered valuable insights into the impact of reduced adipocyte differentiation on mitochondrial function and warrant further investigation.

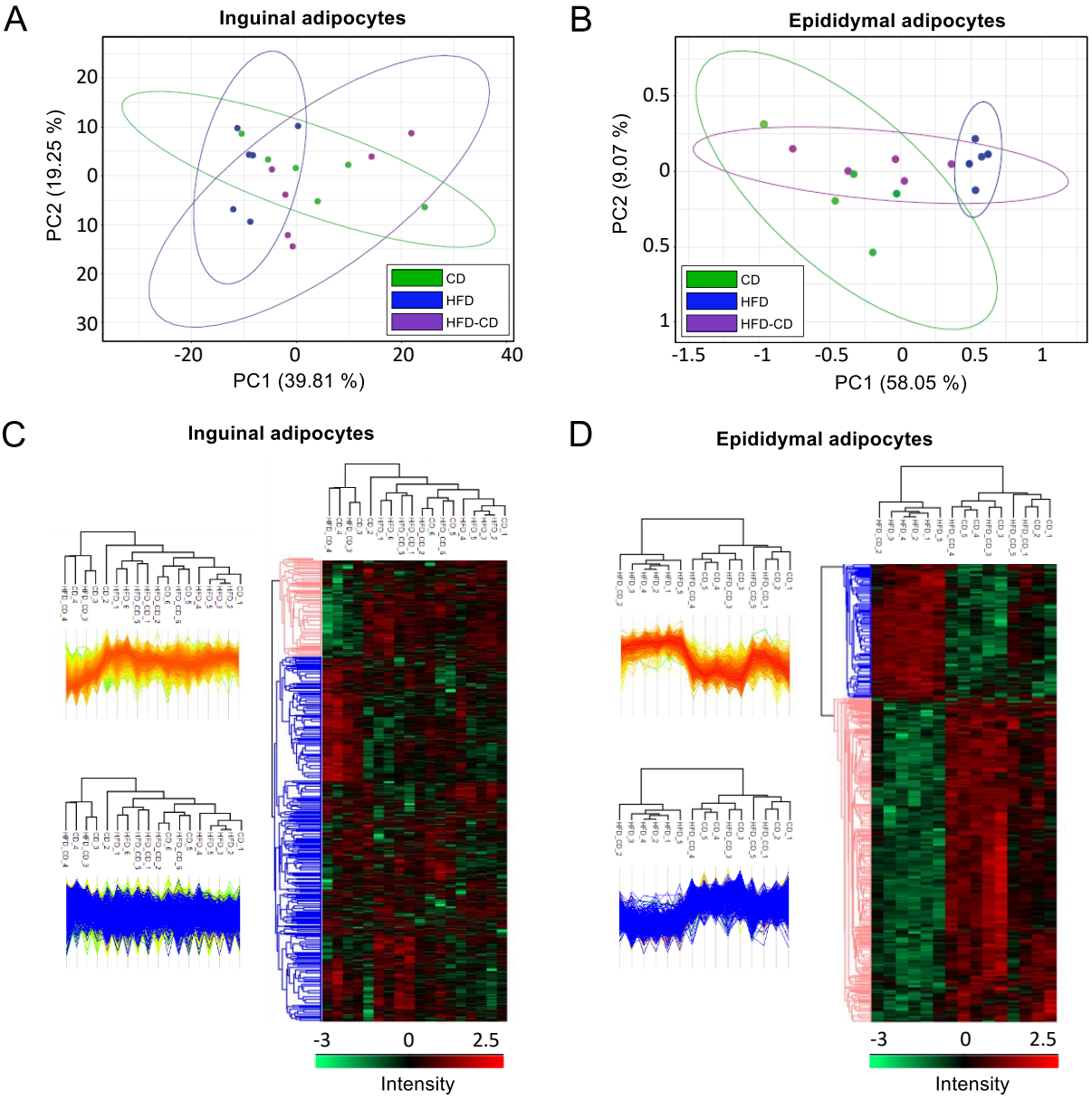
A
Inguinal adipocytes
PC2 (19.25 %)
PC1 (39.81 %)
CD
HFD
HFD-CD
B
Epididymal adipocytes
PC2 (9.07 %)
PC1 (58.05 %)
CD
HFD
HFD-CD
C
Inguinal adipocytes
-3
0
2.5
Intensity
D
Epididymal adipocytes
-3
0
2.5
Intensity

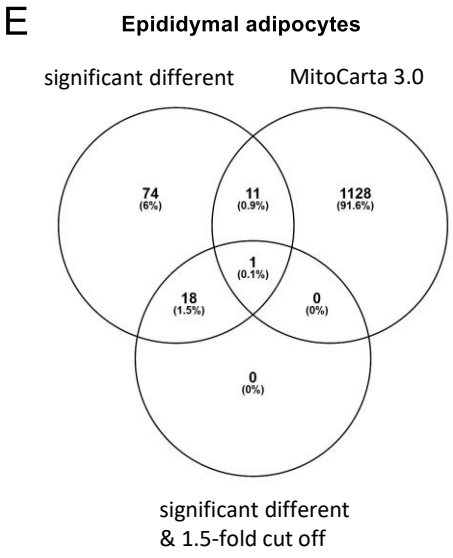
E
Epididymal adipocytes
significant different
MitoCarta 3.0
74
(6%)
11
(0.9%)
1128
(91.6%)
1
(0.1%)
18
(1.5%)
0
(0%)
0
(0%)
significant different
& 1.5-fold cut off

Figure 13: No changes in mitochondrial protein expression in inguinal and epididymal adipocytes. Mass spectrometry proteomics analysis of inguinal and epididymal adipocytes. Data were processed in Perseus. (**A**) Principal compound analysis (PCA) of inguinal adipocytes. (**B**) PCA of epididymal adipocytes. (**C**) Profile plots (left) and hierarchal-clustered heat map (right) of significantly expressed proteins in inguinal adipocytes. The dark blue lines on the profile plot represent the overlap with Gene Ontology Cellular Component (GOCC) terms associated with mitochondria. (**D**) Profile plots (left) and hierarchal-clustered heat map (right) of significantly expressed proteins in epididymal adipocytes. The dark blue lines on the profile plot represent the overlap with GOCC terms associated with mitochondria. (**E**) Vent diagram of significant different proteins in epididymal adipocytes, MitoCarta 3.0 proteins, and significant different proteins with 1.5-fold change in the high-fat diet-control diet (HFD-CD) versus CD group. Significant different proteins were defined as those with $p < 0.05$ for HFD versus CD groups and HFD-CD versus CD groups and a coefficient of variation less than 0.5 between the investigated feeding groups. Data are presented as individual values, n = 5 (epididymal adipocytes) – 6 (inguinal adipocytes) (biological replicates).

Our results showed that the decreased mitochondrial function was not primarily caused by changes in protein expression. Despite the fact that the epididymal adipocytes from obese mice clustered differently from those from lean mice, we did not observe significant changes in mitochondrial protein expression that could account for our previous findings. These findings suggest that signaling factors outside of mature adipocytes, such as from preadipocytes, may contribute to the reduction in mitochondrial function. Furthermore, our data demonstrated that the ability of primary adipocytes to differentiate was diminished in obese mice, and even mature adipocytes displayed decreased differentiation, implying a possible connection between primary and mature adipocytes that leads to a persistent reduction in both the quantity and quality of mitochondria within epididymal adipocytes.

3.2.5 High-fat diet refeeding doubles body mass and fat mass within the first two weeks in comparison to first time high-fat diet feeding

Body mass, composition, and organ masses normalized within an eight-week CD-induced obesity remission phase; even so, epididymal adipocyte mitochondria sustained irreversible alterations. Next, we examined the effect of body mass, body composition, and organ masses after a HFD refeeding period. We sought to determine whether mice that had undergone CD-induced obesity remission were more prone to HFD afterward. Therefore, mice received HFD for 12 weeks either following CD-induced obesity remission or for the first time.

Body mass, fat mass, and lean mass were comparable at 44 weeks of age (**Figure 14 A** – **D**, **I**, and **J**). Body mass and fat mass increased during the 12-week HFD feeding period in both groups (**Figure 14 A** – **D**), while lean mass only increased in the HFD-refed group (**Figure 14 I** and **J**). However, the rate of change in body mass and fat mass was two-fold higher within the first two weeks of HFD refeeding (HFD-CD-HFD group) compared to mice that were switched to HFD for the first time (CD-HFD group) (**Figure 14 E** and **F**), demonstrating that HFD-refed mice are more susceptible to an obesogenic environment. After four weeks of HFD feeding, CD-HFD mice exhibited a faster rate of change in body mass and fat mass compared

to HFD-CD-HFD mice, before both HFD groups demonstrated similar rate changes. Interestingly, the adjusted fat mass was consistent among all three feeding groups at any time point (**Figure 14 G** and **H**). These findings corroborated the notion that mice had an appropriate fat mass relative to their body mass when comparing the three feeding regimes. The organ mass of the iWAT depot significantly increased in the HFD refeeding group (**Figure 14 K**). In contrast, the eWAT depot remained largely unchanged in organ mass in both HFD groups (**Figure 14 L**), potentially due to the limited storage capacity of eWAT at body masses above 40 g (van Beek et al., 2015) and the different behaviors of the fat depots.

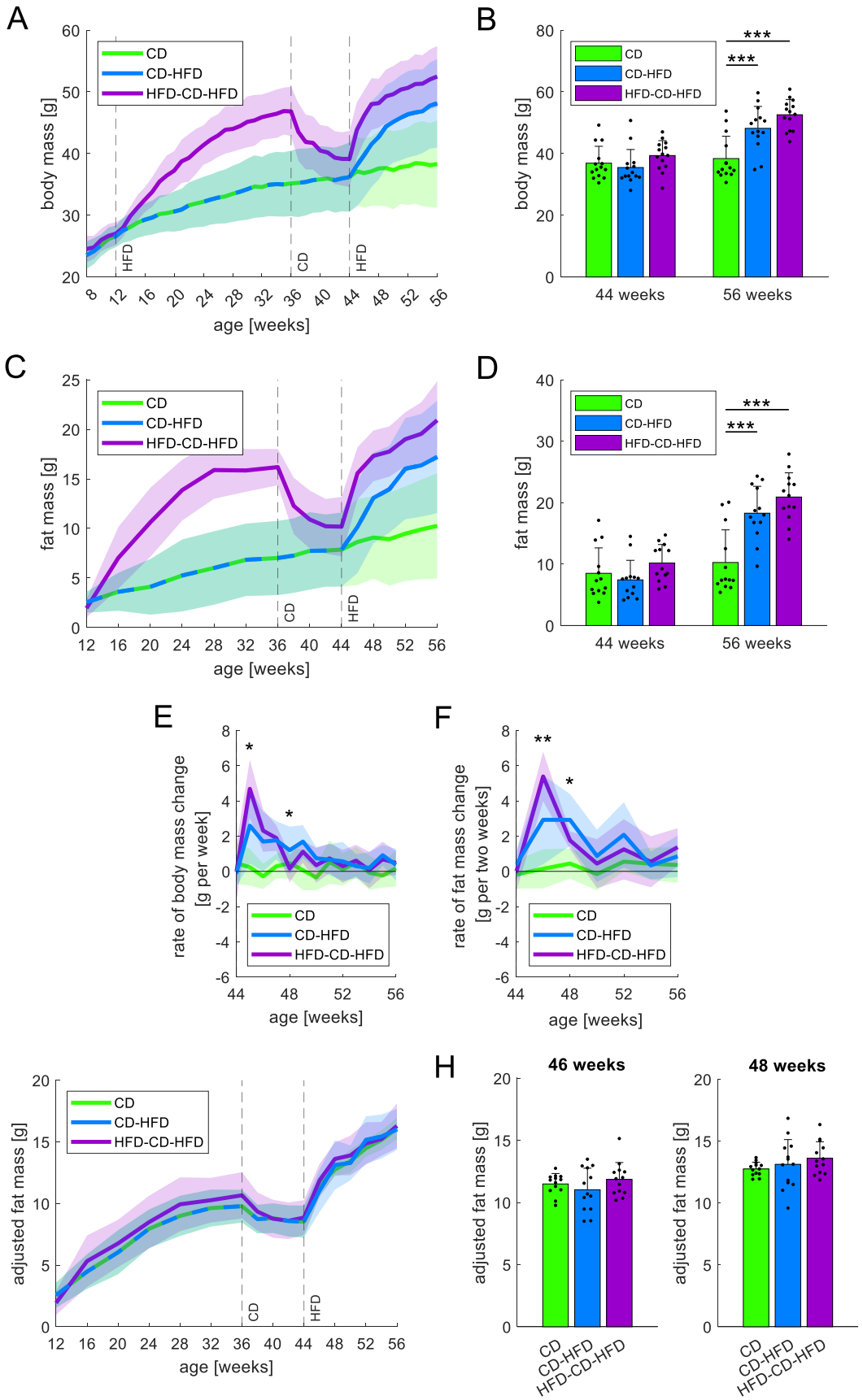

Continue page 64

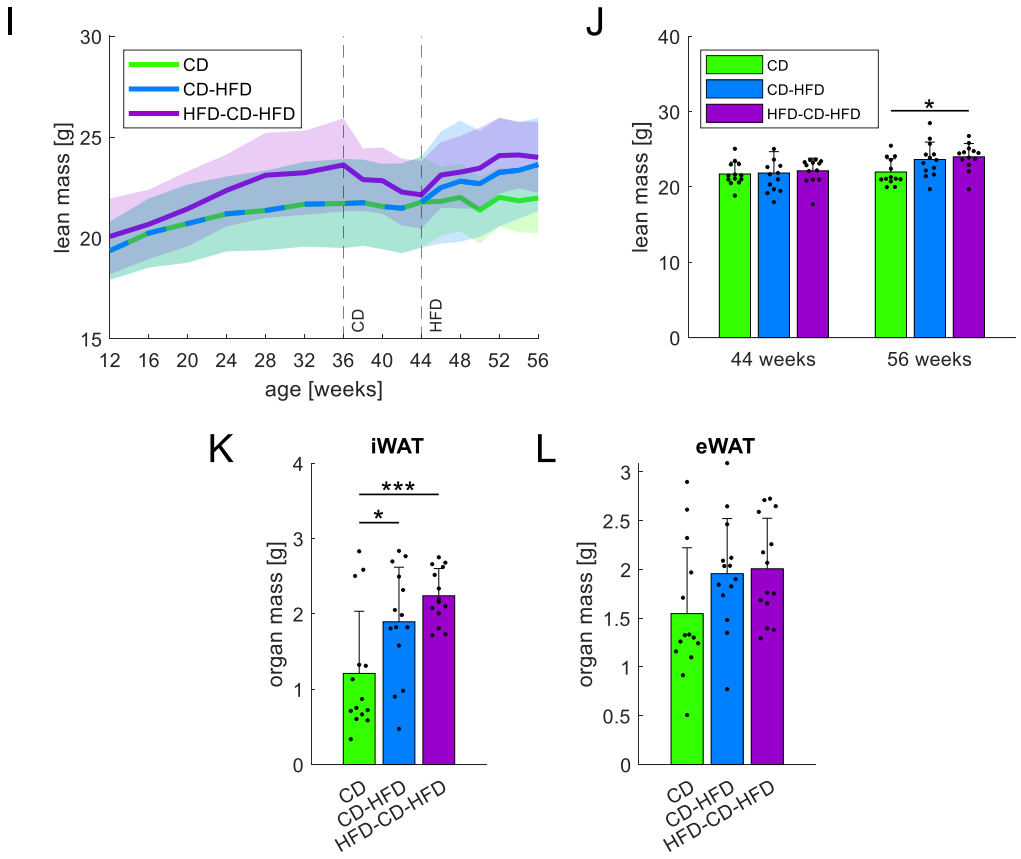

Figure 14: High-fat diet refeeding doubles body mass and fat mass within the first two weeks. All male C57BL/6N mice received a control diet (CD) at 8 weeks of age. High-fat diet (HFD) feeding began at 12 weeks of age for mice in the HFD-CD-HFD group. CD-induced obesity remission began at 36 weeks of age for HFD-CD-HFD mice. At 44 weeks of age, the diet was switched to HFD for HFD-CD-HFD and CD-HFD mice. (**A**) Body mass development between 8 and 56 weeks of age. Body mass was determined weekly. (**B**) Comparison of body mass at 44 and 56 weeks of age between described feeding regimes. (**C**) Fat mass development between 12 and 56 weeks of age. Fat mass was measured monthly until age 36 weeks and biweekly afterward. (**D**) Comparison of fat mass at 44 and 56 weeks of age between depicted feeding regimes. (**E**) Rate of weekly body mass changes upon 44 weeks of age. (**F**) Rate of biweekly fat mass changes upon 44 weeks of age. (**G**) ANCOVA-adjusted fat mass development between 12 and 56 weeks of age. Fat mass was measured monthly until 36 weeks of age and biweekly afterward. (**H**) Comparison of ANCOVA-adjusted fat mass at 46 and 48 weeks of age. (**I**) Lean mass development between age 12 and 56 weeks. Lean mass was measured monthly until 36 weeks of age and biweekly afterward. (**J**) Comparison of lean mass at 44 and 56 weeks of age between three feeding regimes. (**K**) Organ mass of inguinal white adipose tissue (iWAT). (**L**) Organ mass of epididymal white adipose tissue (eWAT). **B**, **D**, **H**, **J**, **K**, and **L** were analyzed by one-way ANOVA (Dunn-Šidák correction). **E** and **F** were analyzed by two-way repeated measures ANOVA (Dunn-Šidák correction) of CD-HFD and HFD-CD-HFD group. Data are presented as means ± standard deviation, n = 13 (**C** - **J**) – 14 (**A**, **B**, **K**, **L**) (biological replicates). * = $p < 0.05$, ** = $p < 0.01$, *** = $p < 0.001$.

Overall, HFD-refed mice exhibited a phenomenon of body mass cycling reminiscent of what is commonly referred to as ‘yo-yo effect’ in humans, and were more prone to HFD. The persistent changes in epididymal adipocyte mitochondria at the start of the HFD refeeding period underscored the critical function of these organelles in metabolism. These data suggest that reduced mitochondrial integrity and abundance alone may lead to irreversible consequences without changes in mitochondrial protein expression.

3.2.6 HFD refeeding impairs epididymal mitochondrial function

HFD-refed mice were more prone to an obesogenic environment. To investigate the impact of HFD refeeding on mitochondrial function, we assessed mitochondrial respiration (states 3 and 4) in permeabilized inguinal and epididymal adipocytes, as well as mitochondrial content and integrity.

Consistent with previous findings, we did not observe significant changes in the mitochondrial respiration rate of inguinal adipocytes between CD, CD-HFD, and HFD-CD-HFD feeding (**Figure 15 A**). In addition, there were no differences in mitochondrial respiration, abundance, and integrity between 12 weeks of HFD feeding and HFD refeeding for 12 weeks (**Figure 15 A – C**). However, in epididymal adipocytes, we observed a decrease in mitochondrial respiration in the HFD-refed group compared to the CD group, while the CD-HFD group already demonstrated a trend towards reduced respiration (**Figure 15 D**). This trend towards reduced mitochondrial respiration was reflected in both HFD groups in terms of mitochondrial content and integrity (**Figure 15 E** and **F**). The more marked reduction in mitochondrial respiration in the HFD refeeding group was due to the greater decrease in mitochondrial abundance, as both HFD feeding groups showed similar reductions in mitochondrial integrity. HFD refeeding did not further reduce mitochondrial integrity compared to HFD feeding for the first time in epididymal adipocytes.

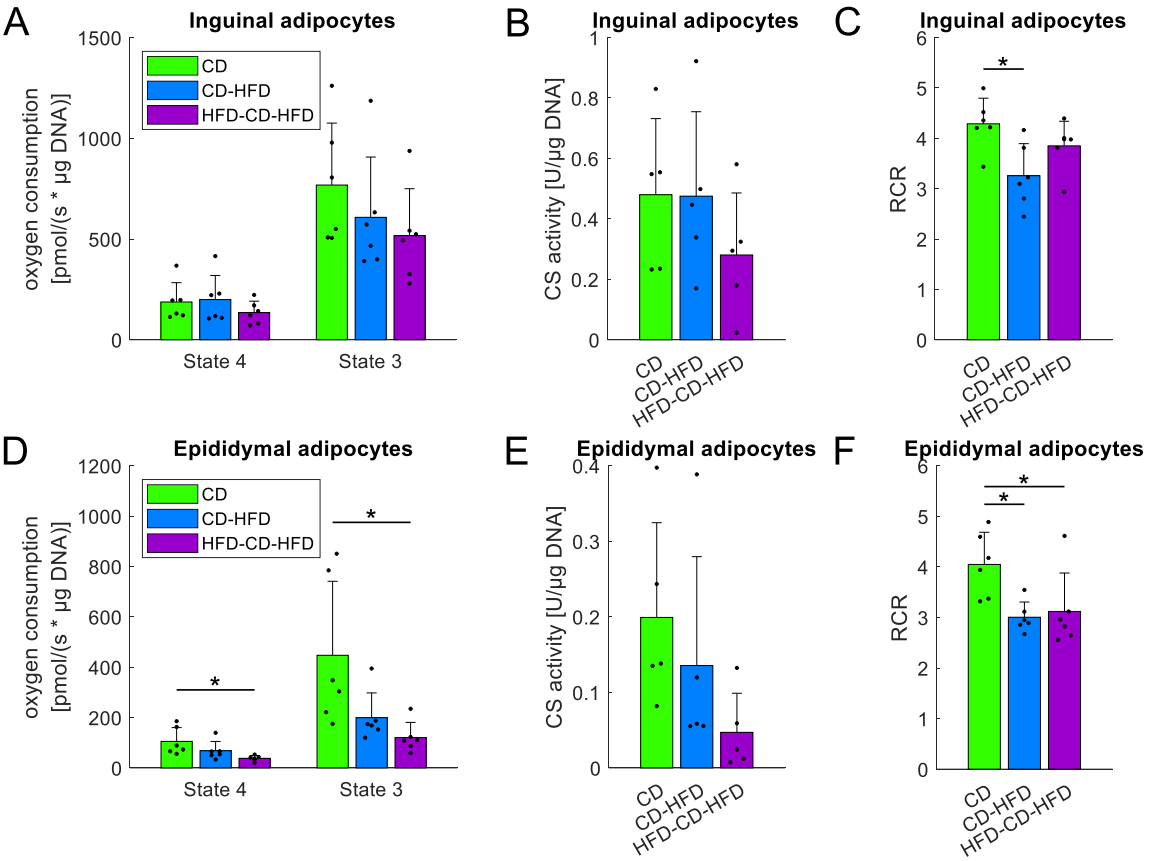

Figure 15: Three-month high-fat diet feeding already alters the mitochondrial capacity, content, and integrity in epididymal adipocytes. (**A**) Bioenergetics of α-chaconine permeabilized inguinal adipocytes in the presence of substrates (pyruvate, malate, succinate). State 4 represents substrate-only respiration. Phosphorylating state 3 respiration was assessed the in presence of substrates and adenosine diphosphate (ADP). Non-biological background respiration was subtracted from respiration rates after electron flow at complex III was blocked with antimycin A. Respiration rates were normalized to deoxyribonucleic acid (DNA) content of the inserted cells. (**B**) Citrate synthase (CS) activity measurements of inguinal adipocytes. CS activity was normalized to DNA content. (**C**) Respiratory control ratio (RCR) of inguinal adipocytes, defined as the ratio of state 3 to state 4 respiration. (**D**) Bioenergetics of α-chaconine permeabilized epididymal adipocytes in the presence of substrates (pyruvate, malate, succinate). State 4 represents substrate-only respiration. State 3 is respiration in the presence of substrates and ADP. Non-biological background respiration was subtracted from respiration rates after electron flow at complex III was blocked with antimycin A. Respiration rates were normalized to DNA content of inserted cells. (**E**) CS activity measurements of epididymal adipocytes. CS activity was normalized to DNA content. (**F**) RCR of epididymal adipocytes. It is defined as ratio of state 3 to state 4 respiration. Data were analyzed by one-way ANOVA (Dunn-Šidák correction). Data are presented as individual values and means ± standard deviation, n = 6 (biological replicates). * = $p < 0.05$. CD = control diet, HFD = high-fat diet.

Our investigation of the effects of HFD feeding for the first time and HFD refeeding on mitochondrial function revealed that 12 weeks of HFD feeding had already caused alterations in the mitochondrial function of epididymal adipocytes, but not in inguinal adipocytes. These findings supported the conclusion that inguinal adipocytes were resistant to re-exposure to an obesogenic environment, while epididymal adipocyte mitochondria demonstrated a trend towards additional reduction in mitochondrial respiration and abundance in comparison to mice consuming HFD for the first time.

3.2.7 HFD refeeding has no effects on the expression of oxidative phosphorylation proteins

To investigate whether HFD refeeding had negative effects on oxidative phosphorylation expression in adipocytes, we performed Western blot analyses of subunits from complex II to V. In order to identify potential compensation of protein expression levels, we also analyzed whole tissue and SVF cells.

Western blot analyses showed only minor changes between the different feeding regimes within adipocytes, whole tissue, and SVF cells in both fat depots (**Figure 16 A** – **F**). As oxidative phosphorylation play only a moderate role in highly proliferative cells (DeBerardinis et al., 2008), SVF cells showed nearly no complex II expression (**Figure 16 C** and **F**). Interestingly, we observed slightly increased expression of all four detected complexes in epididymal SVF cells following HFD refeeding (**Figure 16 F**), while epididymal adipocytes showed slightly reduced expression of oxidative phosphorylation complexes (**Figure 16 D**). In addition, HFD feeding for the first time caused a reduction in complex II expression in the whole eWAT, but this effect did not persist after HFD refeeding. (**Figure 16 E**). Analysis of the ratio of total protein

to organ mass (**Figure 16 H** and **I**) revealed no significant differences between the investigated feeding regimes.

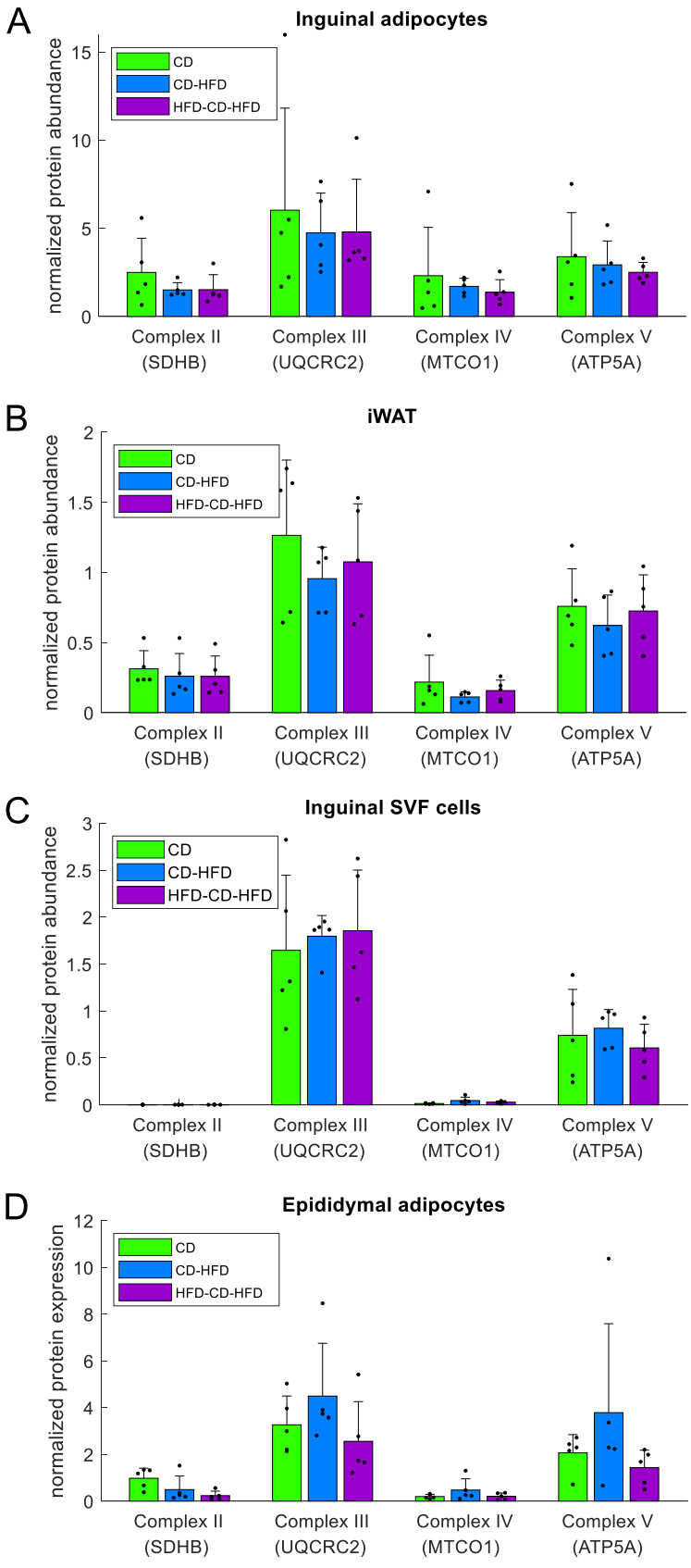

Continue page 68

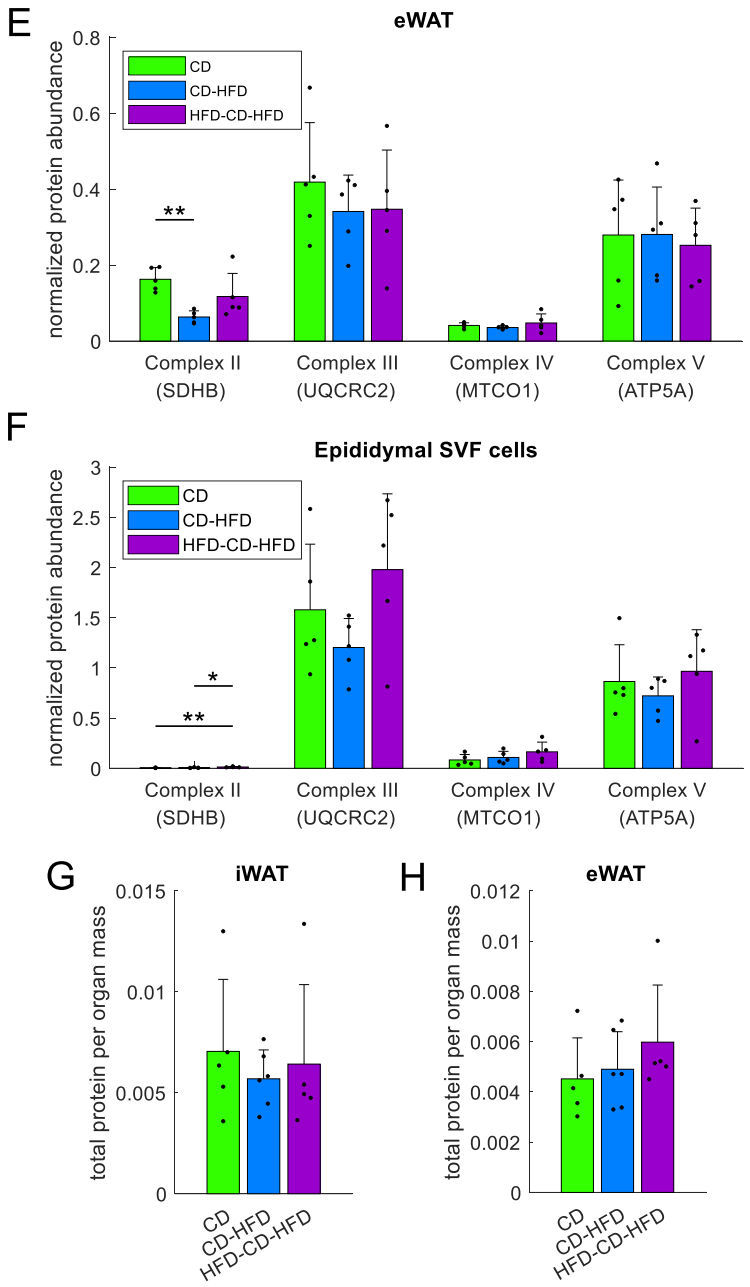

Figure 16: High-fat diet refeeding has only minor effects on protein expression of oxidative phosphorylation complexes. Western blot analysis of oxidative phosphorylation complexes. Complex signals were normalized to vinculin signal. (**A**) Inguinal adipocytes. (**B**) Inguinal white adipose tissue (iWAT). (**C**) Inguinal stromal-vascular fraction (SVF) cells. (**D**) Epididymal SVF cells. (**E**) Epididymal white adipose tissue (eWAT). (**F**) Epididymal SVF cells. (**G**) Total protein concentration of iWAT. (**H**) Total protein concentration of eWAT. Data were analyzed by one-way ANOVA (Dunn-Šidák correction). Data are presented as individual values and means ± standard deviation, n = 5 (biological replicates). * = $p < 0.05$, ** = $p < 0.01$. CD = control diet, HFD = high-fat diet.

In summary, we found that HFD feeding did not significantly affect the expression of mitochondrial oxidative phosphorylation complex subunits or total protein abundance. Thus, HFD refeeding did not appear to alter the expression of these complex subunits. These results highlight the importance of other factors in regulating mitochondrial function in mature adipocytes.

Based on our inability to observe changes in overall protein expression, we also assumed that there would be no changes in the expression of other proteins after HFD refeeding. Our previous data showed that obesity reduces the differentiation potential of primary adipocytes, implying a potential connection between primary and mature adipocytes. This connection led to a sustained decline in the quantity and quality of mitochondria in epididymal adipocytes without affecting general protein expression. In addition, our findings revealed a reduced adipogenic potential due to a HFD-induced increase in the Areg frequency, suggesting that signaling from primary adipocytes plays a crucial role in the regulation of mitochondria in mature adipocytes. In addition, we observed an impaired *in vivo* proliferation rate in obese mice that was further reduced after one week of CD feeding. These findings suggested that the adipogenic potential could be restored after a short-term low-fat CD intervention, but the obesity-induced signals may result in irreversible changes to the mitochondria in epididymal mature adipocytes. Despite the normalization of body and fat mass and the restoration of adipogenic potential, the function of the epididymal mitochondria remained reduced. These results indicated that obesity had far-reaching effects on the epididymal mitochondria, which may contribute to the phenomenon of body mass cycling, commonly known as the ‘yo-yo effect’.

4 Discussion

The persistent increase in the prevalence of obesity and overweight highlights the urgency for further research to identify the underlying causes of disrupted energy balance and develop effective interventions. Despite all the progress to date, the physiological mechanisms that impede the maintenance of reduced body mass after successful body mass loss remain poorly understood. Adults who undergo repeated cycles of caloric restriction (i.e., "dieting") and overeating often experience an increase in body mass, commonly referred to as the ‘yo-yo effect’ (Dulloo and Montani, 2015; OECD/WHO, 2020). Adipose tissue, exhibiting a heterogeneous composition of various fat cell types with diverse function, has emerged as a critical node in the homeostatic system that regulates body mass (Hepler and Gupta, 2017; Macotela et al., 2012; Rosen and Spiegelman, 2014).

Our prior research on the cellular composition of adipose tissue in diet-induced obese mice reveals a restricted mitochondrial function in mature adipocytes (Schottl et al., 2015b). Interestingly, preliminary data from our laboratory suggested a reduction in the adipogenic potential of adipocyte progenitor cells (APCs) that could be restored by short-term exposure to a low-fat diet. Of note, feeding mice for one week a control diet (CD) does not improve mitochondrial function in mature adipocytes (Schottl et al., 2015b). If corroborated, a nutritional programming of adipogenic potential and mitochondrial function plausibly contributes to the accelerated body mass regain. Hence, it is of great interest to investigate the effects of caloric restriction and CD-feeding followed by a high-fat diet (HFD) on adipose tissue growth and mitochondrial function, as these factors contribute to the development of metabolic complications. A better understanding of the underlying cellular mechanisms may provide valuable insights into the effects of repeated cycles of dieting and overeating on body mass regulation in humans.

The present study aimed to examine the impact of APCs on the adipogenic potential and the mitochondrial function in white adipocytes during body mass loss and regain. At first, we investigated the capacity of HFD feeding to deplete the adipogenic stem and precursor cells and to suppress the differentiation of APCs into mature adipocytes. Our findings demonstrated the significance of various adipogenic stem and progenitor cells on the adipogenic potential and their fluctuations after a one-week dietary intervention in obese mice. Secondly, we analyzed the mitochondrial function and protein expression in obese mice and mice undergoing CD-induced obesity remission, which were comparable in body mass to control mice. By refeeding these CD-induced obesity remission mice, we revealed the persistent effects of obesity on mitochondria and the long-lasting impact of nutritional programming on white adipose tissue (WAT) that may contribute to body mass regain in mice.

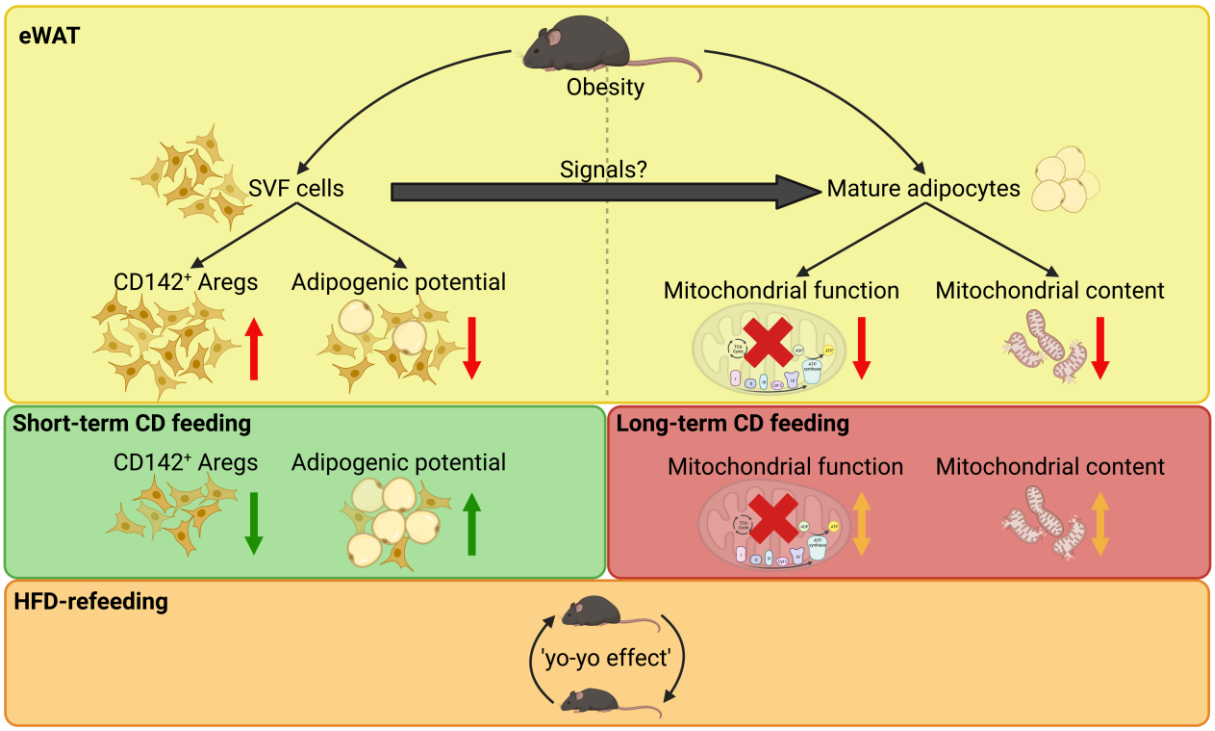

Figure 17: Nutritional programming of epididymal white adipose tissue and its consequences. High-fat diet (HFD) feeding is associated with an increased frequency of CD142⁺ adipogenesis-regulatory cells (Aregs) and reduced adipogenic potential in stromal-vascular fraction (SVF) cells of epididymal white adipose tissue (eWAT) (yellow area left). Furthermore, HFD feeding reduces mitochondrial function and content in mature adipocytes (yellow area right). Upon refeeding with control diet (CD) for one week, the frequency of CD142⁺ Aregs decreases, and the adipogenic potential of SVF cells increases (green area). However, even after normalization of body mass and fat mass following long-term CD feeding, mitochondrial function and content fail to restore (red area). This increased adipogenic potential coupled with diminished mitochondrial function and content renders HFD-refed mice more susceptible to an obesogenic environment and body mass regain (orange area). Created with BioRender.com

4.1 Reversible alterations in cell fate decision and terminal differentiation

The nutritional programming of APCs may contribute to accelerated body mass regain. In a preliminary study, a HFD feeding regime resulted in a reduction of the adipogenic potential of WAT. However, a one-week refeeding of obese mice with a low-fat CD reversed this effect (unpublished). To corroborate and understand these observations, a more detailed investigation was necessary. To that end, we examined both the whole tissue structure and primary adipocyte cultures to assess their adipogenic potential through differentiation analyses. Additionally, we determined the presence and proliferation ability of previously described subpopulations within the adipose tissue (Merrick et al., 2019; Schwalie et al., 2018).

Feeding mice with HFD for several weeks until they reached at least 40 g of body mass and the eWAT expansion plateau (**Figure 3**) resulted in consistent outcomes with previous studies in mice and humans (Pasquet et al., 1992; Schmitz et al., 2016). However, we observed a

huge variation between individual mice. Additionally, lean mass increased steadily during aging and the increase in lean mass in HFD-fed mice plateaued over time, reducing the differences between the CD and HFD groups (**Figure 10**). Despite the potential influence of various factors on body mass development in mice (Anderson et al., 1968; Parra-Vargas et al., 2020; Toth et al., 2015), only slight variations between the different feeding regimes were observed and deemed negligible since no correlations were found with factors such as litter size and housing density. In the group fed with caloric restricted pair-fed (pf) HFD, the mice were provided with food of the same caloric density as the HFD-CD group, but only once a day before the onset of darkness. They consumed the food within a few hours, resulting in starvation for the remaining hours of darkness and throughout the light phase. Therefore, feeding the mice a CD for one week led to a suggestive reduction in fat mass and organ masses, whereas one-week of a pfHFD reduced lean mass significantly, but had a less pronounced effect on organ masses compared to one-week CD feeding. Previous studies on calorie restriction and starvation in humans and mice have also reported a reduction in lean mass (Keys et al., 1950; Schmitz et al., 2016). However, *ad libitum* low-fat diets have more beneficial effects on insulin resistance and a decrease in plasma triglycerides compared to caloric restriction (Muurling et al., 2002), despite the fact that the dietary composition did not result in a significant difference in body mass loss in our study and a previously reported study (Sacks et al., 2009). Our results highlighted the importance of diet quality, rather than solely quantity, in determining body composition during a short phase of body mass loss. This suggests that diet quality is more significant than diet quantity in achieving body mass and fat mass loss, whereas for lean mass, the opposite is true.

Following the initial determination of the change in body mass and body composition during the first series of experiments, subsequent investigations involved a more detailed analysis of the composition of WAT. Adipose tissue can be hypertrophic and/or hyperplastic increasing storage capacity (Jo et al., 2009). iWAT primarily undergoes hypertrophy and limited adipogenesis when exposed to a HFD, whereas eWAT initially experiences hypertrophy followed by hyperplastic growth (Kim et al., 2014; Wang et al., 2013). However, upon reaching a body mass of approximately 40 g, the expansion of the eWAT depot ceases, while iWAT continues to increase proportionally with body mass (van Beek et al., 2015). The morphological analysis of WAT was conducted to assess the differences in terminal differentiation between different feeding regimes and fat depots. Our results (**Figure 4**) confirmed a limited expandability of eWAT and larger adipocytes in eWAT than in iWAT (Madsen et al., 2023; van Beek et al., 2015). After HFD feeding, adipocyte size increased further in both fat depots, but reached its limit earlier in eWAT, suggesting maximal hypertrophy and an elevated adipocyte death opposing the increased hyperplasia in eWAT (Alkhouri et al., 2010; Kim et al., 2014). The increase in adipocyte size can elicit metabolic stress such as endoplasmic reticulum stress and

lipotoxicity, and finally leads to alterations in mitochondrial function, adipokine secretion profiles, and metabolites (Brookheart et al., 2009). Consequently, a plethora of co-occurring medical conditions may arise, such as type 2 diabetes, cardiovascular and renal diseases, and certain types of cancer (Kitahara et al., 2014; Kovesdy et al., 2017; Renehan et al., 2008; Xu et al., 2018). The impact of one week of CD or pfHFD following a prolonged HFD on the overall tissue architecture was negligible. However, one week of CD may had a slightly stronger reverse effect on the morphology of WAT in both fat depots. Overall, both WAT depots were found to be hypertrophic, with an earlier expansion limit observed in eWAT. Moreover, iWAT exhibited a more rapid remodeling of its tissue structure in response to dietary alterations compared to eWAT, indicating a superior physiological adaptation of iWAT. iWAT exhibited a favorable remodeling response to varying caloric challenges, while prolonged exposure to an obesogenic environment caused pathological changes in eWAT, resulting in deleterious effects on the health of the entire organism.

As WAT plays a central role in the pathogenesis of obesity, we conducted a detailed examination of its cellular composition. The stromal-vascular fraction (SVF) comprises the majority of cells in WAT, including APCs (Sarjeant and Stephens, 2012). Even though APCs are only one of several cell populations within WAT, our preliminary data suggested that reduced adipogenic potential of APCs might contribute to the limited expansion of eWAT. Therefore, we proceeded to investigate the adipogenic potential of isolated SVF cells *in vitro* (**Figure 5**). We suggested that inguinal primary adipocytes differentiated appropriately with fewer, but well-differentiated large lipid droplets. On the other hand, epididymal primary adipocytes indicated reduced differentiation capacity, with smaller and less developed lipid droplets within primary adipocytes. However, the results did not support our previous preliminary findings of reduced adipogenic potential in primary adipocytes after HFD feeding, since we still observed proliferating and lipid-storing primary adipocytes in this experiment. In line with observations at the entire tissue morphological level (**Figure 4**), we observed only minor changes within one week of CD or pfHFD feeding. The reversing effects on the morphology were more pronounced in inguinal primary adipocytes compared to epididymal primary adipocytes. Furthermore, one week of CD seemed to have a slightly stronger reversing effect compared to one week of pfHFD, especially in inguinal primary adipocytes. It is worth noting that the aging of the cells (Bonab et al., 2006) may have weakened the differences between the feeding regimes. Contrary to our preliminary data, we could not observe a fully reduced adipogenic potential of APCs. Nevertheless, our data showed a diminished terminal differentiation capacity of epididymal primary adipocytes upon HFD feeding at the morphological level of primary cell cultures.

To enhance our understanding of APCs, we studied their gene expression. The successful expansion of WAT requires a high level of coordination between the numerous cell types present in the SVF (Sun et al., 2011). Moreover, studies have demonstrated alterations in the abundance and expression patterns of specific subpopulations of SVF cells during the progression of obesity (Burl et al., 2018; Cho et al., 2019; Emont et al., 2022; Hepler et al., 2018; Merrick et al., 2019; Sarvari et al., 2021; Schwalie et al., 2018). Therefore, we further evaluated the terminal differentiation capacity of APCs (**Figure 6**). The results of the HFD feeding were in agreement with the observations made at the morphological level (**Figure 4** and **Figure 5**). Inguinal primary adipocytes were unaffected by obesity, while epididymal primary adipocytes indicated a slightly reduced terminal differentiation capacity in obese mice. Intriguingly, there were differences in the gene expression of various terminal differentiation markers in epididymal primary adipocyte. Markers related to lipogenesis (*Fasn*) and lipid biosynthesis (*Plin1*) were more downregulated upon HFD feeding than general adipocyte markers (*Pparg*) as previously described in eWAT (Sarvari et al., 2021). Feeding mice a low-fat CD for one week had no effect on the gene expression levels of terminal differentiation markers and *Pref1* in inguinal primary adipocytes. However, a one-week pfHFD seemed to increase the expression of these markers, suggesting a higher differentiation capacity. These results indicated a slightly differing outcome compared to the morphological investigations of cultured primary adipocytes and entire tissue. Upon further examination of individual mice, it was revealed that one mouse in the pfHFD group (**Figure S3**) heavily influenced the results of the inguinal primary adipocytes. Excluding this mouse from the analysis would indicate that the one-week CD feeding was more effective in increasing the expression of terminal differentiation markers and *Pref1* than the one-week pfHFD. These findings were consistent with our previous morphological findings, with one-week CD feeding resulting in a greater reversion of diet-induced obesity compared to one-week pfHFD. Our results indicated that HFD feeding resulted in a reversible reduction in the terminal differentiation capacity of APCs on a gene expression level. This observation was consistent with the results obtained at the morphological level.

Recently, a multitude of studies has been conducted to explore the various subpopulations of SVF cells. Although the specific subpopulations analyzed may vary among studies in terms of their numbers and names, the overall results consistently demonstrate comparable characteristics and markers within the different defined subpopulations (Burl et al., 2018; Cho et al., 2019; Emont et al., 2022; Ferrero et al., 2020; Hepler et al., 2018; Merrick et al., 2019; Sarvari et al., 2021; Schwalie et al., 2018). After dividing the SVF cell population into subpopulations, some have investigated the adipogenic potential of these subpopulations both *in vivo* and *in vitro*, as well as their development in lean versus obese mice (Merrick et al., 2019; Schwalie et al., 2018). In line with prior research findings (Merrick et al., 2019; Schwalie et al., 2018),

we conducted further investigations to analyze the influence of HFD consumption and the unexplored effects of short-term dietary alterations at the subpopulation level of SVF cells. We examined three distinct subpopulation clusters of the lineage-negative/stem cells antigen 1-positive ($Lin^-/SCA1^+$) cell population in inguinal and epididymal SVF cells: Cluster 1: $CD55^+$ adipocyte stem cells, Cluster 2: Vascular adhesion protein 1-positve ($VAP1^+$) preadipocytes, and Cluster 3: $CD142^+$ adipogenesis-regulatory cells (Aregs). Our data (**Figure 7**) confirmed a connection between $CD142^+$ Aregs and $VAP1^+$ preadipocytes, their shared origins, and their capacity to transit into each other (Emont et al., 2022; Merrick et al., 2019). However, the function of the $CD142^+$ Areg subpopulation and its potential inhibitory effects on adipogenesis are still not fully resolved (Merrick et al., 2019; Sarvari et al., 2021; Schwalie et al., 2018). A recent study underscores the importance of age in determining the function and frequency of $CD142^+$ Aregs (Zachara et al., 2022). Our result aligned with those of other studies investigating diet-induced obesity in mice, showing no significant increase in the $CD142^+$ Areg frequency of inguinal SVF cells upon exposure to a HFD (Emont et al., 2022; Merrick et al., 2019). Furthermore, HFD feeding decreased the pool of $CD55^+$ adipocyte stem cells while increasing the frequency of $VAP1^+$ preadipocytes in inguinal SVF cells. This demonstrated that the differentiation capacity of inguinal SVF cells remained unaffected, as $CD55^+$ adipocyte stem cells differentiate into $VAP1^+$ preadipocytes to meet the growing demand for lipid-storing mature adipocytes. The subpopulation distribution of SVF cells from eWAT differed from that of SVF cells from iWAT. Specifically, the frequency of $CD142^+$ Aregs in SVF cells from eWAT increased in response to HFD feeding in both experimental setups, as previously reported in obese mice (Merrick et al., 2019; Schwalie et al., 2018). However, the frequency of $VAP1^+$ preadipocytes and $CD55^+$ adipocyte stem cells remained unchanged, indicating a minor role for the differentiation capacity of SVF cells initially. Our findings suggested a reduced differentiation capacity in SVF cells of eWAT, supported by the absence of a trajectory of $CD55^+$ adipocyte stem cells towards $VAP1^+$ preadipocytes. As the inhibitory characteristics of $CD142^+$ Aregs increase with age (Zachara et al., 2022), the increase in $CD142^+$ Aregs in SVF cells from eWAT explained the decreased adipogenic potential of epididymal primary adipocytes. In addition, we evaluated the subpopulation distribution after one week of CD feeding and one week of pfHFD feeding. In inguinal SVF cells, the reduction of $VAP1^+$ preadipocytes with one-week pfHFD indicated a decreased demand for preadipocytes to differentiate into mature adipocytes. However, since the $CD142^+$ Areg frequency remained low, the adipogenic potential was not reduced. In the case of epididymal SVF cells, the $CD142^+$ Areg frequency normalized to the control group level after one week CD without alterations in the frequency of $CD55^+$ adipocyte stem cells or $VAP1^+$ preadipocytes. Based on the observed trend towards increased adipogenic potential at the morphological and gene expression levels, without a reduction in infiltrated immune cells (Schmitz et al., 2016; Shirakawa et al., 2017), we suggested that the reduced $CD142^+$ Areg

frequency was a major contributor to these rapid changes. The present study demonstrated that HFD intake had a significant impact on cell fate decisions and the adipogenic process. Our findings indicated that HFD-mediated signals reach the SVF cells and influence their further development. HFD feeding increased the frequency of $CD142^+$ Areg cells in the epididymal SVF, leading to an inhibitory effect on adipogenesis in adult obese mice. The raised frequency of $CD142^+$ Areg cells resulted in a diminished transition of $CD55^+$ adipocyte stem cells into $VAP1^+$ preadipocytes, ultimately hindering the differentiation of $VAP1^+$ preadipocytes into lipid-laden adipocytes. These observations proved that the HFD-induced increase in the frequency of $CD142^+$ Areg subpopulation lowered the adipogenic potential of epididymal SVF cells. However, the inhibitory effect could be rapidly reversed by reducing the frequency of $CD142^+$ Areg, as evidenced by a low-fat diet intervention. These findings emphasized the crucial role of dietary composition in regulating the frequency of $CD142^+$ Areg and the adipogenic potential.

The plateau phenomenon observed in eWAT may results from nutritional programming of the adipogenic potential in progenitor cells derived from eWAT. This may be attributed to APC pool depletion, as well as the silencing of differentiation capacity through an increase in $CD142^+$ Areg frequency during HFD feeding. To assess the impact of diet on cellular proliferation, we performed *in vivo* studies using 5-ethynyl-2'-deoxyuridine (EdU) to monitor deoxyribonucleic acid (DNA) synthesis. Given the low turnover rate of adipocytes (Spalding et al., 2008), we observed a modest rate of proliferation in adipogenic stem and precursor cells (**Figure 8**). Our results indicated that HFD feeding slightly enhanced cell proliferation in SVF cells of iWAT, while in eWAT, a slight reduction in proliferation was observed in response to HFD, albeit without a complete termination of proliferation. Interestingly, one week of CD or pfHFD resulted in a substantial reduction in the proliferation rate of SVF cells in iWAT and a milder reduction in eWAT. On the contrary, our results disproved a HFD-induced proliferation stop and depletion of the adipogenic stem and precursor cells as an explanation of a decreased adipogenic potential in epididymal SVF cells. Additionally, these findings demonstrated that HFD did not limit eWAT expansion through a reduction in cell proliferation. Instead, our data suggested that HFD feeding suppressed the differentiation of adipogenic stem and precursor cells into mature adipocytes, primarily due to the inhibitory effect of the increased $CD142^+$ Areg subpopulation in eWAT of obese mice.

APCs appear to play a vital role in the development and expansion of WAT. To validate our findings regarding APCs, we conducted 3D imaging analysis on eWAT. The results of this image analysis were consistent with our flow cytometry data (**Figure 9**). Additionally, we noted that a majority of the EdU^+ preadipocytes were associated with vessels, as previously reported

(Cawthorn et al., 2012; Schwalie et al., 2018). Upon exposure to HFD, we observed an expected increase in immune cell infiltration in eWAT, which was predominantly organized into crown-like structures (Fischer et al., 2018; van Beek et al., 2015). Our findings indicated that HFD feeding resulted in a reduction of the proliferation rate in tissue-distributed EdU^+ preadipocytes. A short-term obesity intervention was not able to reverse the infiltrated immune cells. However, one-week pfHFD feeding further promoted the immune cell infiltration into eWAT and led to a deterioration of the surrounding vascular structures. Additionally, both obesity intervention groups demonstrated a reduction in the *in vivo* proliferation rate and were in line with our previous findings in the SVF. The analysis confirmed the broad impact of obesity on the structure of eWAT, including infiltration of immune cells and a slight reduction in *in vivo* proliferation in response to a HFD. The increase in the $CD142^+$ Areg subpopulation observed with HFD feeding highlighted their systemic influence on preadipocytes in the entire tissue, with a modest effect on proliferation and a significant impact on differentiation capacity. Our findings also demonstrated the critical role of diet quality in obesity intervention. The implementation of caloric restriction with HFD led to a significant increase in immune cell infiltration, deterioration of surrounding vasculature, and near-complete inhibition of preadipocyte proliferation, whereas these negative effects were not observed after one week of a low-fat diet. These results suggested that body mass reduction achieved through low-fat diet was more sustainable and beneficial compared to energy-restricted HFD.

In summary, a HFD caused a significant increase in body mass, fat mass, and organ mass, while CD for one week resulted in a reduction of fat mass and organ mass. The expandability of eWAT was reduced and the effects of one week of CD on tissue structure were modest, with slower eWAT remodeling compared to iWAT. While the quality of the diet played a more significant role in body mass and fat mass loss, caloric restriction alone may result in a loss of lean mass. HFD reduced the differentiation capacity of adipogenic stem and precursor cells, without preventing cell proliferation, but CD reversed its inhibitory effects. Short-term obesity interventions resulted in a proliferation reduction in both iWAT and eWAT, without reducing immune cell infiltration. Overall, a low-fat diet result in a more sustainable and beneficial reduction of body mass compared to caloric restriction with HFD.

4.2 Persistent mitochondrial impairment

Previous studies have documented adverse effects of obesity on adipocyte mitochondria. It is well known that murine eWAT is more susceptible to the negative impacts of obesity concerning mitochondrial bioenergetics and inflammation compared to iWAT (Giordano et al., 2013; Gonzalez-Franquesa et al., 2022; Schmitz et al., 2016; Schottl et al., 2015b). However, to the best of our knowledge, no studies have yet explored whether obesity has long-lasting effects

on the mature adipocytes of WAT that persist beyond a full remission achieved through switching from a HFD to a low-fat CD. In our study, we compared mice that achieved a full remission from obesity through diet with obese mice and mice that were never obese. Similar to several studies in rodents and humans (Brownell et al., 1986; Pietilainen et al., 2012; Saarni et al., 2006), we investigated body mass cycling in mice. We examined whether mice that recovered from obesity through a low-fat diet were more susceptible to a HFD environment and gained body mass and fat mass more rapidly compared to mice that were exposed to a HFD for the first time.

Initially, we demonstrated that HFD feeding significantly increased body and fat mass with an appropriate fat-to-body mass ratio at all tested time points (**Figure 10**). An eight-week CD-induced obesity remission was sufficient to restore body mass and fat mass. One possible explanation for the steady lean mass was the late onset of our HFD feeding, as we aimed to investigate its effects in adulthood. Compared to a study where lean mass increases during HFD feeding, we switched the diet at 12 weeks of age instead of 4 weeks of age (Schmitz et al., 2016). However, as we observed an increase in lean mass in our study investigating the adipogenic potential (**Figure 3**), we attributed the differences to variations within our mice and their high age. These parameters led to an increase in lean mass in the control group and thus reduced differences in lean mass between CD and HFD-fed mice. After the CD-induced obesity remission, we did not observe a decrease in lean mass, which is in contrast to the findings of decreased lean mass in the Minnesota experiment in humans and the study in mice that started HFD feeding at 4 weeks of age (Keys et al., 1950; Schmitz et al., 2016). However, less decrease in lean mass was observed in heavier lean men in the Minnesota experiment (Dulloo, 2021; Keys et al., 1950). These results, combined with our previous findings, propose that after initial body mass gain, lean mass does not decrease significantly with long-term CD feeding, as the energy deficit is preferentially balanced by energy stored in fat mass rather than lean mass. Therefore, we suggested that lean mass replenishment and subsequent fat overshooting play only a minor role in body mass cycling under regular meals distributed over the day. However, it should be noted that our studies were conducted with mice and thus may differ from findings in humans. Unfortunately, there are no data on lean mass in human studies on co-twins, body mass cycling athletes, or in the Guru-Walla ritual, where an ethnic group from northern Cameroon underwent voluntary overfeeding for approximately two months. Therefore, we can only speculate that lean mass only plays a minor role in body mass regain in these cases (Pasquet and Apfelbaum, 1994; Pietilainen et al., 2012; Saarni et al., 2006). Another interesting observation in our study was the clear distinguishable behavior of iWAT and eWAT organ masses. As previously observed (Giordano et al., 2013; van Beek et al., 2015), iWAT could expand unlimitedly, while eWAT had limited expansion capacity. In contrast, eWAT

has higher levels of inflammation and macrophages content. These macrophages are important for debris removal that results from increased eWAT expenditure and need a long time to finish the task (Giordano et al., 2013). Therefore, inflammation persists even after full remission from obesity with normalized fat cell size (Schmitz et al., 2016; Shirakawa et al., 2017). The reduced eWAT organ mass after CD-induced obesity remission in our study may already indicated ongoing and lasting effects of obesity in terms of crown-like structure removal and reduced regeneration. These findings provided initial evidence for a long-lasting obesity effect on eWAT that could not be reversed by long-term CD feeding for obesity recovery.

After initially determining the change in body mass and composition during the first series of experiments, further investigations involved a detailed analysis of the mitochondria in adipocytes. Mitochondria in WAT play a crucial role in various physiological processes, including lipogenesis, lipolysis, adipokine secretion, and adipocyte differentiation (De Pauw et al., 2009; Koh et al., 2007). However, recent studies in rodent models have consistently demonstrated a reduction in mitochondrial integrity, content, and protein levels during obesity and type 2 diabetes (Fischer et al., 2015; Heinonen et al., 2017; Kusminski and Scherer, 2012; Mustelin et al., 2008; Schottl et al., 2015b; Schottl et al., 2020; Wessels et al., 2019). In-depth examinations have revealed that long-term consumption of a HFD particularly affects epididymal mitochondria, and these alterations cannot be improved by short-term low-fat CD interventions (Schottl et al., 2015b). Therefore, our study aimed to determine the impact of obesity and complete recovery from obesity on mitochondrial bioenergetics and content, investigating whether a full CD-induced remission from obesity is necessary to reverse the effects on mitochondria. For this purpose, we evaluated the respiration capacity, the mitochondrial integrity, and the mitochondrial content in inguinal and epididymal adipocyte mitochondria (**Figure 11**). Our findings regarding inguinal adipocytes were partially in contrast to the results of Schöttl *et al*., who also report no changes in mitochondrial integrity but observe a decrease in mitochondrial content (Schottl et al., 2015b). However, our results were consistent with a study that investigated iWAT and eWAT homogenates before and after reducing body mass and fat mass through caloric restriction of a HFD (45 % fat) and exercise intervention (Gonzalez-Franquesa et al., 2022). The resistant decrease in respiration capacity in the phosphorylating state observed in our data is also reported in eWAT homogenates after caloric restriction of HFD feeding and exercise (Gonzalez-Franquesa et al., 2022). However, examining the whole WAT may detect effects primarily caused by immune cells or SVF cells, not mature adipocytes, as WAT only makes up one-third of mature adipocytes, yet it can account for over 80 % of its tissue volume (Tsiloulis and Watt, 2015). Furthermore, the number of immune cells greatly increases in WAT because of HFD feeding (Gonzalez-Franquesa et al., 2022; Schmitz et al., 2016). Therefore, we employed only mature adipocytes and permeabilized them with α-chaconine at the beginning of the experiment additionally to ensure that the mitochondria had access to all substrates

needed for respiration and to exclude the effects of limited substrate supply. The reduced respiratory capacity of epididymal mitochondria in our data could be partially attributed to reduced mitochondrial content. Another reason for the lowered mitochondrial respiration with HFD feeding was the reduced mitochondrial integrity. Mitochondrial content and integrity did not recover after full remission from obesity, demonstrating a long-lasting effect of obesity on epididymal adipocyte mitochondria and their metabolic flexibility. Furthermore, our results provided clear evidence that HFD feeding has extensive consequences beyond the mitochondrial functionality and content in epididymal adipocytes. For instance, the reduced mitochondrial respiration capacity of epididymal adipocyte mitochondria is in line with reduced mitochondrial fission activity. Obesity disrupts the fusion-fission balance, and reduced fission activity is associated with impaired mitochondrial bioenergetics in diet-induced obese mice and obesity models, indicating a reciprocal metabolic adaptation to reduce excess lipid accumulation in eWAT (Tol et al., 2016). Changes in the physiological behavior of mitochondria in response to obesity may lead to alterations in mitochondrial structure, which are crucial for proper mitochondrial function. One such change observed in response to a HFD is a reduction in the density of the mitochondrial inner membrane *cristae* structure, as well as a decrease in its master regulator, optic atrophy 1 (OPA1), as reported in previous studies (Gonzalez-Franquesa et al., 2022). Moreover, caloric restriction of HFD and physical interventions are insufficient to reverse the effects of HFD (Gonzalez-Franquesa et al., 2022), as also observed in our study. Although it is known that caloric restriction, achieved by switching from HFD to CD, has a body mass reducing effect (Sacks et al., 2009), the reduced mitochondrial function and content in eWAT of obese mice persisted. Another potential contributing factor to our observations is the downregulation of immunometabolic crosstalk between adipocytes and macrophages, which leads to a decrease in mitochondrial uptake from adipocytes to macrophages in the eWAT following HFD feeding. This, in turn, results in an increased immune response (Brestoff et al., 2021). Furthermore, adipocytes also communicate with other cell types, such as myocytes, through paraspeckles and small extracellular vesicles (Crewe et al., 2021; Fox, 2018). This means that the absence of paraspeckles may lead to dysfunctional mitochondria and decreased mitochondrial content, respiration, and fission activity (Fox, 2018). The alterations within the extracellular mitochondrial signaling modulate the whole body physiology. Thereby, circulation mitochondrial DNA may explain a chronic inflammatory state beyond obesity (Boardman et al., 2023). This elevated inflammation persists even after full recovery from obesity (Schmitz et al., 2016). Overall, the impaired mitochondrial transfer and signaling due to obesity have a detrimental impact on the overall organism. The collective findings on altered fusion-fission activity, mitochondrial structure, and communication between adipocytes and non-adipocytes highlight the extensive impact of HFD on mitochondria, which could potentially explain the persistently decreased mitochondrial content and function observed in our study.

Since reduced mitochondrial function and abundance can have multiple contributing factors, we initiated an investigation into their protein expression. Several studies have previously demonstrated the impact of obesity on the expression of mitochondrial OXPHOS proteins. (Gonzalez-Franquesa et al., 2022; Madsen et al., 2023; Schottl et al., 2020). Therefore, we were interested in whether persisting reduced mitochondrial integrity and abundance in epididymal adipocytes was due to a permanent adaptation of the respiratory chain at the protein level. To this end, we investigated the expression of oxidative phosphorylation (OXPHOS) complexes II – V in several adipose tissue samples (**Figure 12**). Our results did not replicate previous findings that reported a decreased expression of OXPHOS proteins in obese mice (Gonzalez-Franquesa et al., 2022; Madsen et al., 2023; Schottl et al., 2020). Interestingly, despite a reversible reduction in complex II expression, the mitochondrial respiration and integrity in inguinal adipocytes remained unaltered, suggesting that the reduction may have been compensated by other mechanisms.

As the absence of alteration in protein expression could indicate that the proteins are present but not functional, we conducted a comprehensive analysis of the proteome of inguinal and epididymal adipocytes from our feeding groups. Of particular interest were mitochondrial proteins, which may have undergone modifications during HFD feeding. Additionally, we sought to examine pathways related to protein misfolding and alterations in mitochondrial structure. Previous studies have reported reduced fission activity in mitochondria in response to HFD, leading to an elongated appearance and compromised respiratory capacity, as well as reduced mitochondrial functions (Giordano et al., 2013; Tol et al., 2016). Furthermore, the lysosomal and proteasome pathways have been found to be altered during HFD feeding, but remain unaltered in whole eWAT homogenates following caloric restriction in combination with exercise intervention. Lysosomal proteins are upregulated, whereas proteasome proteins are downregulated (Gonzalez-Franquesa et al., 2022). In detail, the activation of lysosomal pathways by the cell is an attempt to manage defective mitochondrial proteins (Deus et al., 2020), whereas the downregulation of proteasome proteins resulting from obesity-induced adipocyte senescence and represents the failure of a recycling/removal of dysfunctional proteins (Li et al., 2021; Saez and Vilchez, 2014). Our findings (**Figure 13**) demonstrated a clear distinction in protein expression between the CD and HFD groups in epididymal adipocytes. However, by analyzing the biologically relevant altered protein expression, we detected only very few proteins that were significantly regulated after HFD feeding and remained dysregulated after full remission of obesity in comparison to CD mice. Intriguingly, the majority of the low expressed proteins were involved in adipocyte differentiation, whereas the highly expressed proteins were primarily associated with increased fat mass size and inflammation. Our findings suggested that the altered expression of OXPHOS proteins, as reported in previous studies (Gonzalez-Franquesa et al., 2022; Madsen et al., 2023; Schottl et al., 2020), did not appear to be the

cause of mitochondrial dysfunction in our study. This was supported by our criteria that the protein levels remained unaltered for biological relevance. Furthermore, we did not detect any significant differences in protein expression related to protein misfolding pathways, as described earlier in eWAT homogenates (Gonzalez-Franquesa et al., 2022). Our findings suggested that the altered expression of proteins may not be the primary cause of mitochondrial dysfunction. Instead, the proper differentiation of adipose stem and progenitor cells into mature adipocytes could be a critical factor for mitochondrial function. This differentiation process can be influenced by nutritional programming, resulting in persistent epigenetic modifications in epididymal adipocytes and their mitochondria, which ultimately leads to a reduction in mitochondrial function and content.

Depending on the persistence of reduced mitochondrial abundance and function even after complete recovery from obesity, mitochondria may play a role in body mass cycling. Studies have shown that athletes and identical twins with a history of body mass loss have a higher body mass compared to non-athletes or non-dieting co-twins (Pietilainen et al., 2012; Saarni et al., 2006). The underlying mechanisms of body mass cycling are complex, with evidence supporting the role of mitochondria in both mice and humans (Heinonen et al., 2017; Kusminski and Scherer, 2012; Mustelin et al., 2008; Schottl et al., 2015b; Schottl et al., 2020; Wessels et al., 2019). To further elucidate the intricate subject of body mass cycling, we conducted an experimental investigation into the susceptibility of mice, which had undergone CD-induced obesity remission, to a high-fat environment and their proclivity to the ‘yo-yo effect’. The lean mice that were refed with a HFD showed an increased susceptibility to an obesogenic environment (**Figure 14**). In addition, inguinal iWAT demonstrated proper expansion capability, while eWAT showed no increase in mass due to its early limited storage capacity (van Beek et al., 2015), which was almost reached even in the control group due to age-related body mass gain (Turturro et al., 1999). Our data highlighted the susceptibility of HFD-refed mice to an obesogenic environment and suggested a link between the ‘yo-yo effect’ and the persistence of impaired epididymal adipocyte mitochondria.

After we had observed the susceptibility of HFD-refed mice to an obesogenic environment on the level of body mass and body composition, we were interested whether we can also see further reduction of the mitochondrial function (**Figure 15**). We proved the resistance of inguinal adipocytes against diet-induced obesity and a re-exposure to an obesogenic environment. On the contrary, in mice, eWAT reached its plateau already after 12 weeks of HFD feeding, which could lead to increased inflammation (van Beek et al., 2015) and a reduction in mitochondrial function. HFD refeeding even more decreased the functionality of the mitochondria in epididymal adipocytes by reducing the mitochondrial content. A further increase in the immune response and decrease in mitochondrial bioenergetics during obesity may be promoted

by a diminished immunometabolic crosstalk, reduced fission activity, and decreased density of *cristae* structures (Brestoff et al., 2021; Gonzalez-Franquesa et al., 2022; Tol et al., 2016). However, the inflammatory state in WAT and the reduced density of mitochondrial inner membrane *cristae* structure remain even after a full recovery from obesity (Gonzalez-Franquesa et al., 2022; Schmitz et al., 2016). As these alterations seem to be permanent, we suggested that they contributed to a susceptibly to re-exposing mice to an obesogenic environment. Our data highlighted the vulnerability of epididymal mitochondria and the resistance of inguinal mitochondria to a HFD environment.

To obtain a more profound understanding of the direct impact of body mass cycling, an investigation into the adipocyte protein expression was conducted. Previous studies have shown that obesity results in a reduced expression of mitochondrial OXPHOS proteins in obese cotwins when compared to their non-obese counterparts (Heinonen et al., 2017; Mustelin et al., 2008), and that body mass cycling has a negative effect on body mass in twins (Pietilainen et al., 2012). In light of these observations, we comprehensively examined OXPHOS complexes II – V in various adipose tissue samples (**Figure 16**). Strikingly, we failed to observe the reported decrease in the expression of OXPHOS proteins in obese mice in any of the samples, even after HFD refeeding (Gonzalez-Franquesa et al., 2022; Madsen et al., 2023; Schottl et al., 2020). The reasons for this discrepancy remained elusive. Nonetheless, we supposed no significant differences when analyzing the OXPHOS protein expression using a proteomics approach with strict criteria for detecting only biologically relevant proteins. Our findings suggested that nutritional programming of SVF cells and adipocytes induced persistent alterations that affected the function and abundance of mitochondria within adipocytes, resulting in irreversible changes.

In summary, our investigation unveiled the persistent deleterious effects of obesity on epididymal adipocytes even after complete remission induced by CD. While obesity caused a reversible increase in body mass and fat mass, it had a permanent negative impact on mitochondrial bioenergetics and inflammation in epididymal adipocytes. Notably, the differentiation capacity of adipocytes may play a crucial role in mitochondrial function, beyond differences in protein expression alone. The re-exposure of mice to an obesogenic environment after CD-induced obesity remission resulted in an increased susceptibility to obesity recurrence, likely due to irreversible alterations in mitochondrial function and content contributing to their proclivity to the ‘yo-yo effect’.

4.3 Conclusion and outlook

This dissertation has identified discernible variations in the adipogenic potential of iWAT and eWAT in response to obesity. Notably, we observed a reduction in the adipogenic potential of eWAT, primarily due to changes in the frequency of subpopulations of progenitor cells, in which an increase in the frequency of Aregs induces a reduced adipogenic potential. Prolonged HFD feeding and the subsequent relapse period induce an increase in the number of adipocytes, which can result in the shift of the balance from an available lipid storage to excess storage of lipid. This can contribute to the high rate of body mass regain. Our findings also suggest that HFD feeding does not lead to the arrest of APC proliferation. Nevertheless, the observed diminished adipogenic potential can be reversed through one-week refeeding with a low-fat CD, but not with a calorie-restricted pfHFD, demonstrating the importance of diet quality instead of solely diet quantity. Nutritional programming of adipogenic potential in APCs during the body mass loss phase may enforce the rate of body mass regain by promoting hyperplasia in response to subsequent HFD consumption. On the other hand, during the relapse period, there may be an increased frequency of Areg, which can reduce the adipogenic potential of progenitor cells, limiting the expansion of adipose tissue. As a result, mature adipocytes can enlarge to their maximum capacity, which may trigger cellular stress responses and lead to metabolic complications.

Adipose tissues, beyond serving as fat storage organs, mediate endocrine and paracrine activities. The alteration in the mitochondrial function of mature adipocytes persists even after the full remission of diet-induced obesity. However, we have not been able to attribute these persistent alterations in mitochondrial functionality to changes in the expression of mitochondrial proteins. As body mass increases and is regained, triglyceride stores in adipose tissue accumulate, leading to expansion of adipocytes until a plateau is reached in individuals with severe obesity. The increase in cell size places stress on the adipocytes, resulting in metabolic stress including endoplasmic reticulum stress and lipotoxicity, which finally alters mitochondrial function and communication, adipokine secretion patterns, and metabolite levels. These alterations may cause persistent abnormalities that predispose to relapsing metabolic disease upon refeeding with an obesogenic diet, representing a novel mechanism of nutritional programming.

Further research should be directed towards investigating the interplay between SVF cell signaling and mature adipocytes, particularly in relation to the development of adipogenic stem and precursor cell subpopulations and their impact on mitochondrial function. It is also crucial to consider strategies to restore mitochondrial function and content in eWAT when developing long-term body mass reduction therapeutics to address the issue of body mass cycling.

Overall, the rapid recovery of the adipogenic potential through the generation of new APCs, in conjunction with the persistent reduction in mitochondrial function, may promote body mass regain in mice. Nutritional programming of APCs results in irreversibly changed mitochondrial functionality and crosstalk of adipocytes in obesity, which might be implicated in driving body mass regain and constitute a valuable therapeutic target to preserve body mass reduction.

5 References

Alexson, S.E., and Nedergaard, J. (1988). A novel type of short- and medium-chain acyl-CoA hydrolases in brown adipose tissue mitochondria. J Biol Chem *263*, 13564-13571.

Alkhouri, N., Gornicka, A., Berk, M.P., Thapaliya, S., Dixon, L.J., Kashyap, S., Schauer, P.R., and Feldstein, A.E. (2010). Adipocyte apoptosis, a link between obesity, insulin resistance, and hepatic steatosis. J Biol Chem *285*, 3428-3438.

Anastasiou, C.A., Karfopoulou, E., and Yannakoulia, M. (2015). Weight regaining: From statistics and behaviors to physiology and metabolism. Metabolism *64*, 1395-1407.

Anderson, A., Werboff, J., and Les, E.P. (1968). Effects of environmental temperature-humidity and cage density on body weight and behavior in mice. Experientia *24*, 1022-1023.

Anderson, J.W., Konz, E.C., Frederich, R.C., and Wood, C.L. (2001). Long-term weight-loss maintenance: a meta-analysis of US studies. Am J Clin Nutr *74*, 579-584.

Arner, P., Andersson, D.P., Thorne, A., Wiren, M., Hoffstedt, J., Naslund, E., Thorell, A., and Ryden, M. (2013). Variations in the size of the major omentum are primarily determined by fat cell number. J Clin Endocrinol Metab *98*, E897-901.

Boardman, N.T., Trani, G., Scalabrin, M., Romanello, V., and Wust, R.C.I. (2023). Intra-cellular to inter-organ mitochondrial communication in striated muscle in health and disease. Endocr Rev.

Brand, M.D., and Nicholls, D.G. (2011). Assessing mitochondrial dysfunction in cells. Biochem J *435*, 297-312.

Brestoff, J.R., Wilen, C.B., Moley, J.R., Li, Y., Zou, W., Malvin, N.P., Rowen, M.N., Saunders, B.T., Ma, H., Mack, M.R.*, et al.* (2021). Intercellular Mitochondria Transfer to Macrophages Regulates White Adipose Tissue Homeostasis and Is Impaired in Obesity. Cell Metab *33*, 270-282 e278.

Brookheart, R.T., Michel, C.I., and Schaffer, J.E. (2009). As a matter of fat. Cell Metab *10*, 9-12.

Brownell, K.D., Greenwood, M.R., Stellar, E., and Shrager, E.E. (1986). The effects of repeated cycles of weight loss and regain in rats. Physiol Behav *38*, 459-464.

Burl, R.B., Ramseyer, V.D., Rondini, E.A., Pique-Regi, R., Lee, Y.H., and Granneman, J.G. (2018). Deconstructing Adipogenesis Induced by beta3-Adrenergic Receptor Activation with Single-Cell Expression Profiling. Cell Metab *28*, 300-309 e304.

Cases, S., Smith, S.J., Zheng, Y.W., Myers, H.M., Lear, S.R., Sande, E., Novak, S., Collins, C., Welch, C.B., Lusis, A.J.*, et al.* (1998). Identification of a gene encoding an acyl CoA:diacylglycerol acyltransferase, a key enzyme in triacylglycerol synthesis. Proc Natl Acad Sci U S A *95*, 13018-13023.

Cawthorn, W.P., Scheller, E.L., and MacDougald, O.A. (2012). Adipose tissue stem cells meet preadipocyte commitment: going back to the future. J Lipid Res *53*, 227-246.

Chau, Y.Y., Bandiera, R., Serrels, A., Martinez-Estrada, O.M., Qing, W., Lee, M., Slight, J., Thornburn, A., Berry, R., McHaffie, S.*, et al.* (2014). Visceral and subcutaneous fat have different origins and evidence supports a mesothelial source. Nat Cell Biol *16*, 367-375.

Cho, D.S., Lee, B., and Doles, J.D. (2019). Refining the adipose progenitor cell landscape in healthy and obese visceral adipose tissue using single-cell gene expression profiling. Life Sci Alliance *2*.

Christ, A., Lauterbach, M., and Latz, E. (2019). Western Diet and the Immune System: An Inflammatory Connection. Immunity *51*, 794-811.

Cinti, S. (2005). The adipose organ. Prostaglandins Leukot Essent Fatty Acids *73*, 9-15.

Cottam, M.A., Caslin, H.L., Winn, N.C., and Hasty, A.H. (2022). Multiomics reveals persistence of obesity-associated immune cell phenotypes in adipose tissue during weight loss and weight regain in mice. Nat Commun *13*, 2950.

Cox, J., Hein, M.Y., Luber, C.A., Paron, I., Nagaraj, N., and Mann, M. (2014). Accurate proteome-wide label-free quantification by delayed normalization and maximal peptide ratio extraction, termed MaxLFQ. Mol Cell Proteomics *13*, 2513-2526.

Cox, J., Neuhauser, N., Michalski, A., Scheltema, R.A., Olsen, J.V., and Mann, M. (2011). Andromeda: a peptide search engine integrated into the MaxQuant environment. J Proteome Res *10*, 1794-1805.

Crewe, C., Funcke, J.B., Li, S., Joffin, N., Gliniak, C.M., Ghaben, A.L., An, Y.A., Sadek, H.A., Gordillo, R., Akgul, Y.*, et al.* (2021). Extracellular vesicle-based interorgan transport of mitochondria from energetically stressed adipocytes. Cell Metab *33*, 1853-1868 e1811.

Cristancho, A.G., and Lazar, M.A. (2011). Forming functional fat: a growing understanding of adipocyte differentiation. Nat Rev Mol Cell Biol *12*, 722-734.

Cutter, G., St Jeor, S., Brunner, R., Wolfe, P., Foreyt, J., Dyer, A., and Brownell, K.D. (1996). Methodological issues in weight cycling. Ann Behav Med *18*, 280-289.

De Pauw, A., Tejerina, S., Raes, M., Keijer, J., and Arnould, T. (2009). Mitochondrial (dys)function in adipocyte (de)differentiation and systemic metabolic alterations. Am J Pathol *175*, 927-939.

DeBerardinis, R.J., Lum, J.J., Hatzivassiliou, G., and Thompson, C.B. (2008). The biology of cancer: metabolic reprogramming fuels cell growth and proliferation. Cell Metab *7*, 11-20.

Deus, C.M., Yambire, K.F., Oliveira, P.J., and Raimundo, N. (2020). Mitochondria-Lysosome Crosstalk: From Physiology to Neurodegeneration. Trends Mol Med *26*, 71-88.

Dong, L., Zhang, Y., Yang, L., Liu, G., Ye, J., and Wang, H. (2017). Effects of a High-Fat Diet on Adipose Tissue CD8+ T Cells in Young vs. Adult Mice. Inflammation *40*, 1944-1958.

Droyvold, W.B., Lund Nilsen, T.I., Lydersen, S., Midthjell, K., Nilsson, P.M., Nilsson, J.A., Holmen, J., and Nord-Trondelag Health, S. (2005). Weight change and mortality: the Nord-Trondelag Health Study. J Intern Med *257*, 338-345.

Dulloo, A.G. (2021). Physiology of weight regain: Lessons from the classic Minnesota Starvation Experiment on human body composition regulation. Obes Rev *22 Suppl 2*, e13189.

Dulloo, A.G., and Montani, J.P. (2015). Pathways from dieting to weight regain, to obesity and to the metabolic syndrome: an overview. Obes Rev *16 Suppl 1*, 1-6.

Eguchi, J., Wada, J., Hida, K., Zhang, H., Matsuoka, T., Baba, M., Hashimoto, I., Shikata, K., Ogawa, N., and Makino, H. (2005). Identification of adipocyte adhesion molecule (ACAM), a novel CTX gene family, implicated in adipocyte maturation and development of obesity. Biochem J *387*, 343-353.

Ellulu, M., Abed, Y., Rahmat, A., Ranneh, Y., and Ali, F. (2014). Epidemiology of obesity in developing countries: challenges and prevention. Global Epidemic Obesity *2*.

Emont, M.P., Jacobs, C., Essene, A.L., Pant, D., Tenen, D., Colleluori, G., Di Vincenzo, A., Jorgensen, A.M., Dashti, H., Stefek, A.*, et al.* (2022). A single-cell atlas of human and mouse white adipose tissue. Nature *603*, 926-933.

Ferrero, R., Rainer, P., and Deplancke, B. (2020). Toward a Consensus View of Mammalian Adipocyte Stem and Progenitor Cell Heterogeneity. Trends Cell Biol *30*, 937-950.

Fischer, B., Schottl, T., Schempp, C., Fromme, T., Hauner, H., Klingenspor, M., and Skurk, T. (2015). Inverse relationship between body mass index and mitochondrial oxidative phosphorylation capacity in human subcutaneous adipocytes. Am J Physiol Endocrinol Metab *309*, E380-387.

Fischer, I.P., Irmler, M., Meyer, C.W., Sachs, S.J., Neff, F., Hrabe de Angelis, M., Beckers, J., Tschop, M.H., Hofmann, S.M., and Ussar, S. (2018). A history of obesity leaves an inflammatory fingerprint in liver and adipose tissue. Int J Obes (Lond) *42*, 507-517.

Foster, M.T., Softic, S., Caldwell, J., Kohli, R., de Kloet, A.D., and Seeley, R.J. (2013). Subcutaneous Adipose Tissue Transplantation in Diet-Induced Obese Mice Attenuates Metabolic Dysregulation While Removal Exacerbates It. Physiol Rep *1*.

Fothergill, E., Guo, J., Howard, L., Kerns, J.C., Knuth, N.D., Brychta, R., Chen, K.Y., Skarulis, M.C., Walter, M., Walter, P.J.*, et al.* (2016). Persistent metabolic adaptation 6 years after "The Biggest Loser" competition. Obesity (Silver Spring) *24*, 1612-1619.

Fox, A.H. (2018). A mitochondria-paraspeckle crosstalk. Nat Cell Biol *20*, 1108-1109.

Freedhoff, Y., and Hall, K.D. (2016). Weight loss diet studies: we need help not hype. Lancet *388*, 849-851.

Ghaben, A.L., and Scherer, P.E. (2019). Adipogenesis and metabolic health. Nat Rev Mol Cell Biol *20*, 242-258.

Giordano, A., Murano, I., Mondini, E., Perugini, J., Smorlesi, A., Severi, I., Barazzoni, R., Scherer, P.E., and Cinti, S. (2013). Obese adipocytes show ultrastructural features of stressed cells and die of pyroptosis. J Lipid Res *54*, 2423-2436.

Gnaiger, E., Kuznetsov, A.V., Schneeberger, S., Seiler, R., Brandacher, G., Steurer, W., and Margreiter, R. (2000). Mitochondria in the Cold. G Heldmaier (Ed), Life in the Cold, Springer, Berlin, Heidelberg, New York.

Gonzalez-Franquesa, A., Gama-Perez, P., Kulis, M., Szczepanowska, K., Dahdah, N., Moreno-Gomez, S., Latorre-Pellicer, A., Fernandez-Ruiz, R., Aguilar-Mogas, A., Hoffman, A.*, et al.* (2022). Remission of obesity and insulin resistance is not sufficient to restore mitochondrial homeostasis in visceral adipose tissue. Redox Biol *54*, 102353.

Guillermier, C., Fazeli, P.K., Kim, S., Lun, M., Zuflacht, J.P., Milian, J., Lee, H., Francois-Saint-Cyr, H., Horreard, F., Larson, D.*, et al.* (2017). Imaging mass spectrometry demonstrates age-related decline in human adipose plasticity. JCI Insight *2*, e90349.

Gupta, R.K., Mepani, R.J., Kleiner, S., Lo, J.C., Khandekar, M.J., Cohen, P., Frontini, A., Bhowmick, D.C., Ye, L., Cinti, S.*, et al.* (2012). Zfp423 expression identifies committed preadipocytes and localizes to adipose endothelial and perivascular cells. Cell Metab *15*, 230-239.

Hammarstedt, A., Gogg, S., Hedjazifar, S., Nerstedt, A., and Smith, U. (2018). Impaired Adipogenesis and Dysfunctional Adipose Tissue in Human Hypertrophic Obesity. Physiol Rev *98*, 1911-1941.

Heinonen, S., Muniandy, M., Buzkova, J., Mardinoglu, A., Rodriguez, A., Fruhbeck, G., Hakkarainen, A., Lundbom, J., Lundbom, N., Kaprio, J.*, et al.* (2017). Mitochondria-related transcriptional signature is downregulated in adipocytes in obesity: a study of young healthy MZ twins. Diabetologia *60*, 169-181.

Hepler, C., and Gupta, R.K. (2017). The expanding problem of adipose depot remodeling and postnatal adipocyte progenitor recruitment. Mol Cell Endocrinol *445*, 95-108.

Hepler, C., Shan, B., Zhang, Q., Henry, G.H., Shao, M., Vishvanath, L., Ghaben, A.L., Mobley, A.B., Strand, D., Hon, G.C.*, et al.* (2018). Identification of functionally distinct fibro-inflammatory and adipogenic stromal subpopulations in visceral adipose tissue of adult mice. Elife *7*.

Hocking, S.L., Chisholm, D.J., and James, D.E. (2008). Studies of regional adipose transplantation reveal a unique and beneficial interaction between subcutaneous adipose tissue and the intra-abdominal compartment. Diabetologia *51*, 900-902.

Hocking, S.L., Stewart, R.L., Brandon, A.E., Suryana, E., Stuart, E., Baldwin, E.M., Kolumam, G.A., Modrusan, Z., Junutula, J.R., Gunton, J.E.*, et al.* (2015). Subcutaneous fat transplantation alleviates diet-induced glucose intolerance and inflammation in mice. Diabetologia *58*, 1587-1600.

Hofmann, J., Gadjalova, I., Mishra, R., Ruland, J., and Keppler, S.J. (2020). Efficient Tissue Clearing and Multi-Organ Volumetric Imaging Enable Quantitative Visualization of Sparse Immune Cell Populations During Inflammation. Front Immunol *11*, 599495.

Isakson, P., Hammarstedt, A., Gustafson, B., and Smith, U. (2009). Impaired preadipocyte differentiation in human abdominal obesity: role of Wnt, tumor necrosis factor-alpha, and inflammation. Diabetes *58*, 1550-1557.

Jo, J., Gavrilova, O., Pack, S., Jou, W., Mullen, S., Sumner, A.E., Cushman, S.W., and Periwal, V. (2009). Hypertrophy and/or Hyperplasia: Dynamics of Adipose Tissue Growth. PLoS Comput Biol *5*, e1000324.

Joe, A.W., Yi, L., Even, Y., Vogl, A.W., and Rossi, F.M. (2009). Depot-specific differences in adipogenic progenitor abundance and proliferative response to high-fat diet. Stem Cells *27*, 2563-2570.

Keys, A., Brozek, J., Henschel, A., Mickelsen, O., and Taylor, H.L. (1950). The biology of human starvation. Minneapolis (MN): The University of Minnesota Press.

Kim, J.Y., Tillison, K., Zhou, S., Wu, Y., and Smas, C.M. (2007). The major facilitator superfamily member Slc37a2 is a novel macrophage- specific gene selectively expressed in obese white adipose tissue. Am J Physiol Endocrinol Metab *293*, E110-120.

Kim, S.M., Lun, M., Wang, M., Senyo, S.E., Guillermier, C., Patwari, P., and Steinhauser, M.L. (2014). Loss of white adipose hyperplastic potential is associated with enhanced susceptibility to insulin resistance. Cell Metab *20*, 1049-1058.

Kitahara, C.M., Flint, A.J., Berrington de Gonzalez, A., Bernstein, L., Brotzman, M., MacInnis, R.J., Moore, S.C., Robien, K., Rosenberg, P.S., Singh, P.N.*, et al.* (2014). Association between class III obesity (BMI of 40-59 kg/m2) and mortality: a pooled analysis of 20 prospective studies. PLoS Med *11*, e1001673.

Koh, E.H., Park, J.Y., Park, H.S., Jeon, M.J., Ryu, J.W., Kim, M., Kim, S.Y., Kim, M.S., Kim, S.W., Park, I.S.*, et al.* (2007). Essential role of mitochondrial function in adiponectin synthesis in adipocytes. Diabetes *56*, 2973-2981.

Kolodziejczyk, A.A., Kim, J.K., Svensson, V., Marioni, J.C., and Teichmann, S.A. (2015). The technology and biology of single-cell RNA sequencing. Mol Cell *58*, 610-620.

Kovesdy, C.P., Furth, S.L., Zoccali, C., and World Kidney Day Steering, C. (2017). Obesity and Kidney Disease: Hidden Consequences of the Epidemic. Can J Kidney Health Dis *4*, 2054358117698669.

Kusminski, C.M., Holland, W.L., Sun, K., Park, J., Spurgin, S.B., Lin, Y., Askew, G.R., Simcox, J.A., McClain, D.A., Li, C.*, et al.* (2012). MitoNEET-driven alterations in adipocyte mitochondrial activity reveal a crucial adaptive process that preserves insulin sensitivity in obesity. Nat Med *18*, 1539-1549.

Kusminski, C.M., and Scherer, P.E. (2012). Mitochondrial dysfunction in white adipose tissue. Trends Endocrinol Metab *23*, 435-443.

Lawson, H.A., Zayed, M., Wayhart, J.P., Fabbrini, E., Love-Gregory, L., Klein, S., and Semenkovich, C.F. (2017). Physiologic and genetic evidence links hemopexin to triglycerides in mice and humans. Int J Obes (Lond) *41*, 631-638.

Lee, M.J., Wu, Y., and Fried, S.K. (2010). Adipose tissue remodeling in pathophysiology of obesity. Curr Opin Clin Nutr Metab Care *13*, 371-376.

Li, Q., Hagberg, C.E., Silva Cascales, H., Lang, S., Hyvonen, M.T., Salehzadeh, F., Chen, P., Alexandersson, I., Terezaki, E., Harms, M.J*., et al.* (2021). Obesity and hyperinsulinemia drive adipocytes to activate a cell cycle program and senesce. Nat Med *27*, 1941-1953.

Longo, M., Zatterale, F., Naderi, J., Parrillo, L., Formisano, P., Raciti, G.A., Beguinot, F., and Miele, C. (2019). Adipose Tissue Dysfunction as Determinant of Obesity-Associated Metabolic Complications. Int J Mol Sci *20*.

Lu, R.H., Ji, H., Chang, Z.G., Su, S.S., and Yang, G.S. (2010). Mitochondrial development and the influence of its dysfunction during rat adipocyte differentiation. Mol Biol Rep *37*, 2173-2182.

MacLean, P.S., Higgins, J.A., Giles, E.D., Sherk, V.D., and Jackman, M.R. (2015). The role for adipose tissue in weight regain after weight loss. Obes Rev *16 Suppl 1*, 45-54.

MacLean, P.S., Higgins, J.A., Jackman, M.R., Johnson, G.C., Fleming-Elder, B.K., Wyatt, H.R., Melanson, E.L., and Hill, J.O. (2006). Peripheral metabolic responses to prolonged weight reduction that promote rapid, efficient regain in obesity-prone rats. Am J Physiol Regul Integr Comp Physiol *290*, R1577-1588.

Macotela, Y., Emanuelli, B., Mori, M.A., Gesta, S., Schulz, T.J., Tseng, Y.H., and Kahn, C.R. (2012). Intrinsic differences in adipocyte precursor cells from different white fat depots. Diabetes *61*, 1691-1699.

Madsen, S., Nelson, M.E., Deshpande, V., Humphrey, S.J., Cooke, K.C., Howell, A., Diaz-Vegas, A., Burchfield, J.G., Stockli, J., and James, D.E. (2023). Deep proteome profiling of white adipose tissue reveals marked conservation and distinct features between different anatomical depots. Mol Cell Proteomics, 100508.

Marcelin, G., Ferreira, A., Liu, Y., Atlan, M., Aron-Wisnewsky, J., Pelloux, V., Botbol, Y., Ambrosini, M., Fradet, M., Rouault, C*., et al.* (2017). A PDGFRalpha-Mediated Switch toward CD9(high) Adipocyte Progenitors Controls Obesity-Induced Adipose Tissue Fibrosis. Cell Metab *25*, 673-685.

Merrick, D., Sakers, A., Irgebay, Z., Okada, C., Calvert, C., Morley, M.P., Percec, I., and Seale, P. (2019). Identification of a mesenchymal progenitor cell hierarchy in adipose tissue. Science *364*.

Moreno-Navarrete, J.M., Novelle, M.G., Catalan, V., Ortega, F., Moreno, M., Gomez-Ambrosi, J., Xifra, G., Serrano, M., Guerra, E., Ricart, W*., et al.* (2014). Insulin resistance modulates iron-related proteins in adipose tissue. Diabetes Care *37*, 1092-1100.

Mustelin, L., Pietilainen, K.H., Rissanen, A., Sovijarvi, A.R., Piirila, P., Naukkarinen, J., Peltonen, L., Kaprio, J., and Yki-Jarvinen, H. (2008). Acquired obesity and poor physical fitness impair expression of genes of mitochondrial oxidative phosphorylation in monozygotic twins discordant for obesity. Am J Physiol Endocrinol Metab *295*, E148-154.

Mutt, S.J., Hypponen, E., Saarnio, J., Jarvelin, M.R., and Herzig, K.H. (2014). Vitamin D and adipose tissue-more than storage. Front Physiol *5*, 228.

Muurling, M., Jong, M.C., Mensink, R.P., Hornstra, G., Dahlmans, V.E., Pijl, H., Voshol, P.J., and Havekes, L.M. (2002). A low-fat diet has a higher potential than energy restriction to improve high-fat diet-induced insulin resistance in mice. Metabolism *51*, 695-701.

Nanri, A., Mizoue, T., Takahashi, Y., Noda, M., Inoue, M., Tsugane, S., and Japan Public Health Center- based Prospective Study, G. (2010). Weight change and all-cause, cancer and cardiovascular disease mortality in Japanese men and women: the Japan Public Health Center-Based Prospective Study. Int J Obes (Lond) *34*, 348-356.

National, F.T. (1994). Weight cycling. National Task Force on the Prevention and Treatment of Obesity. JAMA *272*, 1196-1202.

OECD/WHO (2020). Obesity and overweight. Health at a Glance: Asia/Pacific 2020: Measuring Progress Towards Universal Health Coverage *OECD Publishing, Paris*.

Parlee, S.D., Lentz, S.I., Mori, H., and MacDougald, O.A. (2014). Quantifying size and number of adipocytes in adipose tissue. Methods Enzymol *537*, 93-122.

Parra-Vargas, M., Ramon-Krauel, M., Lerin, C., and Jimenez-Chillaron, J.C. (2020). Size Does Matter: Litter Size Strongly Determines Adult Metabolism in Rodents. Cell Metab *32*, 334-340.

Pasquet, P., and Apfelbaum, M. (1994). Recovery of initial body weight and composition after long-term massive overfeeding in men. Am J Clin Nutr *60*, 861-863.

Pasquet, P., Brigant, L., Froment, A., Koppert, G.A., Bard, D., de Garine, I., and Apfelbaum, M. (1992). Massive overfeeding and energy balance in men: the Guru Walla model. Am J Clin Nutr *56*, 483-490.

Pietilainen, K.H., Saarni, S.E., Kaprio, J., and Rissanen, A. (2012). Does dieting make you fat? A twin study. Int J Obes (Lond) *36*, 456-464.

Renehan, A.G., Tyson, M., Egger, M., Heller, R.F., and Zwahlen, M. (2008). Body-mass index and incidence of cancer: a systematic review and meta-analysis of prospective observational studies. Lancet *371*, 569-578.

Rosen, E.D., and Spiegelman, B.M. (2014). What we talk about when we talk about fat. Cell *156*, 20-44.

Saarni, S.E., Rissanen, A., Sarna, S., Koskenvuo, M., and Kaprio, J. (2006). Weight cycling of athletes and subsequent weight gain in middleage. Int J Obes (Lond) *30*, 1639-1644.

Sacks, F.M., Bray, G.A., Carey, V.J., Smith, S.R., Ryan, D.H., Anton, S.D., McManus, K., Champagne, C.M., Bishop, L.M., Laranjo, N.*, et al.* (2009). Comparison of weight-loss diets with different compositions of fat, protein, and carbohydrates. N Engl J Med *360*, 859-873.

Saez, I., and Vilchez, D. (2014). The Mechanistic Links Between Proteasome Activity, Aging and Age-related Diseases. Curr Genomics *15*, 38-51.

Sarjeant, K., and Stephens, J.M. (2012). Adipogenesis. Cold Spring Harb Perspect Biol *4*, a008417.

Sarvari, A.K., Van Hauwaert, E.L., Markussen, L.K., Gammelmark, E., Marcher, A.B., Ebbesen, M.F., Nielsen, R., Brewer, J.R., Madsen, J.G.S., and Mandrup, S. (2021). Plasticity of Epididymal Adipose Tissue in Response to Diet-Induced Obesity at Single-Nucleus Resolution. Cell Metab *33*, 437-453 e435.

Schmitz, J., Evers, N., Awazawa, M., Nicholls, H.T., Bronneke, H.S., Dietrich, A., Mauer, J., Bluher, M., and Bruning, J.C. (2016). Obesogenic memory can confer long-term increases in adipose tissue but not liver inflammation and insulin resistance after weight loss. Mol Metab *5*, 328-339.

Schottl, T., Kappler, L., Braun, K., Fromme, T., and Klingenspor, M. (2015a). Limited mitochondrial capacity of visceral versus subcutaneous white adipocytes in male C57BL/6N mice. Endocrinology *156*, 923-933.

Schottl, T., Kappler, L., Fromme, T., and Klingenspor, M. (2015b). Limited OXPHOS capacity in white adipocytes is a hallmark of obesity in laboratory mice irrespective of the glucose tolerance status. Mol Metab *4*, 631-642.

Schottl, T., Pachl, F., Giesbertz, P., Daniel, H., Kuster, B., Fromme, T., and Klingenspor, M. (2020). Proteomic and Metabolite Profiling Reveals Profound Structural and Metabolic Reorganization of Adipocyte Mitochondria in Obesity. Obesity (Silver Spring) *28*, 590-600.

Schwalie, P.C., Dong, H., Zachara, M., Russeil, J., Alpern, D., Akchiche, N., Caprara, C., Sun, W., Schlaudraff, K.U., Soldati, G.*, et al.* (2018). A stromal cell population that inhibits adipogenesis in mammalian fat depots. Nature *559*, 103-108.

Shevchenko, A., Tomas, H., Havlis, J., Olsen, J.V., and Mann, M. (2006). In-gel digestion for mass spectrometric characterization of proteins and proteomes. Nat Protoc *1*, 2856-2860.

Shirakawa, K., Endo, J., Katsumata, Y., Yamamoto, T., Kataoka, M., Isobe, S., Yoshida, N., Fukuda, K., and Sano, M. (2017). Negative legacy of obesity. PLoS One *12*, e0186303.

Song, X.H., He, N., Xing, Y.T., Jin, X.Q., Li, Y.W., Liu, S.S., Gao, Z.Y., Guo, C., Wang, J.J., Huang, Y.Y.*, et al.* (2021). A Novel Age-Related Circular RNA Circ-ATXN2 Inhibits Proliferation, Promotes Cell Death and Adipogenesis in Rat Adipose Tissue-Derived Stromal Cells. Front Genet *12*, 761926.

Spalding, K.L., Arner, E., Westermark, P.O., Bernard, S., Buchholz, B.A., Bergmann, O., Blomqvist, L., Hoffstedt, J., Naslund, E., Britton, T.*, et al.* (2008). Dynamics of fat cell turnover in humans. Nature *453*, 783-787.

Stehling, O., Wilbrecht, C., and Lill, R. (2014). Mitochondrial iron-sulfur protein biogenesis and human disease. Biochimie *100*, 61-77.

Sun, K., Kusminski, C.M., and Scherer, P.E. (2011). Adipose tissue remodeling and obesity. J Clin Invest *121*, 2094-2101.

Tang, W., Zeve, D., Suh, J.M., Bosnakovski, D., Kyba, M., Hammer, R.E., Tallquist, M.D., and Graff, J.M. (2008). White fat progenitor cells reside in the adipose vasculature. Science *322*, 583-586.

Tol, M.J., Ottenhoff, R., van Eijk, M., Zelcer, N., Aten, J., Houten, S.M., Geerts, D., van Roomen, C., Bierlaagh, M.C., Scheij, S.*, et al.* (2016). A PPARgamma-Bnip3 Axis Couples Adipose Mitochondrial Fusion-Fission Balance to Systemic Insulin Sensitivity. Diabetes *65*, 2591-2605.

Tormos, K.V., Anso, E., Hamanaka, R.B., Eisenbart, J., Joseph, J., Kalyanaraman, B., and Chandel, N.S. (2011). Mitochondrial complex III ROS regulate adipocyte differentiation. Cell Metab *14*, 537-544.

Toth, L.A., Trammell, R.A., and Ilsley-Woods, M. (2015). Interactions Between Housing Density and Ambient Temperature in the Cage Environment: Effects on Mouse Physiology and Behavior. J Am Assoc Lab Anim Sci *54*, 708-717.

Tran, T.T., Yamamoto, Y., Gesta, S., and Kahn, C.R. (2008). Beneficial effects of subcutaneous fat transplantation on metabolism. Cell Metab *7*, 410-420.

Tsiloulis, T., and Watt, M.J. (2015). Exercise and the Regulation of Adipose Tissue Metabolism. Prog Mol Biol Transl Sci *135*, 175-201.

Turturro, A., Witt, W.W., Lewis, S., Hass, B.S., Lipman, R.D., and Hart, R.W. (1999). Growth curves and survival characteristics of the animals used in the Biomarkers of Aging Program. J Gerontol A Biol Sci Med Sci *54*, B492-501.

Tyanova, S., Temu, T., and Cox, J. (2016). The MaxQuant computational platform for mass spectrometry-based shotgun proteomics. Nat Protoc *11*, 2301-2319.

van Beek, L., van Klinken, J.B., Pronk, A.C., van Dam, A.D., Dirven, E., Rensen, P.C., Koning, F., Willems van Dijk, K., and van Harmelen, V. (2015). The limited storage capacity of gonadal adipose tissue directs the development of metabolic disorders in male C57Bl/6J mice. Diabetologia *58*, 1601-1609.

Vazquez-Sandoval, A., Velez-delValle, C., Hernandez-Mosqueira, C., Marsch-Moreno, M., Ayala-Sumuano, J.T., and Kuri-Harcuch, W. (2023). FAM129B is a cooperative protein that regulates adipogenesis. Biochem Biophys Res Commun *638*, 66-75.

Vernochet, C., Mourier, A., Bezy, O., Macotela, Y., Boucher, J., Rardin, M.J., An, D., Lee, K.Y., Ilkayeva, O.R., Zingaretti, C.M.*, et al.* (2012). Adipose-specific deletion of TFAM increases mitochondrial oxidation and protects mice against obesity and insulin resistance. Cell Metab *16*, 765-776.

Wajchenberg, B.L., Giannella-Neto, D., da Silva, M.E., and Santos, R.F. (2002). Depot-specific hormonal characteristics of subcutaneous and visceral adipose tissue and their relation to the metabolic syndrome. Horm Metab Res *34*, 616-621.

Wang, Q.A., Tao, C., Gupta, R.K., and Scherer, P.E. (2013). Tracking adipogenesis during white adipose tissue development, expansion and regeneration. Nat Med *19*, 1338-1344.

Wessels, B., Honecker, J., Schottl, T., Stecher, L., Klingenspor, M., Hauner, H., and Skurk, T. (2019). Adipose Mitochondrial Respiratory Capacity in Obesity is Impaired Independently of Glycemic Status of Tissue Donors. Obesity (Silver Spring) *27*, 756-766.

Wing, R.R., and Hill, J.O. (2001). Successful weight loss maintenance. Annu Rev Nutr *21*, 323-341.

Woo, C.Y., Jang, J.E., Lee, S.E., Koh, E.H., and Lee, K.U. (2019). Mitochondrial Dysfunction in Adipocytes as a Primary Cause of Adipose Tissue Inflammation. Diabetes Metab J *43*, 247-256.

Xu, H., Cupples, L.A., Stokes, A., and Liu, C.T. (2018). Association of Obesity With Mortality Over 24 Years of Weight History: Findings From the Framingham Heart Study. JAMA Netw Open *1*, e184587.

Xu, Z., You, W., Zhou, Y., Chen, W., Wang, Y., and Shan, T. (2019). Cold-induced lipid dynamics and transcriptional programs in white adipose tissue. BMC Biol *17*, 74.

Yang, W.S., Lee, W.J., Huang, K.C., Lee, K.C., Chao, C.L., Chen, C.L., Tai, T.Y., and Chuang, L.M. (2003). mRNA levels of the insulin-signaling molecule SORBS1 in the adipose depots of nondiabetic women. Obes Res *11*, 586-590.

Yenjerla, M., Panopoulos, A., Reynaud, C., Fotedar, R., and Margolis, R.L. (2013). TD-60 is required for interphase cell cycle progression. Cell Cycle *12*, 837-841.

Yousof, T., Byun, J.H., Chen, J., and Austin, R.C. (2022). Pleckstrin Homology-Like Domain, Family A, Member 1 (PHLDA1): A Multifaceted Cell Survival Factor that Drives Metabolic Disease. Engineering

Zachara, M., Rainer, P.Y., Hashimi, H., Russeil, J.M., Alpern, D., Ferrero, R., Litovchenko, M., and Deplancke, B. (2022). Mammalian adipogenesis regulator (Areg) cells use retinoic acid signalling to be non- and anti-adipogenic in age-dependent manner. EMBO J *41*, e108206.

6 Appendix

6.1 Material

Table 14: List of used chemicals.

Chemical	Cat#	Supplier
1-Thioglycerol	Cay20824-5	Biomol
2-acrylamido-2-methylpropane sulfonic acid (AMPS)	9592	Carl Roth
4-(2-hydroxyethyl)-1-piperazineethanesulfonic acid (HEPES)	H0887	Sigma-Aldrich
5,5'dithiobis(2-nitrobenzoic acid (DTNB)	D21800	Sigma-Aldrich
5-ethynyl-2'-deoxyuridine (EdU)	A10044	ThermoFisher Scientific
α-chacconie	1553 S	Extrasynthese
Acetyl coenzyme A sodium salt	A2056	Sigma-Aldrich
Adenosine diphosphate (ADP) monopotassium hydrate salt	A5285	Sigma-Aldrich
Ammonium chloride	5470	Carl Roth
Amphotericine B	A2612	Biochrom
Antimycin A	A8674	Sigma-Aldrich
β-mercaptoethanol	M3148	Sigma-Aldrich
Bovine serum albumin (BSA) Fatty Acid Free	A3803	Sigma-Aldrich
Bovine serum albumin (BSA) fraction	8076	Carl Roth
Bromphenol blue	B0126	Sigma-Aldrich
Chloroform p.a.	Y015.1	Carl Roth
Collagenase type I	C 1-22	Biochrom
Dexamethasone	D4902	Sigma-Aldrich
Diethylpyrocarbonate (DEPC)	D5758	Sigma-Aldrich
Dimethyl sulfoxide (DMSO)	4720	Carl Roth

Dipotassium hydrogen phosphate	T875	Carl Roth
Dulbecco's modified eagle medium (DMEM) - high-glucose	D5796	Sigma-Aldrich
Eosin	7089	Carl Roth
Ethanol 70 %, denatured	T913	Carl Roth
Ethanol 96 %, denatured	T171	Carl Roth
Ethanol 99.8 % p.a.	9065	Carl Roth
Ethyl cinnamate	W243000	Sigma-Aldrich
Ethylenediaminetetraacetic acid (EDTA)	V432B	Promega
Ethylene glycol tetraacetic acid (EGTA)	3054	Carl Roth
Fetal bovine serum (FBS)	S0615	Biochrom
Formaldehyde 4 % (v/v)	97135000	VWR
Gentamycin	A2712	Biochrom
Glucose	HN06	Biochrom
Glycerin	3783	Carl Roth
Hank's balanced salt solution (HBSS) w/o Mg^{2+}, Ca^{2+}	14025-050	Invitrogen
Hematoxylin	3870.2500	VWR
Hydrogen chloride	0281	Carl Roth
Indomethacin	I7378	Sigma-Aldrich
Insulin	I9278	Sigma-Aldrich
Isobutylmethylxanthine	I5879	Sigma-Aldrich
Isopropanol	I9516	Sigma-Aldrich
Lactobionic acid	153516	Sigma-Aldrich
Magnesium chloride	M8266	Sigma-Aldrich
Malate disodium salt	M9138	Sigma-Aldrich
Methanol	4627	Carl Roth
Mounting medium	1.00579.0500	VWR
Nonidet® P-40	NP40S	Sigma-Aldrich
Nuclease-free water	129114	Qiagen
Oligomycin	O4876	Sigma-Aldrich
Oil Red O	O0625	Sigma-Aldrich
Oxaloacetic acid	O4126	Sigma-Aldrich

PageRuler Prestained Protein Ladder	26616	ThermoFisher Scientific
Paraffin	361336E	VWR
Penicillin/Streptomycin	A2212	Biochrom
Phosphate Buffered Saline (PBS) Tablets	18912-014	Gibco
Potassium chloride	P9541	Sigma-Aldrich
Potassium hydroxide	6751	Carl Roth
Potassium pyruvate	COM448637111	Sigma-Aldrich
Protease inhibitor	P8340	Sigma-Aldrich
Rosiglitazone	Cay71740	Biomol
ROTI® Phenol/Chloroform/Isoamyl alcohol	A156	Carl Roth
ROTIPHORESE® Gel 30 (37.5:1)	3029	Carl Roth
Sodium chloride	3957	Carl Roth
Sodium deoxycholate	D6750	Sigma-Aldrich
sodium dodecyl sulfate (SDS)/Sodiumlaurylsulphate	4360	Carl Roth
Succinate	398055	Sigma-Aldrich
Sucrose	84097	Sigma-Aldrich
Taurine	4721	Carl Roth
Tetramethylethylenediamine (TEMED)	2367	Carl Roth
Triiodothyronine (T3)	T6397	Sigma-Aldrich
Tris	4855	Carl Roth
Tris-HCl	9090	Carl Roth
TRISure	BIO-38033	BioLine
Triton X-100	85111	ThermoFisher Scientific
Trypan blue 0.4 % (v/v)	1680	Carl Roth
Tween 20	9127	Carl Roth
Xylene	28973.363	VWR

Table 15: List of precast buffers.

Buffer	Cat#	Supplier
eBioscience™ Intracellular Fixation & Permeabilization Buffer Set	88-8824-00	ThermoFisher Scientific
ROTI® Load Sample buffer	K929	Carl Roth
ROTIPHORESE® SDS-Gel Buffer 10x	3060	Carl Roth

Table 16: List of commercial kit systems.

Kit system	Cat#	Supplier
CellTiter-Glo® Luminescent Cell Viability Assay	G7570	Promega
Click-iT™ EdU Alexa Fluor™ 488 Imaging Kit	C10637	ThermoFisher Scientific
Pierce™ BCA Protein Assay	23225	ThermoFisher Scientific
SensiFAST™ cDNA Synthesis Kit	BIO-65054	BioLine
SensiMix SYBR® No-Rox	QT650-20	BioLine
SV Total RNA Isolation System	Z3105	Promega

Table 17: List of consumables.

Consumable	Cat#	Supplier
Cell culture plate 12 well	*83.3921*	*Sarstedt*
Cell scraper	*83.3951*	*Sarstedt*
Cell strainer 40 µM	352340	BD Biosciences
Filter tips (10 µl, 200 µl, 1000 µl)	701130210, 70760211, 70.3050.355	Sarstedt
Micro 96 well plate nunc	260895	VWR
Microscope Cover Slips	MENZBB024060M113	VWR
Nitril gloves	112-2755	VWR
Nitrocellulose	926-31092	Li-Cor
Nylon Mesh 250 µm	510-9526	VWR

Omnifex® 50 ml Luer Lock syringe	4617509F	Zefa
Pasteur pipette	7477 70	VWR
PCR tubes	72.991.992	Sarstedt
Pipette tips (10 µl, 100 µl, 1000 µl)	70.1130, 70.760.002, 70.762	Sarstedt
Screw cap tube (5 ml, 15 ml, 50 ml)	62558201, 62.554.502, 62.547.254	Sarstedt
Serological pipette (5 ml, 10 ml, 25 ml)	861253001, 861254001, 861685001	Sarstedt
SuperFrost® Microscope slides	12372098	ThermoFisher Scientific
Syringe filter CA 25 mm, 0.22 µm	1302601	Zefa
Tubes (1.5 ml, 2 ml)	72.690.001, 72.691	Sarstedt

6.2 Supplementary figure

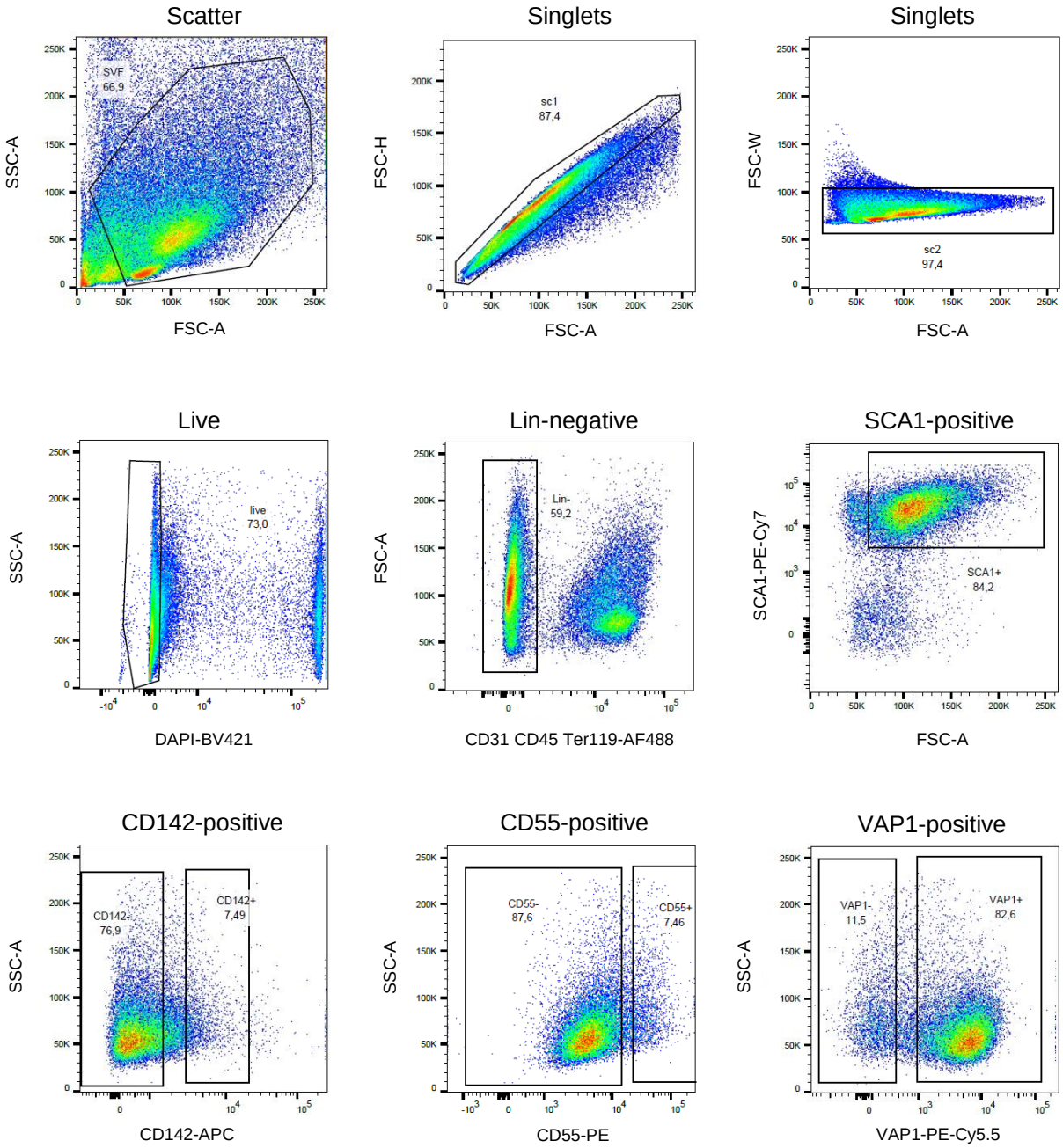

Figure S1: Gating strategy for live cell surface staining to identify three adipogenic stem and precursor cell subpopulations. The gating strategy example shows stromal-vascular fraction (SVF) cells from epididymal white adipose tissue (eWAT) of mice fed a control diet (CD), with gating performed from left to right and top to bottom. Fluorescence minus one (FMO) controls were implemented to accurately differentiate between positive and negative subpopulations. AF = Alexa Fluor®, APC = allophycocyanine, BV = blue violet, Cy = Cyanine, DAPI = 4′,6-diamidino-2-phenylindole, FSC-A = forward scatter area, FSC-H = forward scatter height, FSC-W = forward scatter width, Lin = Lineage, PE = phycoerythrin, SSC-A = side scatter area, SCA1 = stem cells antigen 1, VAP1 = vascular adhesion protein 1.

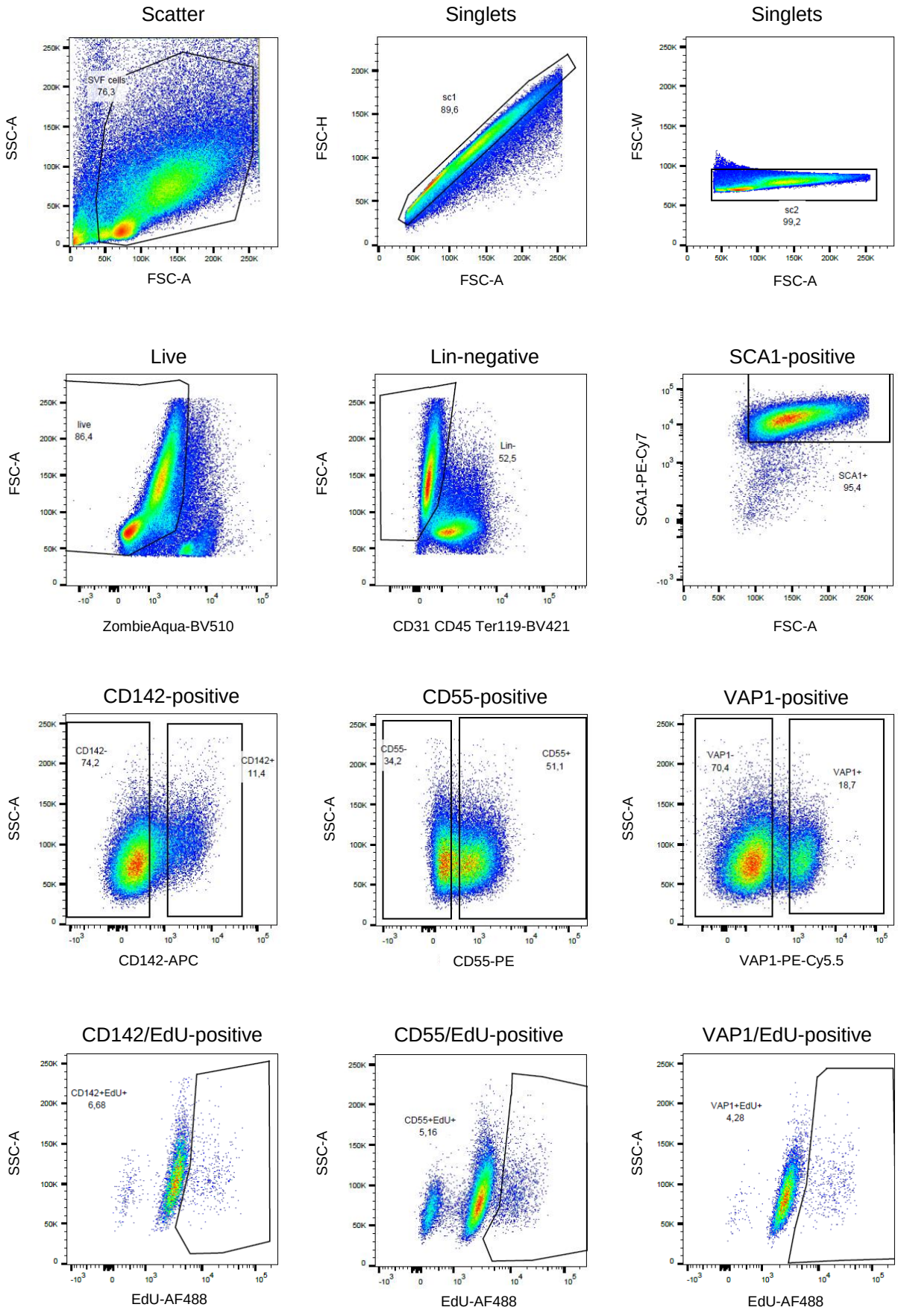

Figure S2: Gating strategy for intracellular staining to identify three adipogenic stem and precursor cell subpopulations and cell proliferation. The gating strategy example shows stromal-vascular fraction (SVF) cells from inguinal white adipose tissue (iWAT) of mice fed a control diet (CD), with

gating performed from left to right and top to bottom. Fluorescence minus one (FMO) controls were implemented to accurately differentiate between positive and negative subpopulations. AF = Alexa Fluor®, APC = allophycocyanine, BV = Blue violet, Cy = Cyanine, DAPI = 4′,6-diamidino-2-phenylindole, EdU = 5-ethynyl-2'-deoxyuridine, FSC-A = forward scatter area; FSC-H = forward scatter height, FSC-W = forward scatter width, Lin = Lineage, PE = phycoerythrin, SSC-A = side scatter area, SCA1 = stem cells antigen 1, VAP1 = vascular adhesion protein 1.

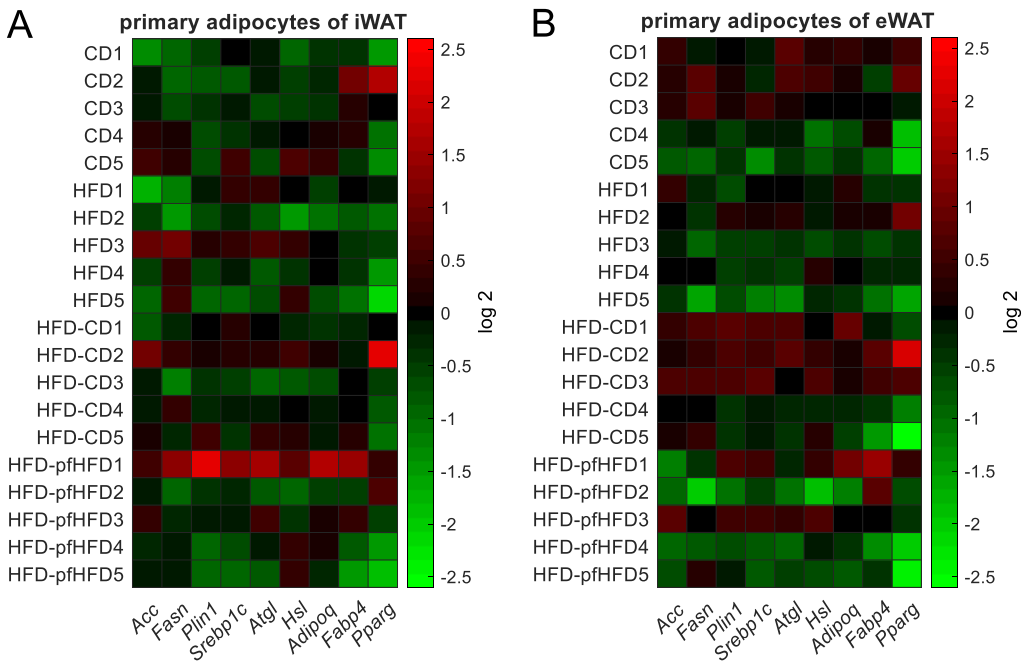

Figure S3: Influence of high-fat diet and short-term obesity interventions on terminal differentiation makers of the adipogenic potential. Isolated stromal-vascular fraction (SVF) cells were cultured until confluence, induced for 48 h, and differentiated for six days. Terminal differentiation capacity was determined by real-time quantitative polymerase chain reaction (RT-qPCR) (**A**) Heat map of selected terminal differentiation markers in differentiated inguinal primary adipocytes in four feeding regimes. Every value represents one mouse (biological replicate) with three technical replicates. Values are standardized in a way that each column (single protein) has the same mean (0) and standard deviation (1). (**B**) Heat map of selected terminal differentiation markers in differentiated epididymal primary adipocytes in four feeding regimes. Every value represents one mouse (biological replicate) with three technical replicates. Values are standardized in a way that each column (single protein) has the same mean (0) and standard deviation (1). All data were analyzed by one-way ANOVA (Dunn-Šidák correction). n = 5 (biological replicates). CD = control diet, HFD = high-fat diet, pf = pair-fed.

7 Acknowledgment

Diese Arbeit wäre nicht möglich gewesen ohne die großartige Hilfe und Unterstützung mehrerer Personen, denen ich an dieser Stelle herzlich danken möchte.

An erster Stelle möchte ich meinen Doktorvater Prof. Dr. Martin Klingenspor danken. Vielen Dank für die Bereitstellung des Themas und die tollen 4,5 Jahre an deinem Lehrstuhl, die vielen neuen Methoden die ich erlernen konnte und die Verantwortung die ich für meine Projekte und Mäuse übernehmen durfte. Zusätzlich möchte ich dir für die konstruktiven Diskussionen, Anregungen, Ratschläge und die Unterstützung zu meinem Thema danken.

Ein herzliches Dankeschön geht an PD Dr. Tobias Fromme. Vielen Dank für die vielen Stunden in denen wir uns durch alle Daten und Abbildungen gewälzt haben und in denen du dich mit meinem Paper-Manuskript und dieser Arbeit beschäftig hast.

Ich möchte mich bei der gesamten Arbeitsgruppe für die angenehme Arbeitsatmosphäre, die Hilfsbereitschaft, die Ratschläge und vielen schönen Momenten bedanken. Ein besonderer Dank geht an meine Kollegen und Hiwis, Sabine, Manuela, Anna und Philipp, die mich Tatkräftig unterstützt haben. Des Weiteren möchte ich Prof. Dr. Yongguo Li für die vielen Unterhaltungen zu meinen Versuchen in unserem Büro danken. Danke auch an Johanna, Akim, Sebastian, Josef, Katharina und alle Tierpfleger vom Kleintierforschungszentrum Weihenstephan, die mich Rund um das Thema Mäuse unterstützt haben. Meiner ehemaligen Masterstudentin Julia möchte ich ebenfalls für ihre Arbeit und Engagement danken.

Ein Dankeschön für das Korrekturlesen dieser Arbeit geht an PD Dr. Tobias Fromme, Dr. Eva Rath und Theresa Lutz.

Vielen Dank auch an meine Kollaborationspartner Dr. Christina Ludwig (Bayerisches Zentrum für Biomolekulare MassenSpektrometrie), Dr. Selina Keppler und Marie Goëss (Institut für Klinische Chemie und Pathobiochemie) für eure Arbeit und Unterstützung. Ein Dankeschön geht auch an Dr. Pratigya Subba, die mich bei der Auswertung der Proteomics Daten mit unterstützt hat.

Des Weiteren möchte ich mich bei der Else-Kröner-Fresenius-Stiftung für die Finanzierung dieser Arbeit bedanken.

Danken möchte ich auch meiner Prüfungskommission, Prof. Dr. Dietmar Zehn als Vorsitzendem und Prof. Dr. Martin Klingenspor sowie Prof. Dr. Alexander Bartelt als Prüfern.

Schlussendlich geht der allergrößte Dank an meine Familie, meinen Freund und meine Freunde. Ohne eure Unterstützung und den Glauben an mich, hätte ich es niemals bis hierhergeschafft. Vielen Dank!

8 Statement of Authorship

Eidesstattliche Erklärung

Ich, Kristina Then, erkläre an Eides statt, dass ich die bei der promotionsführenden Einrichtung TUM School of Life Sciences der TUM zur Promotionsprüfung vorgelegte Arbeit mit dem Titel:

Nutritional programming of white adipose tissue growth and metabolism in adulthood

am Lehrstuhl für Molekulare Ernährungsmedizin

unter der Anleitung und Betreuung durch: Prof. Dr. Martin Klingenspor

ohne sonstige Hilfe erstellt und bei der Abfassung nur die gemäß § 7 Abs. 6 und 7 angegebenen Hilfsmittel benutzt habe.

Ich habe keine Organisation eingeschaltet, die gegen Entgelt Betreuer*innen für die Anfertigung von Dissertationen sucht, oder die mir obliegenden Pflichten hinsichtlich der Prüfungsleistungen für mich ganz oder teilweise erledigt.

Ich habe die Dissertation in dieser oder ähnlicher Form in keinem anderen Prüfungsverfahren als Prüfungsleistung vorgelegt.

Die vollständige Dissertation wurde noch nicht veröffentlicht.

Ich habe den angestrebten Doktorgrad noch nicht erworben und bin nicht in einem früheren Promotionsverfahren für den angestrebten Doktorgrad endgültig gescheitert.

Ich habe keine Kenntnis über ein strafrechtliches Ermittlungsverfahren in Bezug auf wissenschaftsbezogene Straftaten gegen mich oder eine rechtskräftige strafrechtliche Verurteilung mit Wissenschaftsbezug.

Die öffentlich zugängliche Promotionsordnung sowie die Richtlinien zur Sicherung guter wissenschaftlicher Praxis und für den Umgang mit wissenschaftlichem Fehlverhalten der TUM sind mir bekannt, insbesondere habe ich die Bedeutung von § 27 PromO (Nichtigkeit der Promotion) und § 28 PromO (Entzug des Doktorgrades) zur Kenntnis genommen. Ich bin mir der Konsequenzen einer falschen Eidesstattlichen Erklärung bewusst.

Mit der Aufnahme meiner personenbezogenen Daten in die Alumni-Datei bei der TUM bin ich einverstanden.

Ort, Datum, Unterschrift